学位論文

Study of deep ocean circulations in the North Pacific using lowered acoustic Doppler current profiler (LADCP)

降下式音響ドップラー流速計(LADCP)を用いた北太平洋の深層循環の研究

平成 19 年 6 月　博士(環境学)申請

東京大学大学院新領域創成科学研究科
自然環境学専攻

小牧　加奈絵

A doctoral dissertation

Study of deep ocean circulations in the North Pacific using lowered acoustic Doppler current profiler (LADCP)

Kanae Komaki

June 2007

Department of Natural Environment,

Graduate School of Frontier Science, The University of Tokyo

Abstract

A lowered acoustic Doppler current profiler (LADCP) enables to measure current velocity at full depth during a conductivity-temperature-depth profiler (CTD) measurement. However, the data from LADCP produce unrealistic velocities at depths greater than 1000 m at low and middle latitudes where intensity of sound pulse reflected by scatterers in water (called echo intensity) is relatively weak. The present this thesis devised a correcting method of the LADCP velocity that is necessary for studying the deep circulation, and examined application of echo intensity data from LADCP to deep water-mass analysis. Moreover, using these methods for analyzing LADCP data, the pathways and structures of deep circulation currents in the North Pacific were clarified.

Echo intensity of the reflected sound pulse is highly correlated with magnitude of the difference in vertical shear of velocity between downcast and upcast, which indicates an error in velocity shear. Then, the velocity shear was corrected using echo intensity; the correction values were determined as to fit LADCP velocity to shipboard ADCP (SADCP) and LADCP bottom-tracked velocities. The presented method is as follows. Initially, a profile of relative velocity to sea surface is obtained by integration of vertical shears of velocity after low-quality data are rejected. Second, the relative velocity is fitted to the velocity at 100–800 dbar measured by SADCP and an "absolute" velocity profile is obtained. Third, the velocity shear is corrected using the relationship of the errors in velocity shears with echo intensity, in order to adjust the velocity at sea bottom to the bottom-tracked velocity measured by LADCP. Finally, the velocity profile is obtained from the SADCP-fitted velocity at depths less than 800 dbar and the

corrected velocity shear at depths greater than 800 dbar. This method is valid for a full-depth LADCP cast throughout which the echo intensity is relatively high (greater than 75 dB in the present analysis). The corrected data produced qualitatively good current structures that were consistent with the deep current structures inferred from silicate distribution, although the processed velocity may include errors of 1–2 cm s^{-1}.

The present analysis concluded that zooplankton and sinking particle are the largest contributor to echo intensity at depths shallower than 3000 m and at the greater depths, respectively. As a result, their distributions produce the meridional variations of echo intensity that it is higher in the subpolar and equatorial regions and lowest in the subtopics. Echo intensity at each latitude deviates from the averaged meridional variation. The deviation of echo intensity is partly due to the existence of water masses with different origins. In the lower deep layer at depth greater than 3500 m, high dissolved oxygen of the Lower Circumpolar Water (LCPW) carried by the deep circulation from the Antarctic corresponds to low deviation of echo intensity, and validity of the deviation of echo intensity for the analysis of deep water masses was concluded.

Using the above method and conclusion, deep circulation currents in the North Pacific were examined with the data of velocity and echo intensity from LADCP. The deep circulation current in the lower deep layer finally flows into the Northeast Pacific Basin from south of the Aleutian Trench, south of Hawaiian Ridge and the Main Gap of the Emperor Seamounts Chain. The present thesis clarified the inflow through the Main Gap and its downstream pathway. The current in the Main Gap flows eastward with the maximum velocity of 10 cm s^{-1} at a depths of 5400 m carrying LCPW characterized by high oxygen and low echo intensity. From this and the distribution of

LCPW, it was concluded that a portion of the eastern branch current of the deep circulation flows into the Northeast Pacific Basin through the Main Gap. Moreover, it was clarified that this current flows along the northern slope of the Hess Rise and then approximately 38°N to 165°W. In the northeastern region of the Norhteast Pacific Basin, LCPW is transformed into the North Pacific Deep Water (NPDW), characterized by high silica and low oxygen, in the over-turning process, i.e., upwelling to and spreading in the upper deep layer at depth of 2000-3500 m. The present analysis showed that NPDW flows westward at 36.5-44.5°N, 165°W, due to the deep circulation current in the upper deep layer.

Moreover, the present thesis examined the deep circulation current in the upper deep layer from the Antarctic, and clarified the detailed structure of the current over the northeastern slope of the Solomon Rise in the Melanesian Basin. The upper deep current comprised the western and eastern cores located over the bottom slope at water depth of approximately 3000 and 4000 m, respectively. Between the double cores, a thick countercurrent presents in a width of more than 100 km over the bottom slope at water depth of approximately 3500 m. The countercurrent carried water with extremely high echo intensity which is characteristics of equatorial water. This indicates that the countercurrent comes from the western region near the equator.

Contents

Chapter 1

General introduction

Deep ocean circulation conveys cold, dense and oxygen-rich water sinking in the polar regions, advects heat and substance on a large distance, and impacts on oceanic environment and global climate. In order to understand the deep circulation, data of current velocity and water-mass properties have to be observed precisely and analyzed sufficiently. The Lower Circumpolar Water (LCPW) in the Antarctic Circumpolar Current originating from the North Atlantic Deep Water (NADW) flows into the Pacific Ocean, and is carried northward by deep western boundary current, and finally gathers in the Northeast Pacific Basin (Mantyla and Reid, 1983; Fig. 1.1ab). The property of NADW is diluted during the transportation, and LCPW in the North Pacific has much less characteristics of NADW. Therefore, current velocity data are important for the deep circulation analysis especially in the North Pacific, together with high-quality data of water-mass properties.

Moored current meters measure current velocity at a certain point continuously, but the operation of many moorings needs much work. On the other hand, a lowered acoustic Doppler current profiler (LADCP) enables to measure current velocity at full depth relatively easily, although the data procedure is not easy as studied in the present thesis. The data from LADCP are expected to contribute largely to study on deep circulation in the North Pacific. However, the LADCP data produce unrealistic velocities at depths greater than 1000 m at low and mid latitudes where echo intensity of reflected sound pulse is weak (e.g., Wijffels et al., 1998). Therefore, a correcting method of the LADCP velocity needs to be devised for clarifying deep currents in the North Pacific.

The deep circulation current in the North Pacific flows into the Northeast Pacific Basin through south of the Hawaiian Ridge at 20°N from the Central Pacific Basin and through south of the Aleutian Trench, and the Main Gap at 39°N in the Emperor Seamount Chain from the Northwest Pacific Basin (Mantyla and Reid, 1983; Hamann and Taft, 1984). The

deep western boundary current is separated into the eastern and western branches in the southern region of the Central Pacific Basin, which pass the Central Pacific Basin and the East Mariana Basin on way to the Northwest Pacific Basin, respectively (Johnson and Toole, 1993; Kawabe et al., 2003). Part of the eastern branch current is supposed to pass the Main Gap toward the Northeast Pacific Basin (Kawabe and Taira, 1995).

The present thesis proposes a new correction method of LADCP velocity data and an application of echo intensity to water-mass analysis, and examines the deep circulation currents in the North Pacific using the LADCP data of velocity and echo intensity. In Chapter 2, I examined the relationship between echo intensity and errors in velocity from LADCP, and attempted to devise a new method to process and correct LADCP velocity data. In Chapter 3, I investigated the spatial properties and relationship of echo intensity to zooplankton and particles in seawater, and proposed to apply echo intensity to water-mass analysis of deep water. Using these methods, the pathway of the deep circulation current through the Main Gap in the Emperor Seamounts Chain and the pathway of the western branch current were examined in Chapter 4. The conclusions of the present study were summarized in Chapter 5.

(a)

(b)

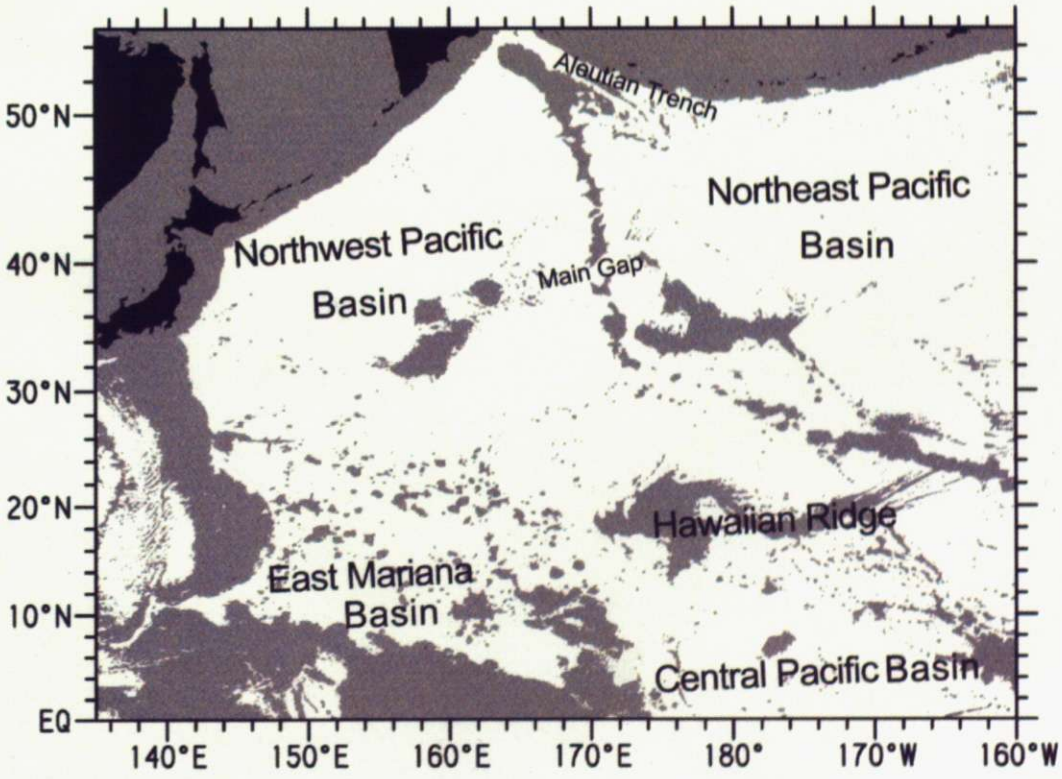

Fig. 1.1: Dissolved oxygen (ml l^{-1}) in the Pacific Ocean at depths of (a) sea bottom sited from Mantyla and Reid (1983) and (b) map of the North Pacific. Shade indicates areas at depths less than 4500 m.

Chapter 2

Correction method for full-depth current velocity with LADCP

2.1. Introduction

Current velocity is a key parameter in oceanography, and its direct measurement is important for oceanographic study and environmental monitoring. Surface drifters are used to survey currents in wide areas of the sea surface. Floats and shipboard acoustic Doppler current profilers (SADCPs) are used to observe subsurface currents on an isobaric or isopycnal surface and in a layer of a few to several hundred meters depth from the sea surface, respectively. For subsurface and deep currents, moored current meters and moored ADCPs are useful to obtain the time series of current velocity at mooring points and in a layer of a few hundred meters depth, respectively. These instruments are practical for horizontal or temporal measurement of current velocity.

Vertical continuous full-depth measurement of current velocity was first realized with a free-falling velocity profiler that was tracked acoustically. However, it requires complex ship maneuver and a long observation time, and is not suitable for measuring current velocity at many points. In contrast, a lowered acoustic Doppler current profiler (LADCP) enables current velocity measurement at full depth at many points. It is attached to the frame of a conductivity-temperature-depth profiler (CTD), and is lowered and lifted together with the CTD underwater unit. In the same way as SADCP and moored ADCP, LADCP discharges sound pulses from four transducers and catches returning pulses that are reflected by floating particles in water and have Doppler-shifted frequencies. The frequency shift is proportional to the speed of scatterers relative to the movement of the LADCP. Since the scatterers float due to current, the current velocity relative to LADCP is estimated from the frequency shift of the reflected sound pulses.

Current observation with LADCP was first conducted in 1989 by Firing and Gordon (1990) and has increased since the mid 1990s. Many full-depth CTD/LADCP casts were

carried out in the World Ocean Circulation Experiment (WOCE), at the lines of the WOCE Hydrographic Programme (WHP) P10, P13, P14, P16, P17, P18, and P19 in the Pacific Ocean (Firing et al., 1998; Wijffels et al., 1998; Firing, 1998; Roden, 2000). However, the published LADCP data are restricted to almost the equatorial region at 14.5°S–6°N and the subtropical and subarctic regions north of 30°N, and there are no LADCP velocity data published in low latitude areas at almost 6°–30°N. The lack of data is thought to be due to the weak echo intensity at depths greater than 1000 m in the low latitude areas (Wijffels et al., 1998; Firing, 1998). Generally, echo intensity is relatively strong in the equatorial and subarctic regions but weak in between in the Pacific Ocean. The weak echo intensity may decrease the range of depth at which sound pulse is reflected and thus the number of current velocity data, thereby reducing the accuracy of current velocity measurement (Fischer and Visbeck, 1993; Firing, 1998).

Differences in horizontal velocity between different depths (vertical shears of velocity) are calculated with data obtained from one LADCP sound pulse (Firing and Gordon, 1990; Fischer and Visbeck, 1993). The averaged vertical shear is integrated downward from the sea surface, and the relative velocity profile is obtained. The vertical shears have low accuracy and need to be corrected, when they are obtained from data with weak echo intensity.

Another remaining serious problem is how to estimate the reference velocity necessary to transform relative velocity to absolute velocity. Fischer and Visbeck (1993) determined reference velocity by removing the integration of relative velocity and ship drift during the whole cast from the integration of velocity measured by LADCP during the whole cast. Hall et al. (2004) adjusted the velocity profile to the SADCP velocity profile at depths of less than 500 m. In the case of a deep cast close to sea bottom, the absolute

velocity at near bottom can be obtained by estimating the movement of LADCP with the bottom-reflected pulse (Cunningham et al., 1997). Visbeck (2002) sought an absolute velocity profile from raw LADCP velocity data and ship's navigation data with the inverse method, using the bottom-tracked velocity as the reference velocity. This method options constraints of SADCP velocity data and variable weights for the inverse solutions.

In the present study, we carefully examine the relationship between echo intensity and errors in velocity from LADCP, and attempt to devise a new method to process and correct LADCP velocity data, in which SADCP velocity and bottom-tracked LADCP velocity are used as reference velocities at the uppermost and lowermost depths, respectively.

2.2. Observations and data

We made CTD/LADCP casts at 36 stations C01–C36 between 8°50′N and 44°30′N along 165°W in the North Pacific in June 2003 on the R.V. *Hakuho Maru* KH-03-1 cruise (Fig. 2.1). We used a 300-kHz LADCP manufactured by RD Instruments. The first bin depth and the bin interval of reflected sound pulses were set at 6 m below the instrument and 4 m, respectively. Current velocity measurement was performed with the sound pulses reflected from 40 bins, and the maximum depth of the sound reflection was 162 m. The time interval of sound pulses discharging and data recording was one second.

Current velocity in the surface and intermediate layers was also measured with a 38-kHz SADCP manufactured by RD Instruments. The first bin depth, the bin interval, and the maximum bin depth of SADCP were set at 38 m, 16 m, and 1040 m, respectively. The current velocity data were averaged at intervals of 2.5 minutes.

Poor-quality data from LADCP were rejected following the procedure of Fischer and Visbeck (1993). (1) Current velocity data have large errors due to tilting of the LADCP, and the data were rejected when the tilt from the horizontal level was greater than 18 degrees. (2) The error velocity, defined as the difference between vertical velocities estimated by two groups of the opposite transducers, was quite large at the first bin; thus, the velocity data at the first bin were rejected. (3) The velocity data were rejected if the error velocity deviated by more than the standard deviation from the mean at each station. (4) The vertical velocities at all bins measured from each sound pulse, which are almost equal to the vertical move of the LADCP instrument of approximately 1 m s^{-1}, must be the same. Therefore, the velocity data were rejected if the vertical velocity deviated by more than three times the standard deviation from the mean of vertical velocities for one sound pulse.

After rejection of poor-quality data, the number of velocity data became maximum at

the third bin that was neither far from nor close to the transducers. Therefore, we selected to use echo intensity data only at the third bin, in order to do away with the difficult correction for decay of echo intensity during a propagation in water. Echo intensity data were transformed into relative backscattering intensity using the conversion equation provided by RD Instruments (1996), and the transformed value is called echo intensity in the present paper.

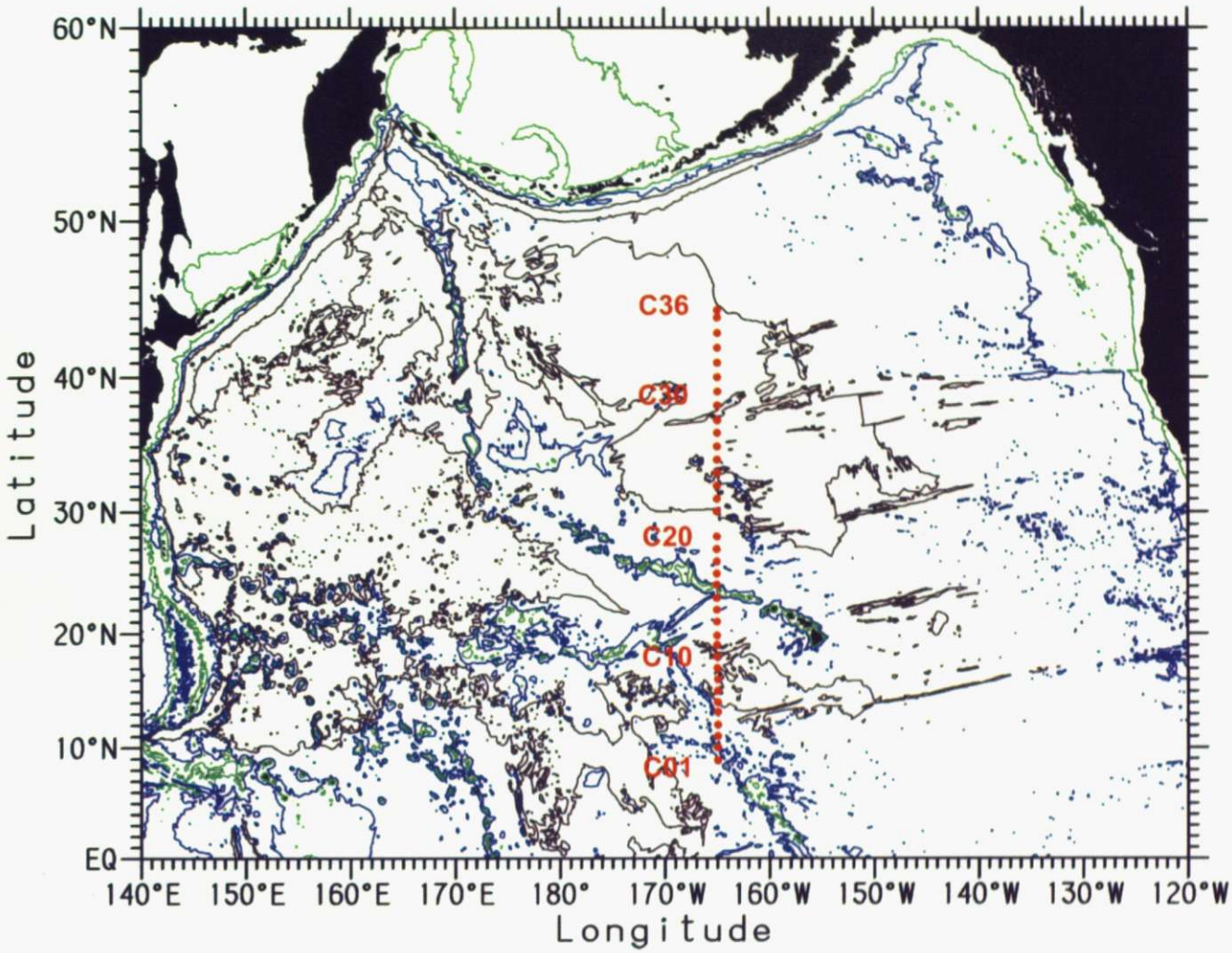

Fig. 2.1: Stations of lowered acoustic Doppler current profiler (LADCP) at 165°W in *Hakuho Maru* cruise KH-03-1 (red dots). Green, blue, and gray lines indicate 2000 m, 4000 m and 5500 m isobaths, respectively.

2.3. Adjustment of relative velocity profile to make absolute velocity

The method of calculating vertical shear of velocity, which was described by Firing and Gordon (1990) and Fischer and Visbeck (1993), was used to obtain the relative velocity profile. The vertical shears were calculated with velocities 5-m depth apart obtained from one transmitted sound pulse, and were averaged in layers of 5 and 200 m at depths less and greater than 1000 dbar, respectively. The averaged shears were integrated from sea surface to sea bottom, and a profile of relative velocity to sea surface was obtained.

The SADCP on R.V. *Hakuho Maru* usually measures current velocity down to depths greater than 900 m. Since it takes almost 15 minutes to lower an LADCP to this depth in a CTD/LADCP cast, the SADCP velocities averaged for 15 minutes at the beginning and end of the LADCP cast were used for comparison with LADCP relative velocity profiles. The absolute values of the difference in vertical shear between SADCP and LADCP velocities were averaged in every 50 m depth cell for all stations (Fig. 2.2). For both downcast and upcast, the differences in vertical shear at depths of 100–800 m are significantly smaller than those at depths less than 100 m and greater than 800 m, having minimums at depths between 400 m and 700 or 750 m. This implies that the SADCP velocity in a layer of 100–800 m depth is suitable to adjust the LADCP relative velocity. Therefore, the LADCP relative velocity profile was fitted to the SADCP velocity at depths of 100–800 m by the least squares method and was transformed to the "absolute" velocity profile.

Moreover, we used bottom-tracked velocity as another reference velocity (see Section 2.4). Bottom tracking was conducted in the range of 140 dbar above sea bottom. With increasing distance from sea bottom, the number of bottom-tracked data and the number of stations decreases, and the mean velocity and its 95% confidence interval increase upward almost monotonously (Table 2.1). The decrease of data and station numbers and the

increase of the 95% confidence interval are particularly remarkable between the third and fourth layers from sea bottom. As a result, in the fourth to seventh layers, the 95% confidence interval is comparable to or larger than the mean velocity. As reference velocity, the bottom-tracked velocities in the first to third layers from sea bottom are more suitable than those in the fourth to seventh layers. In particular, the number of data in the first layer is the largest, and the mean velocity is most significant statistically. Therefore, the bottom-tracked velocity averaged at 0–20 dbar from sea bottom, shown in Fig. 2.3, is used as the reference velocity for the LADCP "absolute" velocity. The eastward near-bottom velocity at 12°–22°N in Fig. 2.3 corresponds to the high-oxygen tongue south of the Hawaiian Ridge which suggests a branch of the deep circulation carrying the Lower Circumpolar Water (LCPW) to the Northeast Pacific Basin (Mantyla and Reid, 1983).

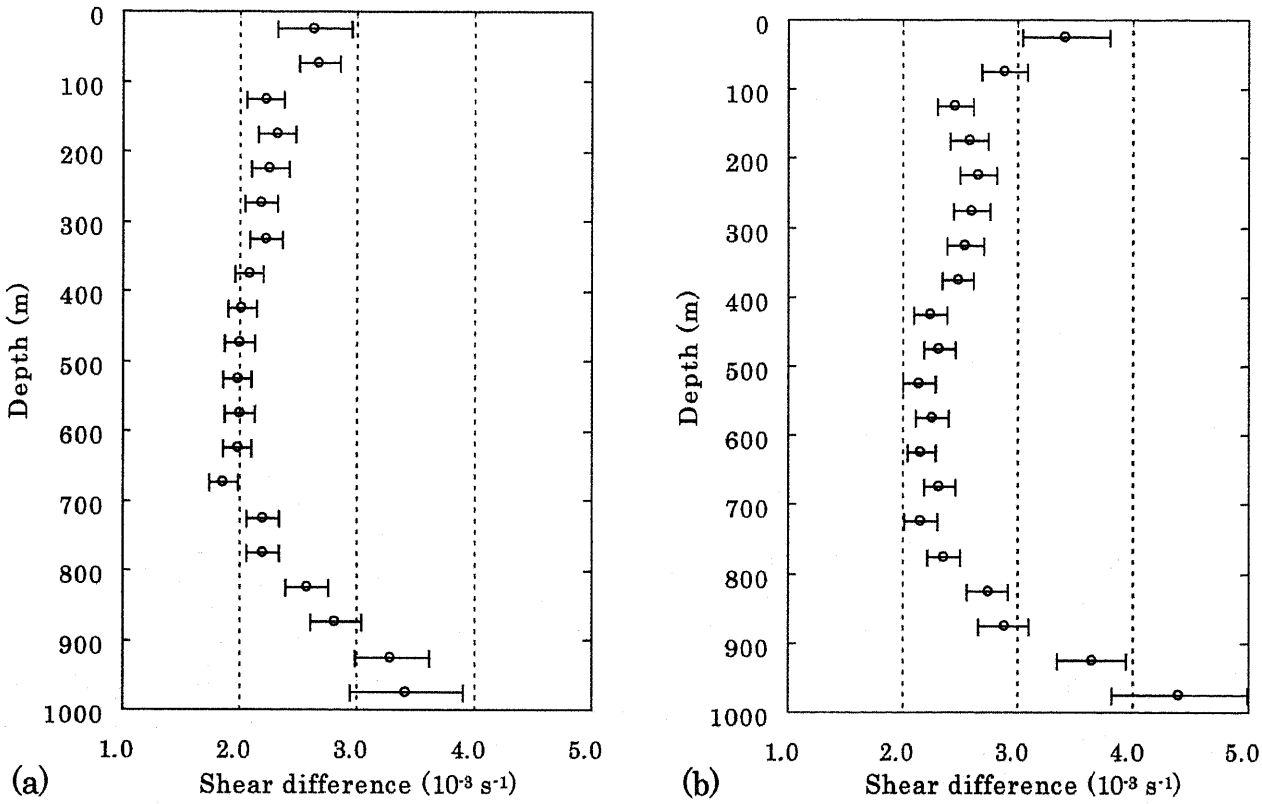

Fig. 2.2: Amplitudes of the difference in vertical shear between SADCP and LADCP velocities averaged for C01–C36 during downcast (a) and upcast (b). The differences are calculated at 5-m intervals for zonal and meridional velocity components, and their absolute values are summed and averaged every 50 m. Horizontal bars show 95% confidence intervals of the means.

Table 2.1: Mean and 95% confidence interval of bottom-tracked velocity for stations C01–C36 calculated at 20-dbar intervals from sea bottom. The numbers of bottom-tracked data and stations are also shown.

Distance from sea bottom (dbar)	Mean ± 95% confidence interval u (cm s^{-1})	v (cm s^{-1})	Number of data	Number of stations
0 – 20	3.0 ± 1.2	3.1 ± 1.2	4644	36
20 – 40	4.0 ± 2.0	4.1 ± 2.4	1728	36
40 – 60	5.2 ± 2.8	5.9 ± 3.2	1155	35
60 – 80	6.1 ± 5.7	4.7 ± 5.0	551	29
80 – 100	9.5 ± 6.1	5.0 ± 5.5	170	15
100 – 120	3.9 ± 6.8	6.8 ± 10.8	99	11
120 – 140	16.5 ± 10.1	12.2 ± 10.1	9	3

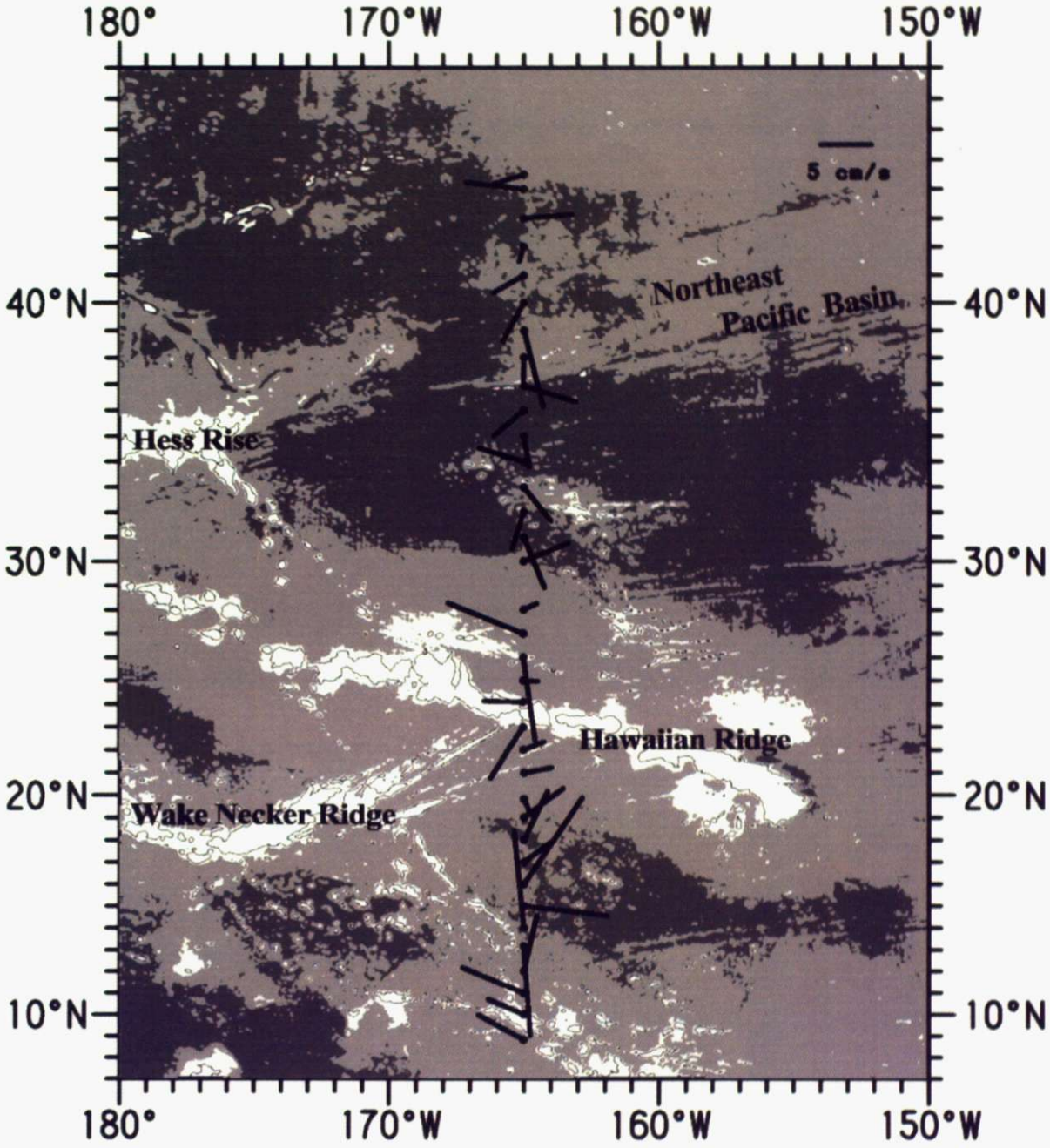

Fig. 2.3: Mean vectors of bottom-tracked velocities at 0-20 dbar from sea bottom at C01–C36, 165°W in the Northeast Pacific Basin. Dark and light shades show water depths greater than 5500 m and 4500 m, respectively. Thin line shows a 3500 m isobath.

2.4. Correction for vertical shears of velocity

2.4.1. Relation of echo intensity with errors in velocity

After the LADCP relative velocity was fitted to the SADCP velocity at depths of 100–800 m, the vertical shears of LADCP velocity have to be corrected in order to fit the bottom velocity to the bottom-tracked velocity at near bottom. The amplitude of correction for vertical shear of velocity probably differs depending on the acoustic environment in water, as indicated by echo intensity. Then, we examine how the reliability of the velocity shear data is related to echo intensity.

The echo intensity along 165°W shows large spatial variations (Fig. 2.4a). The echo intensity north of 32°N is much higher than that south of 32°N at full depth except at near surface (shallower than 100 dbar). A meridional maximum at depths greater than 2000 dbar stands at 39°N, whereas a minimum (< 70 dB) exists in the bottom layer at 14°–20°N. In the surface layer, a vertical minimum of echo intensity is found around 300 dbar (upper broken line in Fig. 2.4a), and maxima are found at near surface and around 500 dbar (lower broken line). They are present clearly at 13°–32°N.

These characteristics in distribution of echo intensity are similar to those of the number of velocity shear in every 5-m depth cell (Fig. 2.4b). The number of velocity shear north of 32°N is much greater than that south of 32°N, and has a meridional maximum at 39°N at depths greater than 2000 dbar and a near-bottom minimum at 14°–20°N. A vertical minimum exists around 300 dbar particularly south of 32°N, and two maxima exist around 100 and 500 dbar. Except the maximum at 100 dbar, these are quite similar to the distribution of echo intensity. The maximum of the number of velocity shear at 100 dbar may be ascribed to data decrease due to sound reflection and noise near the sea surface where echo intensity is higher than approximately 100 dB. This must be one reason why

the number of velocity shear decreases when echo intensity exceeds 100 dB (Fig. 2.5). In the echo intensity range less than 100 dB, the number of velocity shear is strongly correlated with the echo intensity, particularly in the range less than 95 dB. Therefore, echo intensity can be used as an indicator of the number of velocity shear.

If the data of velocity shear is reliable, the velocity shear would not be so different between downcast and upcast. Therefore, reliability of the data may be shown by the difference in velocity shear between downcast and upcast. In this process, velocities were averaged in every 200-m depth cell, and the velocity shear was calculated at intervals of 200 m for zonal and meridional velocities. The absolute value of the difference in velocity shear between downcast and upcast was calculated for the zonal and meridional components, and the average of the absolute values for the both components is termed the magnitude of the difference in velocity shear in this paper. The magnitude of the difference is almost the same as the root mean square (RMS) of the difference, and the RMS can also be used in this method instead of the magnitude.

The magnitude of the difference in velocity shear between downcast and upcast decreases from more than $5 \times 10^{-4}\,s^{-1}$ at sea surface to approximately $2.5 \times 10^{-4}\,s^{-1}$ at 1000 dbar (Fig. 2.6). The relatively large difference at near surface may be due to large changes of surface currents between downcast and upcast. A meridional minimum around 39°N ($< 2.5 \times 10^{-4}\,s^{-1}$) and a maximum at 12°–22°N ($> 1.5 \times 10^{-3}\,s^{-1}$) correspond well to the meridional maximum and minimum of echo intensity, respectively.

The low value of approximately $2.5 \times 10^{-4}\,s^{-1}$ continues to sea bottom north of 35°N (C26), and corresponds to a high echo intensity exceeding 77 dB (Figs. 2.4a and 2.6). Figure 2.7 clearly shows that the magnitude of the difference in velocity shear between downcast and upcast is small for echo intensities exceeding 77 dB, whereas it increases sharply as

the echo intensity decreases in the range of low echo intensity less than 77 dB. The averages in 1-dB bands of the absolute values of the difference in velocity shear are higher than $5 \times 10^{-4}\,s^{-1}$ for echo intensities less than 75 dB and greater than 99 dB, and are lowest and least variable between 79 and 91 dB (Fig. 2.8).

Another indicator of the reliability of LADCP data is the difference between downcast and upcast in the LADCP "absolute" velocity obtained by fitting to SADCP velocity. The difference in zonal velocity is small for echo intensities exceeding 88 dB, increases for low echo intensities, and becomes large and dispersive for echo intensities less than 75 dB (Fig. 2.9). The similar result is also obtained from the difference in meridional velocity. These show that the correction for LADCP velocity is not needed for echo intensities exceeding 88 dB, and may be impossible for echo intensities less than 75 dB. Therefore, the correction for velocity shear of LADCP data was made for echo intensities between 75 and 88 dB.

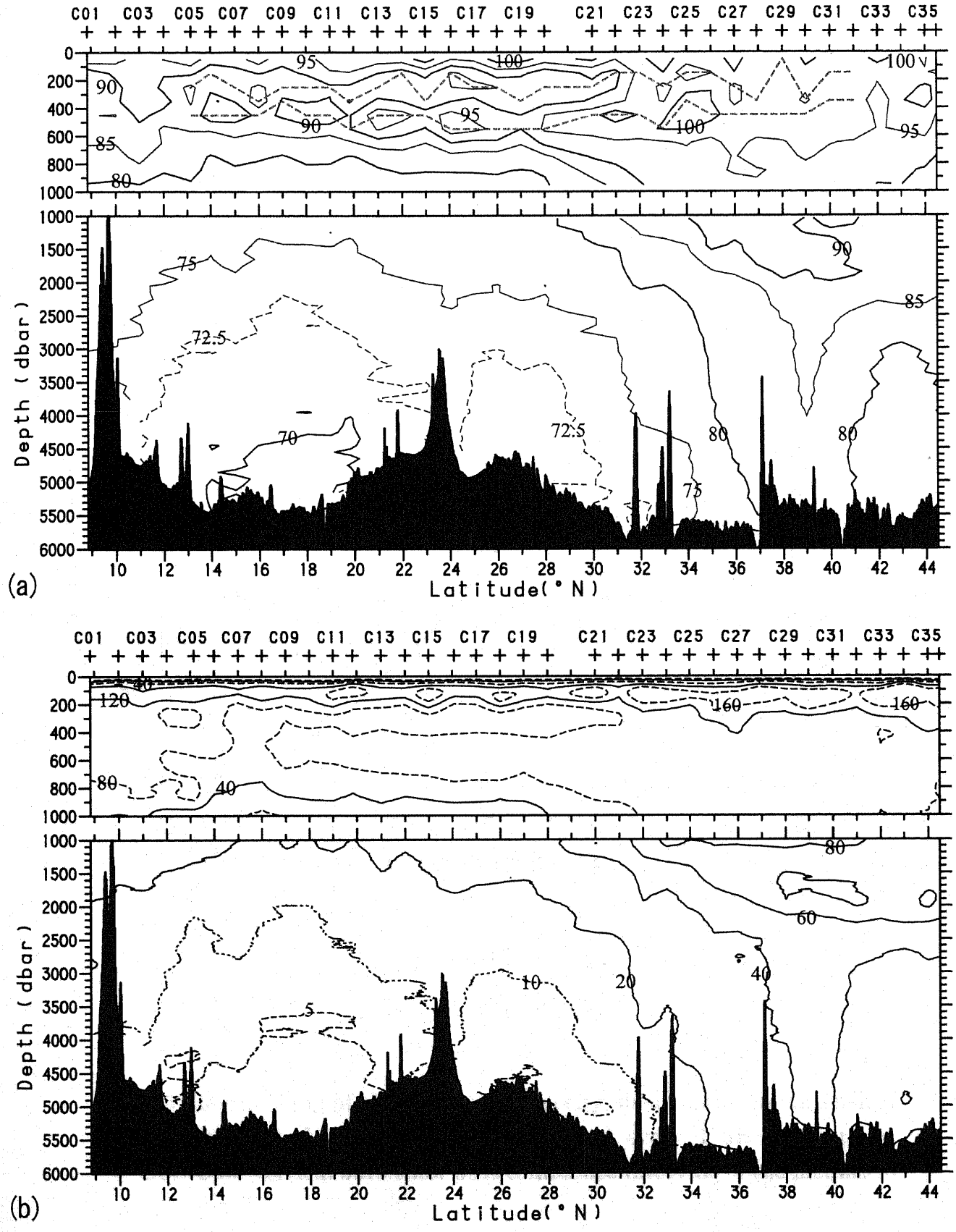

Fig. 2.4: Sections at 165°W of echo intensity (dB) (a) and the number of velocity shear in every 5-m depth cell (b). Mean values for downcast and upcast are shown. Pluses at the top of each panel indicate LADCP stations. In (a), the vertical minimum and maximum of echo intensity around 200 and 400 dbar are shown by broken lines.

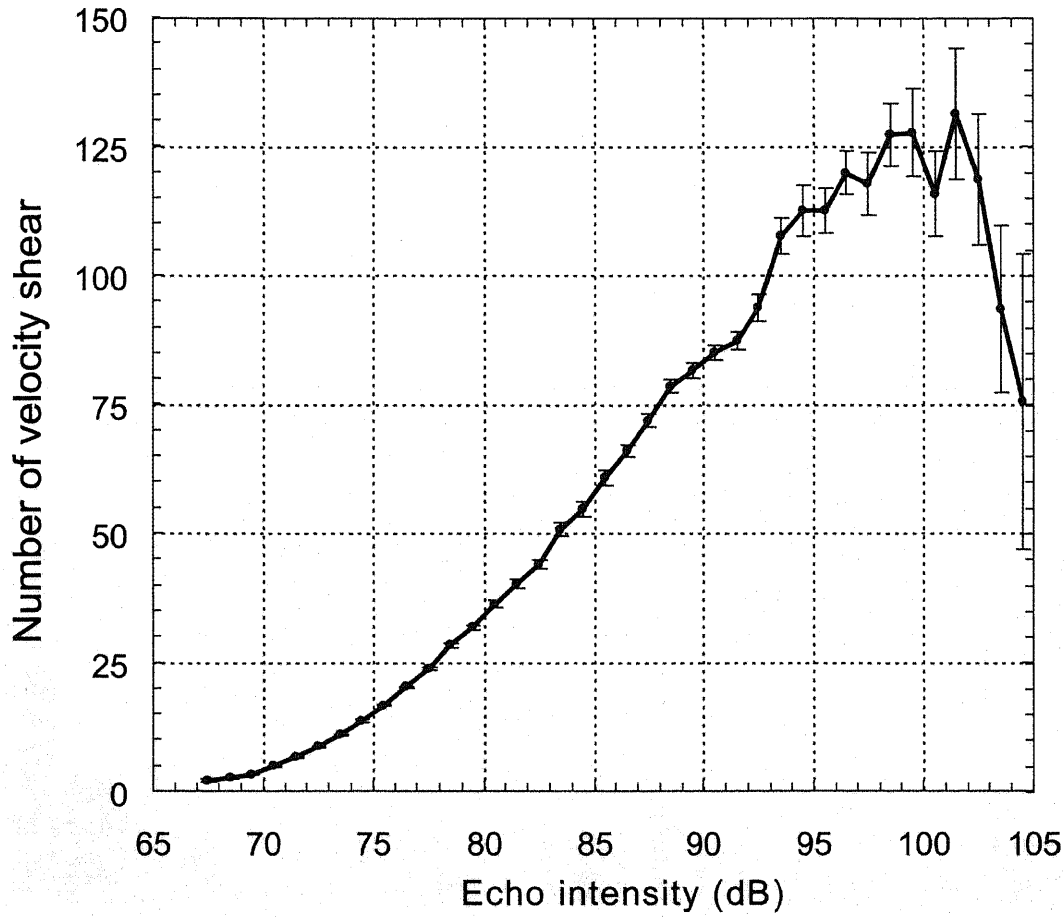

Fig. 2.5: Relationship of the number of velocity shear with echo intensity. The number of velocity shear is averaged every 1 dB for stations C01–C36. Vertical bars show 95% confidence intervals of the means.

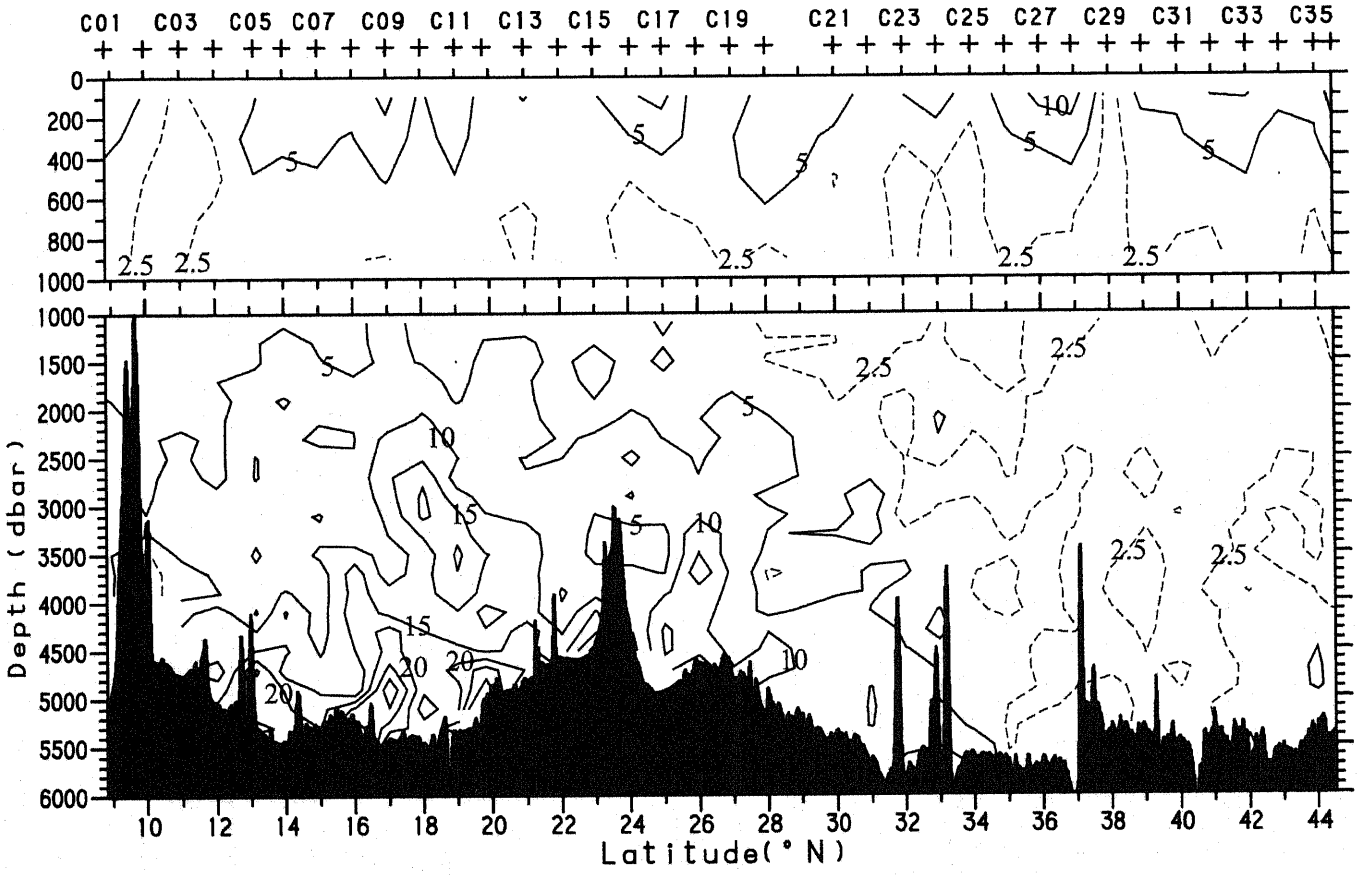

Fig. 2.6: Section at 165°W of the magnitude of the difference in velocity shear (10^{-4} s^{-1}) between downcast and upcast. The vertical shear of velocity was calculated in every 200-m depth cell from an average of 40 local velocity shears at intervals of 5 m. The shear differences were calculated for zonal and meridional components, and their absolute values were averaged. Broken lines indicate small difference value of 2.5×10^{-4} s^{-1}. Pluses at the top of each panel indicate LADCP stations.

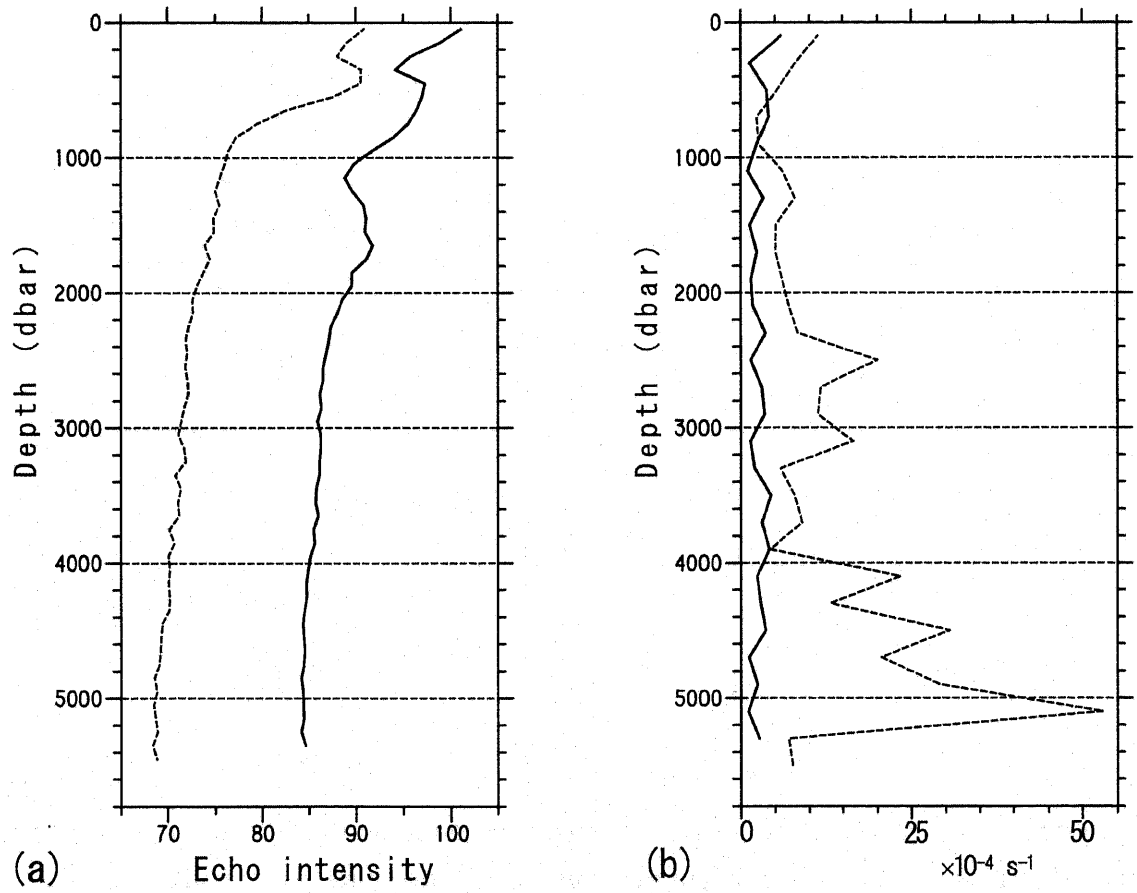

Fig. 2.7: Vertical profiles at C09 (broken lines) and C30 (solid lines) of the mean echo intensity at downcast and upcast (a), and the magnitude of the difference in velocity shear between downcast and upcast (b).

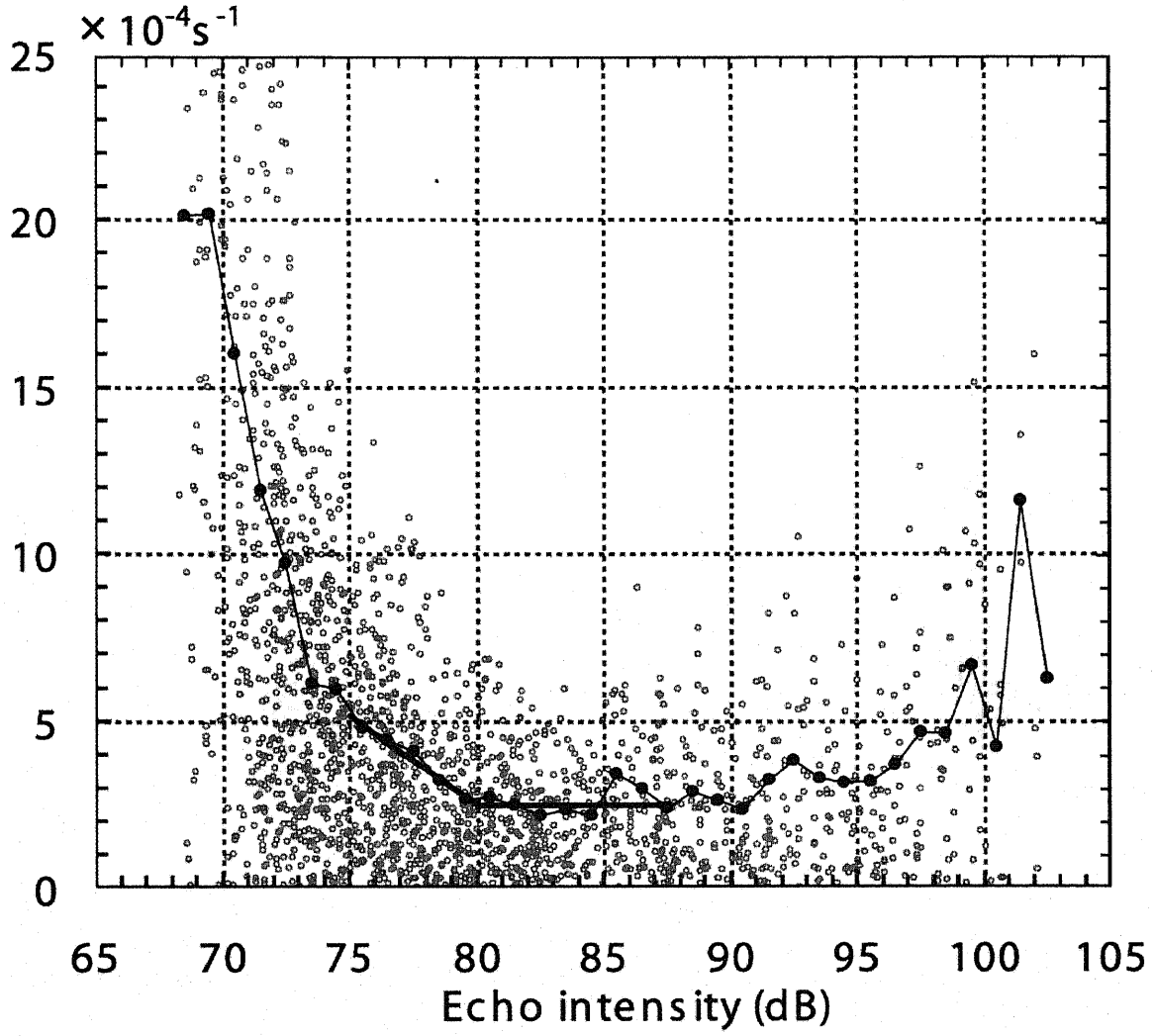

Fig. 2.8: Absolute values of the difference in velocity shear between downcast and upcast for the zonal and meridional components at C01-C36 with respect to echo intensity (small circles), and their averages in 1-dB bands (thin line with dots). The thick line shows the approximation between 75 and 80 dB, and between 80 and 88 dB.

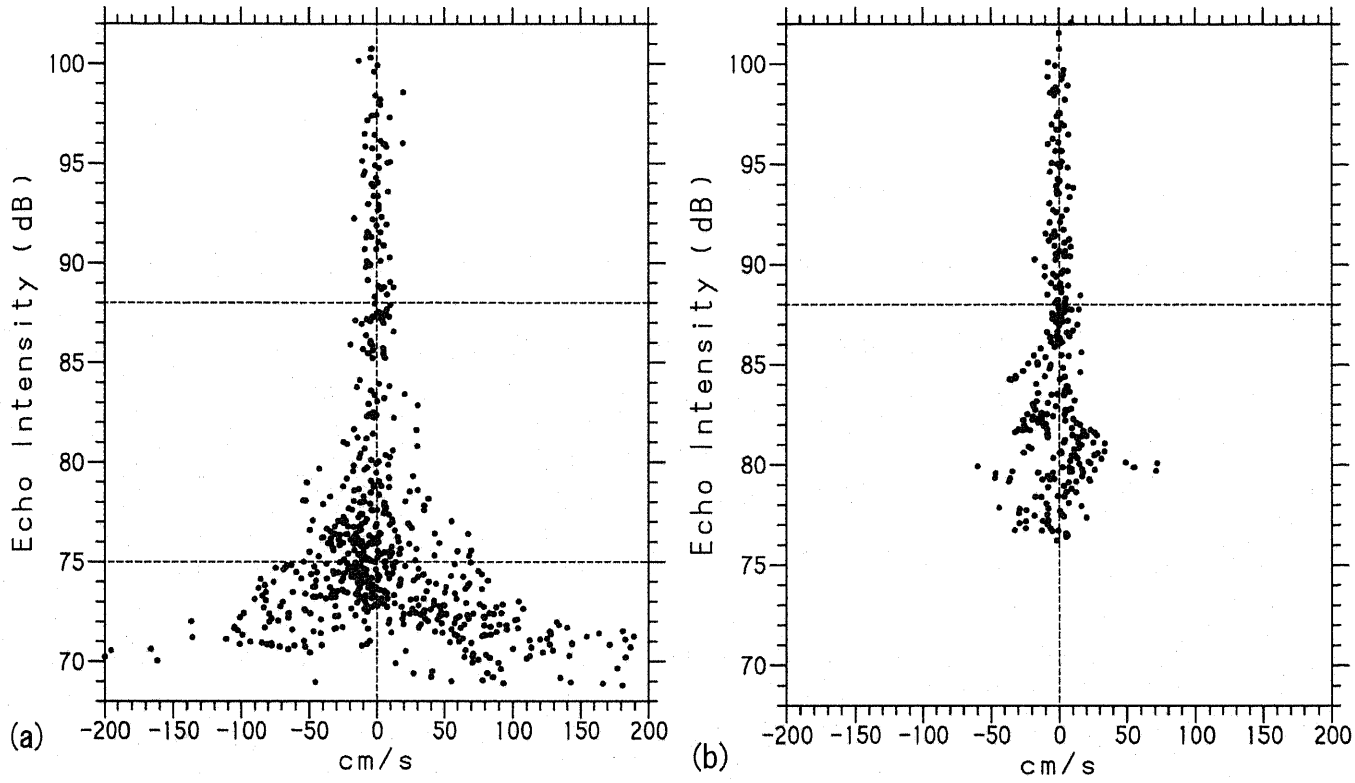

Fig. 2.9: Relationship of echo intensity with the difference in LADCP zonal velocity fitted to SADCP velocity (cm s^{-1}) between downcast and upcast (downcast – upcast), for C01–C25 (a) and C26–C36 (b).

2.4.2. Correction for velocity shears to match near-bottom velocity to bottom-tracked velocity

We assume that the amplitude of the correction of vertical shear of velocity is proportional to the absolute values of the difference in velocity shear between downcast and upcast. The absolute values of the difference in velocity shear are related to the echo intensity as shown in Fig. 2.8. It is approximated by the average of $2.5 \times 10^{-4}\ s^{-1}$ for echo intensities between 80 and 88 dB, and the linear equation $(-0.5375\ EI + 45.5) \times 10^{-4}\ s^{-1}$ for echo intensities between 75 and 80 dB, where EI is echo intensity (dB). Therefore, the correction for velocity shear ζ, which is added to the measured shear of velocity, is

$$\zeta = \begin{cases} 0 & for \quad 88 < EI \\ 2.5\times10^{-4}\cdot k & for \quad 80 < EI \le 88 \\ (-0.5375\cdot EI + 45.5)\times10^{-4}\cdot k & for \quad 75 < EI \le 80 \end{cases} \tag{1}$$

where k is a proportional coefficient that differs by station.

The velocities fitted to the SADCP velocity at downcast and upcast were averaged, and the averaged velocity profile was obtained for each station. If we express the averaged velocity by u, the measured shear of velocity is $\partial u/\partial z$, and the corrected shear of velocity is $\partial u/\partial z + \zeta$. Therefore, the correct velocity at a depth of $z = z_0$, U_0, is expressed as

$$\begin{aligned} U_0 &= \int_{z_{btm}}^{z_0} (\partial u/\partial z + \zeta)\,dz + U_{btm} \\ &= u_0 - u_{btm} + U_{btm} + \int_{z_{btm}}^{z_0} \zeta\,dz \end{aligned}, \tag{2}$$

where z_{btm} is the depth of sea bottom, z is the upward coordinate, u_0 and u_{btm} are the averaged velocities at $z = z_0$ and sea bottom, and U_{btm} is the bottom-tracked velocity. If we take z_0 as the depth at the echo intensity of 88 dB (Section 2.4.1), u_0 is correct velocity fitted

to the SADCP velocity, and $u_0 = U_0$. Using this relation, Equation (2) is transformed to

$$\int_{z_{btm}}^{z_0} \zeta \cdot dz = u_{btm} - U_{btm} \quad . \tag{3}$$

Equations (1) and (3) give the equation for k by using echo intensity data, and the value of k is determined to adjust the velocity at sea bottom to U_{btm}. The determined value of k gives the correction for velocity shear ζ by Equation (1), and ζ gives the correct shear of velocity and, in turn, the correct velocity profile. The values of k at C26–C36 range from −0.38 to 0.15 with an average of −0.12 for the zonal velocity component, and from −0.28 to 0.37 with an average of 0.09 for the meridional component.

Figure 2.10 shows velocity profiles before and after the correction at C26, C33, and C36 for example. The correction changes an overall tilt of velocity profile without largely altering the small-scale vertical variations, since the sign of ζ is constant at a station.

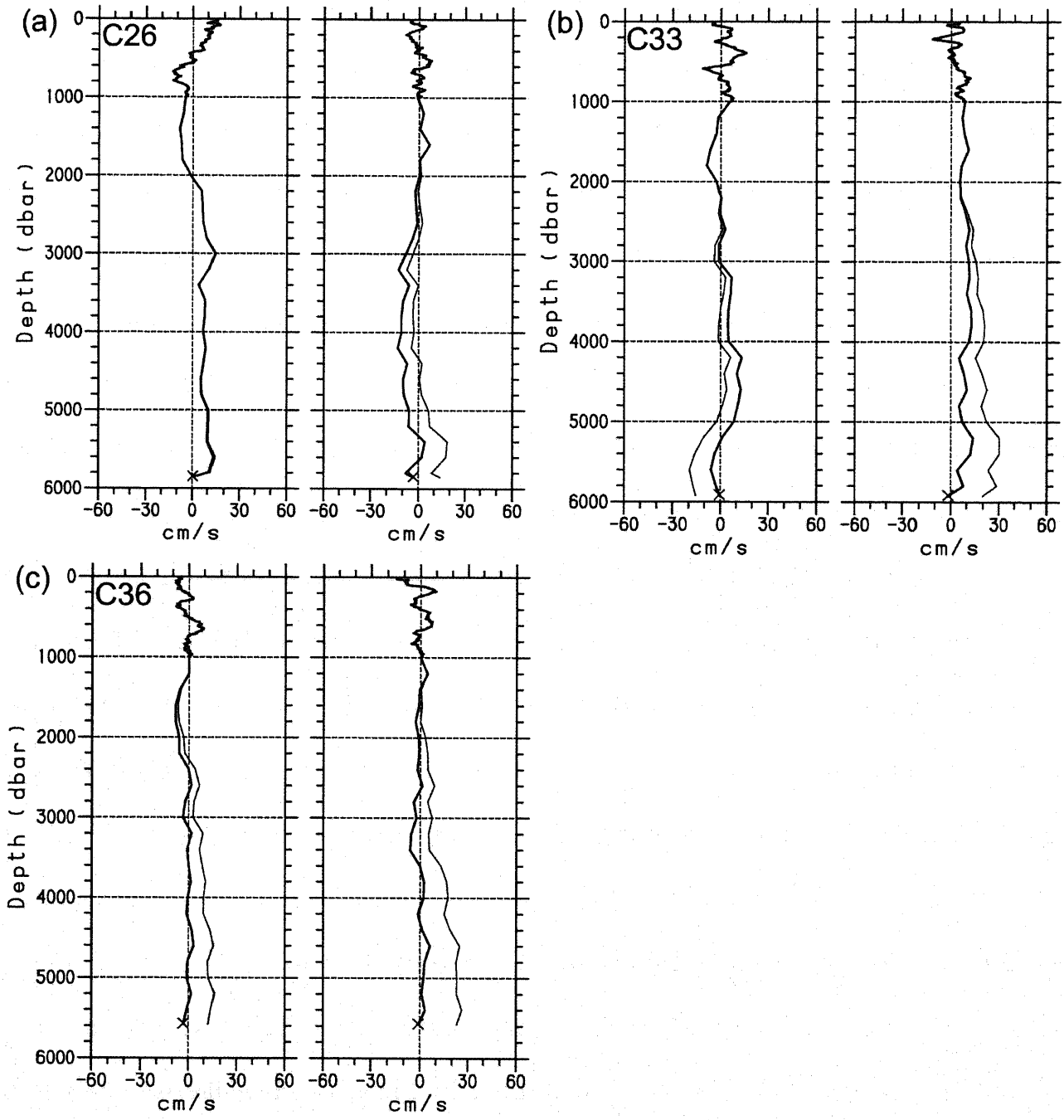

Fig. 2.10: Vertical profiles at C26 (a), C33 (b), and C36 (c) of zonal (left panel) and meridional (right panel) velocities (cm s^{-1}) before and after the correction of velocity shear (thin and thick lines). Crosses show the bottom-tracked velocity.

2.5. Comparison of results between data processing methods

For comparison, we calculated zonal and meridional velocities with the method of Visbeck (2002), based on the constraints of SADCP velocity, ship's navigation and bottom-tracked velocity, using the version 8b software (http://ladcp.ldeo.columbia.edu/ladcp/). The Visbeck (2002) method produces the resemble velocity distribution at the surface and intermediate depths to that from the present method (Figs. 2.11 and 2.12), although the velocity amplitude from the Visbeck (2002) method is smaller particularly for the meridional velocity at 31°N and 36°N. In the deeper layer, the two methods produce different velocity structures. The velocities from the Visbeck (2002) method at depths greater than 1000 dbar are almost less than 2.5 cm s^{-1} with small-scale vertical variations, and large-scale vertical variations are depressed. On the other hand, the present method concludes a relatively organized velocity structure.

We examine the result by the present method for the lower ($\theta < 1.2$°C) and upper ($1.2° < \theta < 2.0$°C) deep layers in which the LCPW and the North Pacific Deep Water (NPDW) are present, respectively (Johnson and Toole, 1993). Deep water colder than 1.2°C, located at depths greater than 4000 dbar, flows eastward at 36.5°–44.5°N toward the high-silicate region located east of 145°W at 37°–50°N (Fig. 2.13a). This suggests that the deep water carried by the eastward current receives silicate from sediment and particles in water in the eastern region. The deep water probably upwells there and expands to a depth of 2300 m (Fig. 2.13b). Water of 1.2°–2.0°C, which is almost present in a layer of 2000–4000 dbar, is westward at 36.5°–44.5°N. The westward current corresponds well to the high-silicate tongue more than 175 μ mol L^{-1} that extends westward. Immediately south of the high-silicate tongue, an eastward current was estimated in the low-silicate region less than 175 μ mol L^{-1}. The zonal velocity averaged at 36.5°–44.5°N is westward between

1000-4000 dbar and eastward at greater depths, with significantly different from that by the Visbeck (2002) method (Fig. 2.14). Thus, the deep current calculated by the present method is consistent with the silicate distribution, and is similar to the flow distribution inferred by Johnson et al. (2006). The present result seems to be realistic qualitatively.

However, the current velocity by the present method is overestimated, as the total volume transport at 36.5°–44.5°N is 25.2 Sv (1 Sv = 10^6 m^3 s^{-1}) eastward in the lower deep layer ($\theta < 1.2$°C) and 42.0 Sv westward in the upper deep layer (1.2°–2.0°C). The volume transport of LCPW carried into the Northeast Pacific Basin is probably 10 Sv or a little more at most, since it is composed of the inflows of LCPW to the Northwest Pacific Basin which are approximately 4 Sv through Wake Island Passage and 2–3 Sv from the East Mariana Basin (Kawabe et al., 2003, 2005) as well as another branch flow south of the Wake Necker Ridge (Mantyla and Reid, 1983). The volume transports estimated with the present method are much larger than the transport of LCPW. The large volume transport may primarily be due to errors in the velocity estimation, although it may include part of an eddy.

One of the errors must be an error of the bottom-tracked velocity. Since the error is 1.2 cm s^{-1} in the deepest column (Table 1), the error of the estimated velocity may be of 1 cm s^{-1} order at least. An error of 1 cm s^{-1} in the zonal velocity brings about an error of more than 16 Sv at maximum in the total volume transport at 36.5°–44.5°N in the respective layer of the upper and lower deep layers. Therefore, the current velocity obtained by the present method may contain an error of 1–2 cm s^{-1}.

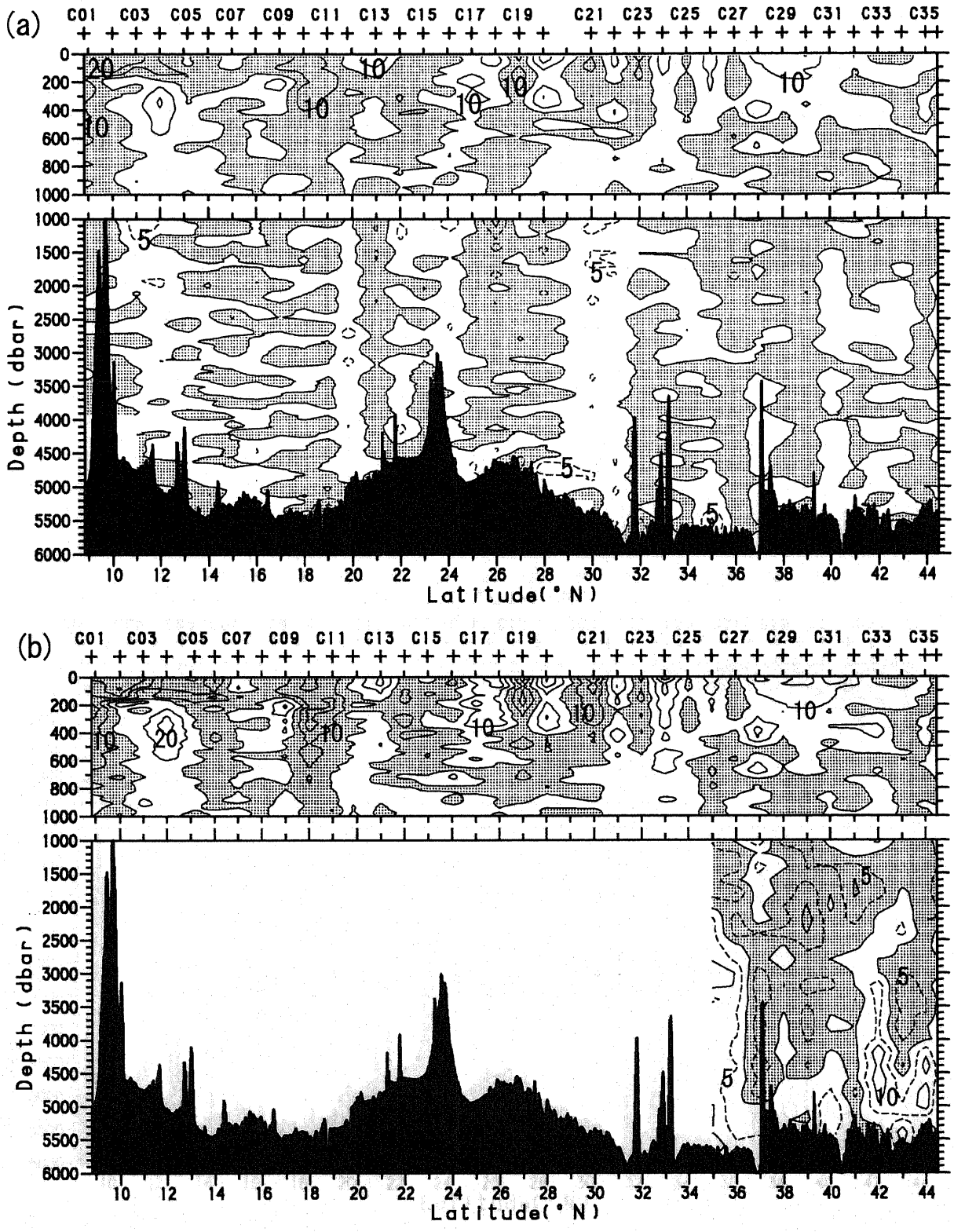

Fig. 2.11: Sections of zonal velocity (cm s^{-1}) at 165°W calculated with the method of Visbeck (2002) (a) and the present method (b). Shade shows westward velocity. The barotropic tidal velocity estimated with the tide model of Egbert (1994) was removed. Contour interval of solid lines is 10 cm s^{-1}. Broken lines show the velocity of 5 cm s^{-1}. The velocity at depth greater than 1000 dbar in (b) is shown only for the stations at which echo intensity exceeds 75 dB at full depth, where the present method of the correction for velocity shear is valid.

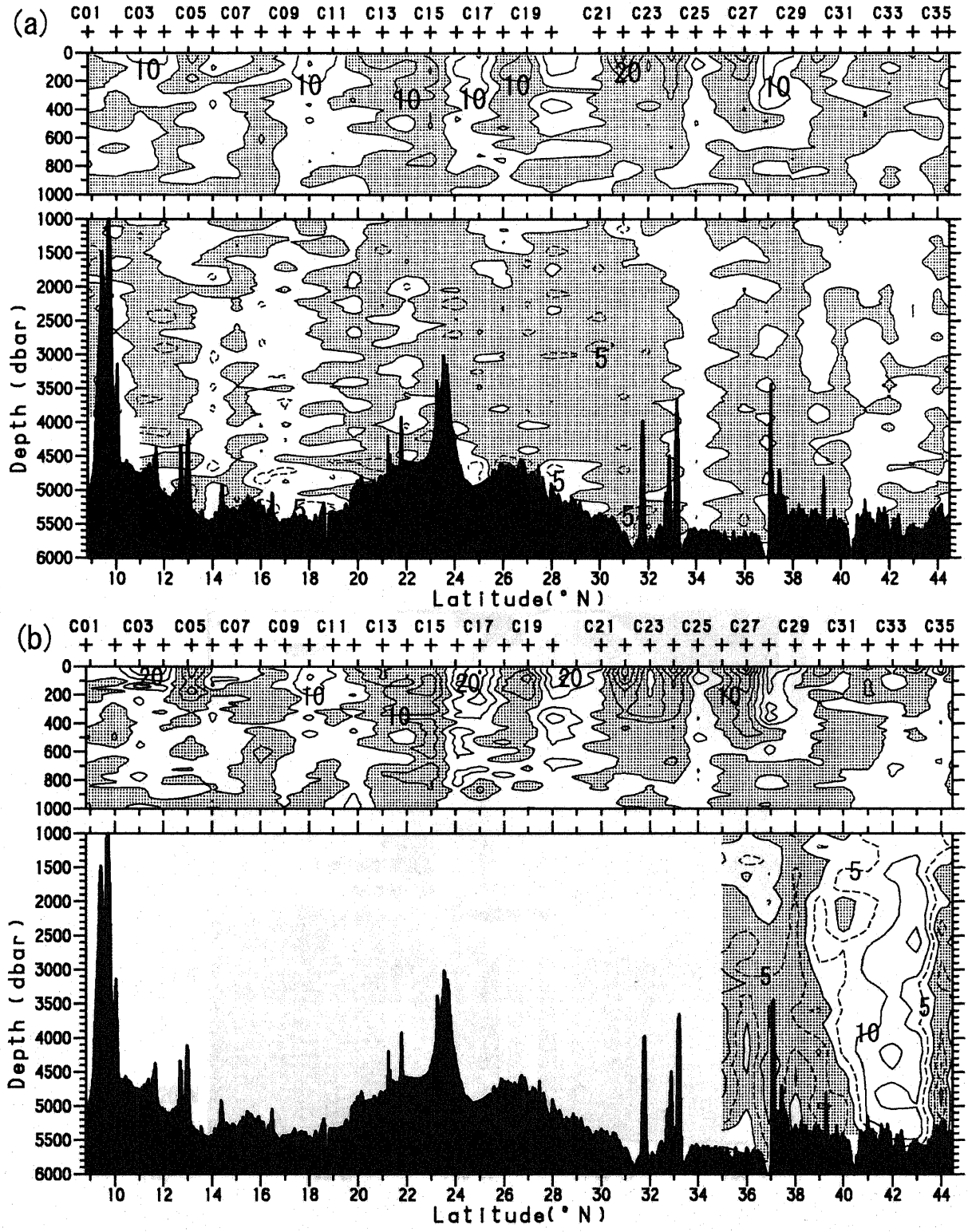

Fig. 2.12: Same as Fig. 11 but for the meridional velocity (cm s^{-1}). Shade shows southward velocity.

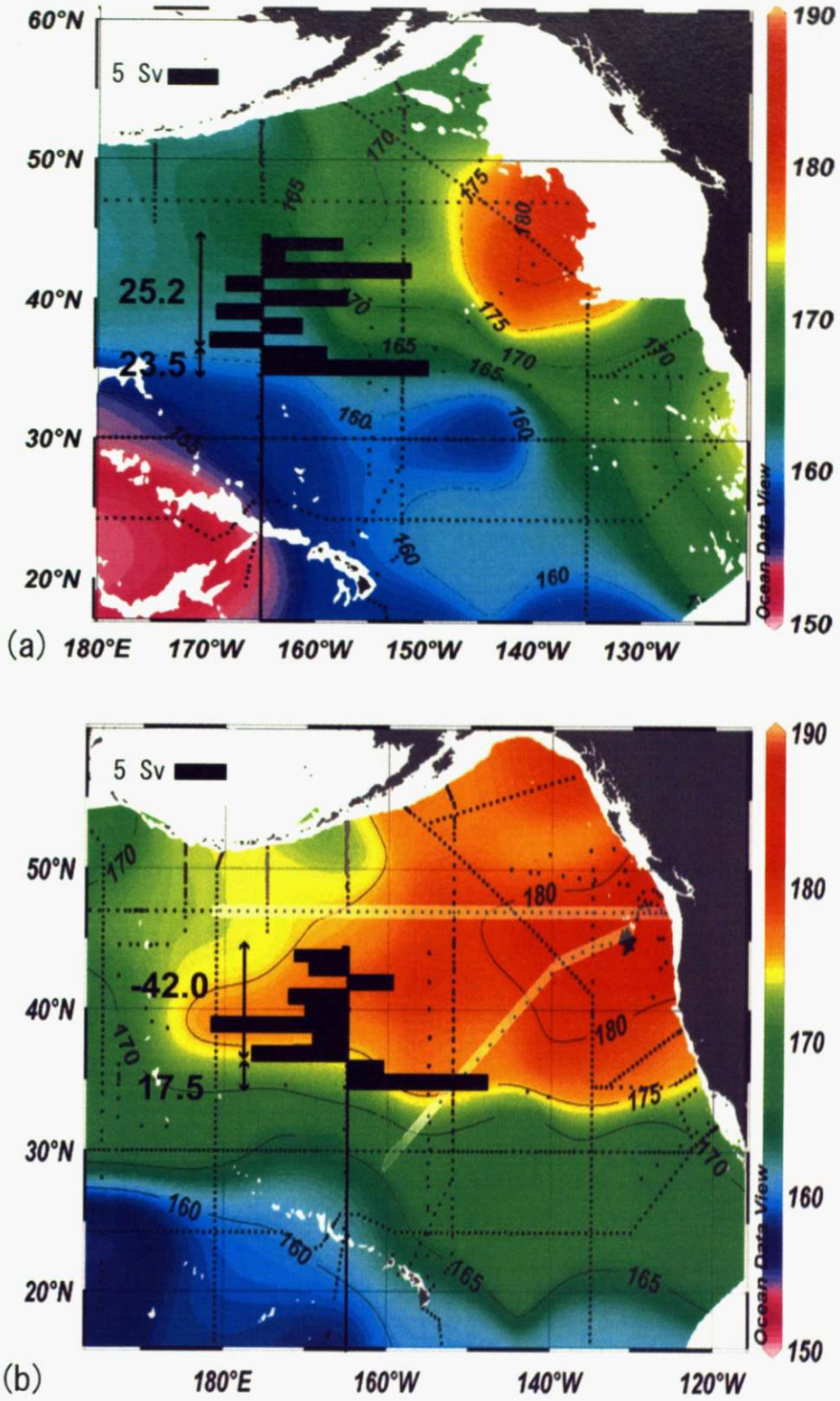

Fig. 2.13: Zonal volume transport in the lower deep layer of $\theta < 1.2°C$ (a) and the upper deep layer of $1.2° < \theta < 2.0°C$ (b) calculated with the present method (black bars). Numbers on the left side of the bars show values of the integrated transport in a range of arrows. Background colors show the lateral distributions of silicate (μ mol L^{-1}) at depths of 4000 m (a) and 2300 m (b), which were reproduced from Johnson et al. (2006). Small dots show the stations of silicate observation.

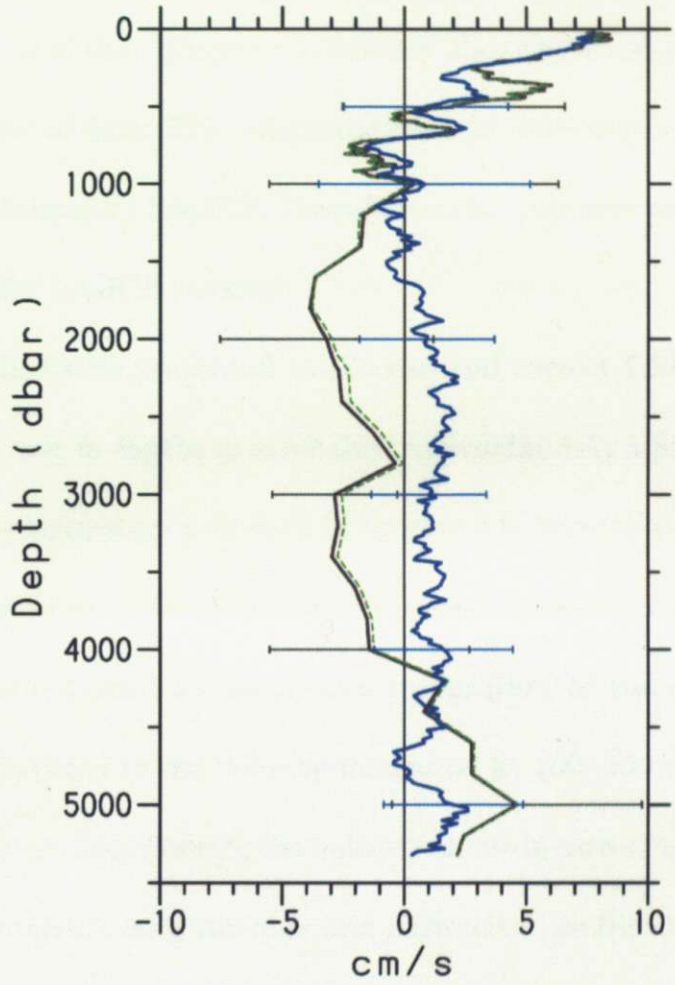

Fig. 2.14: Vertical profiles of zonal velocity (cm s^{-1}) averaged at 36.5°–44.5°N (C28–C36) calculated with the present method (black), the present method but using SADCP velocity in a layer of 100–300 dbar (green broken), and the method of Visbeck (2002) (blue). Horizontal bars represent standard deviations of the zonal velocities at 9 stations (C28-C36) calculated with the present method (black bars) and the method of Visbeck (2002) (blue bars) at 500, 1000, 2000, 3000, 4000 and 5000 dbar depths.

2.6. Conclusions

Using full-depth LADCP data obtained at 8°50′–44°30′N along 165°W, it was shown that the echo intensity of a reflected sound pulse except at near surface is highly correlated with the number of vertical shear of velocity calculated in every 5 m-depth cell, as well as with the magnitude of the difference in velocity shear between downcast and upcast, which indicates reliability of data. This suggests that echo intensity is an indicator of the error of velocity shear obtained by LADCP. Therefore, echo intensity was taken into consideration in the correction for LADCP velocity.

A new method was presented to process and correct LADCP velocity data obtained from a full-depth cast to depths greater than approximately 1000 m. First, low-quality data are rejected by the procedure proposed in Section 2.2. Second, vertical shears of velocity are calculated with velocity data obtained from one transmitted sound pulse, and a relative velocity profile is obtained by successive integration of the velocity shears. Third, the relative velocity is fitted to the velocity measured at 100–800 dbar by SADCP to make an "absolute" velocity profile. Fourth, the velocity shear is corrected with Equations (1) and (3), which use echo intensity as a variable and parameter, so that the velocity at sea bottom is adjusted to the bottom-tracked velocity. Concretely, k in Equation (1) is determined by Equation (3), the correction for velocity shear is given by Equation (1) using the determined value of k, and the velocity shear is obtained by adding the correction to the measured velocity shear. The final velocity profile is obtained from the SADCP-fitted velocity obtained at depths less than 800 dbar, and the corrected velocity shear at depths greater than 800 dbar.

The present correction for velocity shears changes an overall tilt of vertical profile of velocity without largely altering small-scale vertical variations. This method is valid for an

LADCP cast down to near-bottom in which the echo intensity is high at full depths (greater than 75 dB in the present study). Due to this limitation of echo intensity, it may not be valid for subtropics. This implies that an LADCP must be improved to obtain higher echo intensity for velocity measurement in subtropics. The present method, however, gives qualitatively good results for subarctic area so as to produce organized deep current structures that are consistent with the flow pattern inferred from silicate distribution, although the amplitude of current velocity may include errors of 1–2 cm s^{-1}. The deep current velocities averaged at 36.5°–44.5°N are significantly different from those calculated by the method of Visbeck (2002).

Lastly, we mention the use of SADCP data. SADCP data at depths of 100–800 dbar were used in the present study, but those in such a thick layer are not always necessary for obtaining the "absolute" velocity of LADCP. Similar velocities averaged at 36.5°–44.5°N are obtained by fitting to the SADCP data at depths of 100–300 dbar (Fig. 2.14), although the velocities at each station are different by a few cm s^{-1}. SADCPs equipped at many vessels measure velocity at depths less than 300 or 500 m, and the measurements do not reach a depth of 800 m. However, they are also useful for the present data process of LADCP.

Chapter 3

Spatial properties, relation to zooplankton and particles, and application to water-mass analysis of echo intensity measured by LADCP

3.1. Introduction

An acoustic instrument discharging a sound pulse measures an intensity of sound pulse reflected by scatterers. An echo sounder and a fish finder with frequency 10–200 kHz detect sea bottom and a school of fish from strength of echo intensity, respectively. Strengths of echo intensity of sound pulse with higher frequency 500–3000 and 200–3000 kHz are correlated with the number of 0.1–5 mm zooplankton per unit mass (Holliday and Pieper, 1980) and the concentration of suspended sediment less than 0.1 mm (Braithwaite, 1974; Young et al., 1982; Vincent et al., 1982; Hey, 1983), respectively. Echo intensity from an acoustic Doppler current profiler (ADCP) with frequency 75–1200 kHz is useful to observe zooplankton in surface water (Heywood et al., 1991; Ashjian et al., 1994; Ashjian et al., 1998; Liljebladh and Thomasson, 2001); for instance, the vertical migration of zooplankton was found from diurnal changes in vertical distribution of echo intensity observed by a mooring ADCP (Kaneko et al., 1996). Thus, echo intensities of transmitted sound pulses with different frequencies have been used for various purposes.

A lowered acoustic Doppler current profiler (LADCP) with frequency 150 or 300 kHz measures echo intensity during its cast and obtains vertical profiles of echo intensity. The profiles show that the echo intensity is high at near-surface and weakens sharply to a depth of approximately 1000 m (Chapter 2; Fischer and Visbeck, 1993; Wijffels et al., 1998). The echo intensity in the North Pacific is relatively strong in equatorial and subarctic regions and weak in between for the North Pacific (Firing, 1998). It was considered that the spatial distributions at near-surface were due to those of zooplankton (White et al., 1995; O'Brien et al., 2002) and sinking and suspended particles (Honjo, 1995; Kawahata, 2002). Thus, the basic field of echo

intensity seems to be determined by the distribution of zooplankton and particles in water.

Echo intensity, moreover, shows deviations from the basic field significantly. What do the deviations of echo intensity indicate? They may partly be due to the difference in amount of zooplankton and particle involved in water masses, because water masses formed in different conditions at near-surface must have different concentrations of the scatterers of sound pulse originally. If this is true, we may be able to use echo intensity for water-mass analysis. In the present chapter, I investigate the spatial properties of echo intensity measured by LADCP, discuss the causes for the basic field of echo intensity and the deviations from that, and examine an application of echo intensity to water-mass analysis.

3.2. Observations and data

We cast the 300-kHz LADCP manufactured by RD Instruments at 221 stations in the North Pacific (2°00′N-44°30′N, 140°E-165°W) on the R. V. Hakuho Maru cruises of KH-99-1, KH-03-1, and KH-04-4 (Fig. 3.1). The major three lines are named 18.3°N line, Melanesian line and 165°W line. Although the bin of sound reflection were set in a different way by cruise, echo intensity reflected from 12 m below the LADCP instrument was commonly measured at the third bin on the KH-99-1 and KH-03-1 cruises and the first bin on the KH-04-4 cruise, and is used in this chapter. Echo intensity data were transformed into the value relative to the backscattering intensity using the conversion equation provided by RD Instruments (1996), and the transformed value is called echo intensity in the present study.

The strength of echo intensity is highly correlated with the maximum distance from the LADCP instrument, in which LADCP obtains reflected sound pulses significantly, and is accordingly correlated with the data number of velocity shear (Chapter 2). This correlation is found for all cruises, but the relation of the maximum distance of sound reflection with echo intensity is different by cruise (Fig. 3.2). The curves of the maximum distance of sound reflection in KH-03-1 leg1 and KH-99-1 almost coincides with that in KH-03-1 leg2 if the echo intensity increases by approximately 4 dB. The corrected curves in KH-03-1 leg 1 and KH-99-1 are used for comparing echo intensities among the cruises. Echo intensity in KH-04-4 is also adjusted to that in KH-03-1 leg 2 separating into some groups, because echo intensity weakened during the cruises as time elapsed during the cruise, perhaps due to a trouble of the instrument.

On the KH-05-4 cruise, we sampled zooplankton in a layer of 0-3000 dbar at three

stations of LADCP (A-C) at 38°N east of Japan in December 2005, using the Vertical Multiple Plankton Sampler (VMPS) with mesh size of 0.33 mm and mouth opening of 0.25 m^2 (Fig. 3.1; Table 3.1). A each station, VMPS was cast once in a layer less than 800 dbar and three times in a deeper layer. The sampled zooplankton was divided into two groups of size, 0.33-1 and 1-4 mm, and wet weight of the biomass was measured for each group.

Moreover, I used data of concentration of particulate organic carbon (POC) measured by water sampling at 0°-48°N on 175°E in August-September 1993 and April-May 1994 (Fig. 3.1), under the project of the Northwest Pacific Carbon Cycle Study (NOPACCS) (NEDO, 1993, 1995).

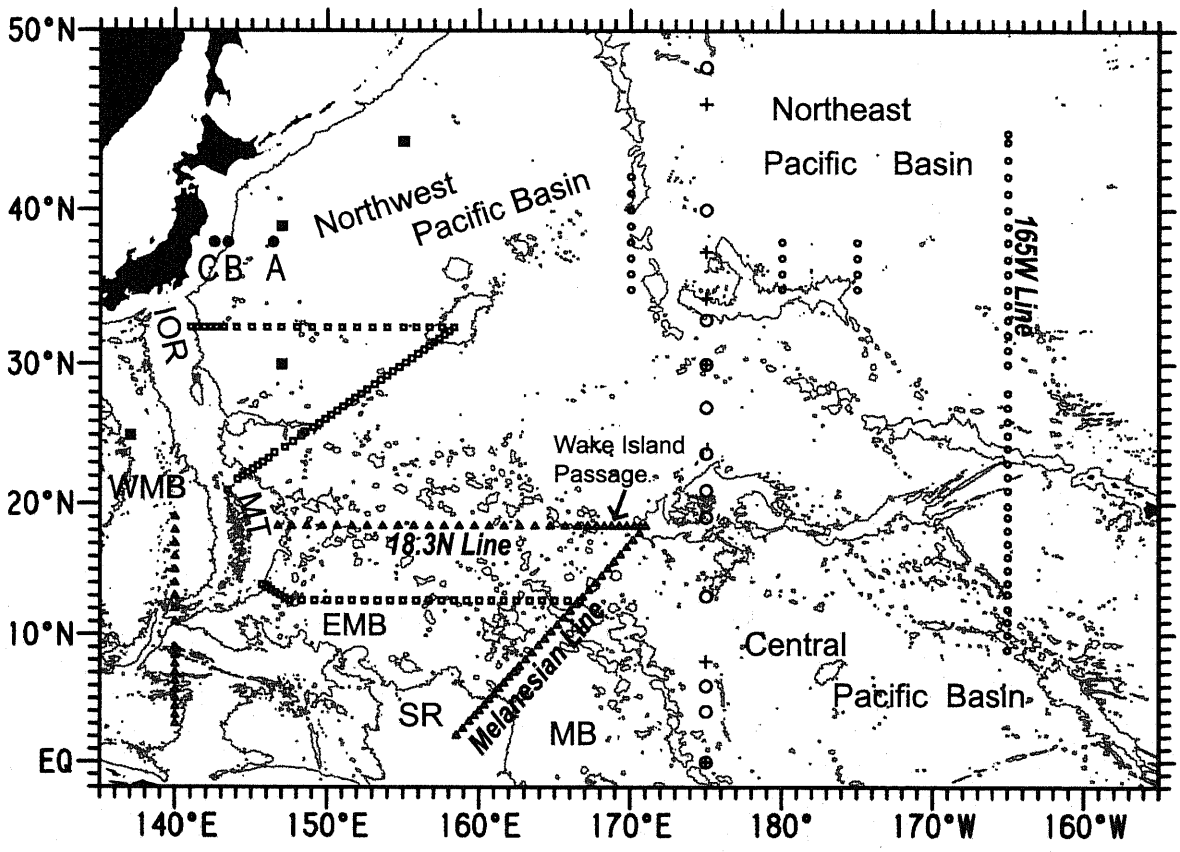

Fig. 3.1: LADCP stations in the North Pacific in *Hakuho-Maru* cruises KH-99-1 (triangles), KH-03-1(small circles) and KH-04-4 (open squares), LADCP/VMPS stations A-C in *Hakuho-Maru* cruise KH-05-4 (dots), VMPS stations sited from Yamaguchi et al. (2004) (solid squares), stations of sediment trap for sinking particles sited from Kawahata (2002) (pluses), and stations of water sampling for POC (large open circles). Solid lines indicate 4000 m isobaths. MB, Melanesian Basin; SR, Solomon Rise; MT, Mariana Trench; EMB, East Mariana Basin; WMB, West Mariana Basin; IOR, Izu-Ogasawara Ridge.

(a)

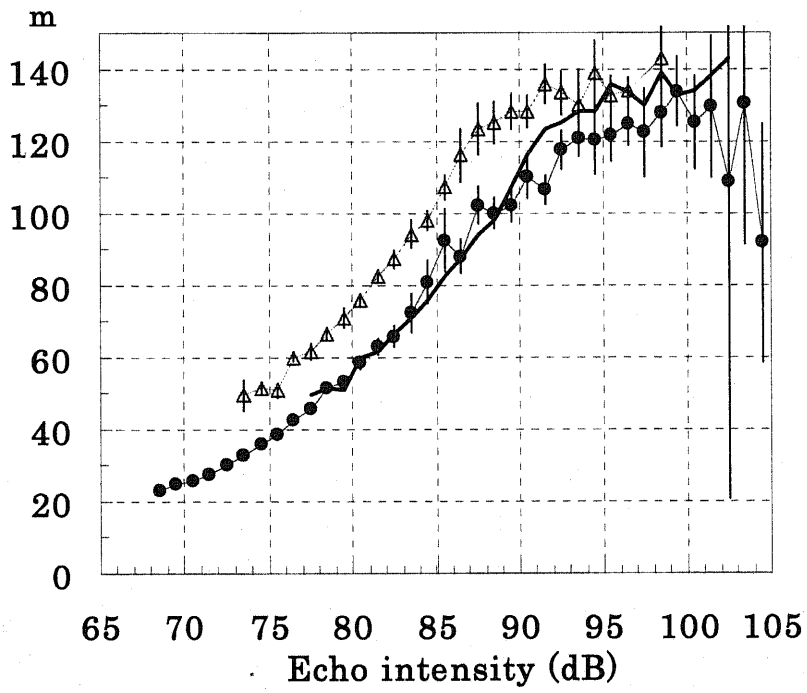

(b)

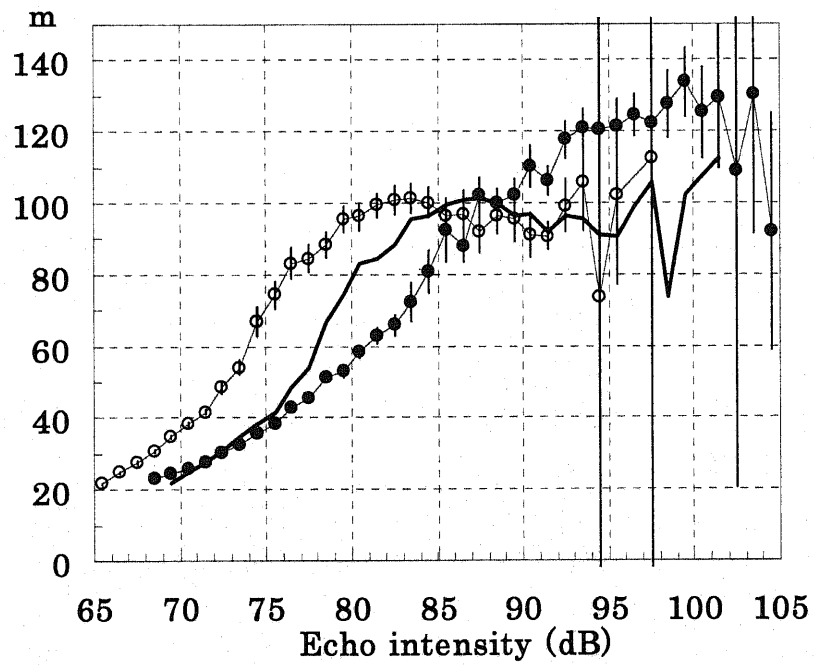

Fig. 3.2: Maximum distance of sound reflection with respect to echo intensity (dB) in KH-03-1 leg1 (triangles) (a) and KH-99-1 (open circles) (b), together with that in KH-03-1 leg2 (dots). Solid lines indicate the curves corrected for echo intensities to adjust to the curve in KH-03-1 leg2.

Table 3.1: Sampling layers of zooplankton observation and the biomass (mg Wet Weight m^{-3}) of smaller than1 mm and 1-4 mm zooplankton at stations A, B, and C during daytime and nighttime off the Sanriku coast of Japan in December 2005 on the KH-05-4 cruise, using the Vertical Multiple Plankton Sampler (VMPS) of 0.33 mm mesh size and 0.25 m^2 mouth opening. Averages of echo intensity at a sampling layer are shown in parentheses.

Sampling layer (dbar)	Station			
	A	B	C(day)	C(night)
< 1mm Biomass (Echo intensity)				
0 — 100	17.44 (113)	4.28 (104)	4.16 (103)	10.84 (111)
100 — 200	3.96 (105)	3.92 (102)	5.16 (109)	7.08 (109)
200 — 300	2.68 (97)	7.44 (104)	10.36 (111)	7.44 (111)
300 — 400	4.44 (103)	7.68 (100)	7.60 (105)	7.04 (107)
400 — 600	3.48 (97)	3.24 (103)	3.58 (100)	4.94 (102)
600 — 800	1.46 (95)	3.17 (99)	2.40 (98)	2.18 (97)
800 — 1000	2.64 (93)	3.49 (97)	- (97)	- (97)
1000 — 2000	0.91 (92)	1.68 (95)	- -	- -
2000 — 3000	0.23 (88)	1.67 (96)	- -	- -
0-800dbar mean	4.80 (100)	4.52 (101)	4.91 (103)	5.83 (104)
1-4mm Biomass (Echo intensity)				
0 — 100	34.16 (113)	8.40 (104)	7.76 (103)	15.08 (111)
100 — 200	12.08 (105)	5.44 (102)	9.76 (109)	14.64 (109)
200 — 300	6.72 (97)	11.68 (104)	10.08 (111)	19.28 (111)
300 — 400	15.20 (103)	36.44 (100)	22.88 (105)	35.88 (107)
400 — 600	12.30 (97)	108.42 (103)	32.10 (100)	39.24 (102)
600 — 800	12.94 (95)	19.36 (99)	20.84 (98)	25.94 (97)
800 — 1000	10.92 (93)	26.90 (97)	- (97)	- (97)
1000 — 2000	8.44 (92)	11.67 (95)	- -	- -
2000 — 3000	3.89 (88)	34.34 (96)	- -	- -
0-800dbar mean	14.83 (100)	39.69 (101)	19.55 (103)	26.91 (104)

3.3. Contributions of sound scatterers to echo intensity

Echo intensity observed at 15°–42°N in the western North Pacific has sharp maxima at two vertical positions at sea surface and approximately 500 dbar, and decreases downward exponentially below a depth of 500 dbar (Fig. 3.3a). This property of vertical profile of echo intensity is common for all latitudes. However, magnitudes of echo intensity and its vertical changes are different among the southern and northern subtropics and the subarctic region. At every depth, echo intensity increases from southern to northern subtropics and further to the subarctic region. In particular below a depth of 1000 dbar, the subarctic echo intensity is markedly larger than the subtropical echo intensities, as the subarctic decrease below a depth of 500 dbar is relatively small. Moreover, subarctic echo intensity has a tiny maximum around 2000 db and decreases significantly from that to approximately 2500 dbar. In a deep layer below 3000 dbar, subarctic echo intensity is much larger by nearly 10 dB than the subtropical echo intensities, whereas the difference between southern and northern subtropics is small.

Such characteristics of echo intensity must reflect the concentration of scatterers in water such as zooplankton and material particles. It is showed that zooplankton biomass in subarctic region is much larger at depths less than 3000 m than that in subtropics, whereas the difference between subarctic and subtropical regions is small at depths greater than 3000 m (Fig. 3.3b). Moreover, zooplankton biomass has maximum and minimum at depths less than 1000 m (Yamaguchi et al., 2004). These correspond to the larger magnitude of subarctic echo intensity and the existence of maximum and minimum in surface and subsurface layers of echo intensity, but not to larger subarctic echo intensity at depths greater than 3000 m.

Total fluxes of sinking particles show two distinct properties (Fig. 3.3c). One is that the amount of sinking particles is little different between depths of 1500 and 4500 m. This suggests that the flux is almost constant from near-surface to sea bottom. This is because the sinking speed, being approximately 200 m day^{-1} (Kawahata et al., 1998), is so large that material particles do not significantly resolve during the fall to sea bottom. The other is that the amount of sinking particles increases northward from tropical to subarctic regions, although the amount on equator is larger than that in tropics and similar to that in subtropics. This corresponds well to the meridional variations of echo intensity, although this cannot be a cause for small-scale vertical variations of echo intensity such as maximum and minimum above a depth of 1000 m.

Concentration of particulate organic carbon (POC) from suspended particles is large at sea surface and decreases downward markedly at near-surface (Fig. 3.3d). The concentration is not different between tropics, subtropics, and the subarctic region, except at depths of 0-800 m. This does not correspond to the meridional difference of echo intensity. The suspended particles with sizes less than approximately 2 μm may be too small to reflect sound pulses, although they do not yet lose a possibility that the large amount near sea surface contributes to the formation of maximum of echo intensity at sea surface.

Figure 3.3 gives the following suggestions. Sinking particles contribute to echo intensity at full depth uniformly. The contribution of sinking particles may be predominant at depths greater than 3000 m. Echo intensity at depths less than 3000 m is contributed by not only sinking particles but also zooplankton significantly. The contribution of zooplankton may increase as the depth decreases.

The contribution of zooplankton to echo intensity should be examined by observing them at the same time. We obtained data of zooplankton biomass and echo intensity at three stations A, B, and C in relatively small area of the mixed-water region east of Japan between the Kuroshio and Oyashio fronts. The data show two properties that the total biomass is markedly different between small (< 1 mm) and large (1–4 mm) zooplanktons, and that the biomass has remarkable maximums and minimums at each cast (Table 3.1).

The former property is clearly shown by the mean values of zooplankton biomass at depths of 0–800 dbar. The mean values during the daytime at station A, B, and C are 4.8, 4.5, and 4.9 mg WW m^{-3} for small zooplankton (< 1 mm) and 15, 40, and 20 mg WW m^{-3} for large zooplankton (1–4 mm), respectively. Thus, the biomass of small zooplankton is spatially uniform, whereas that of large zooplankton is much larger and spatially variable. The mean echo intensity at depths of 0–800 dbar during the daytime is 100, 102, and 103 dB at A, B, and C, respectively. The spatial difference in echo intensity is small, and its tendency is different from that of biomass of large zooplankton. This suggests that echo intensity is related to small zooplankton. Zooplankton biomass at 0–800 dbar increases from daytime to nighttime due to the migration of zooplankton from depths greater than 800 dbar. The increasing rate is 1.19 for small zooplankton (from 4.9 to 5.8 mg WW m^{-3}) and 1.38 for large zooplankton (from 20 to 27 mg WW m^{-3}), and is much larger for large zooplankton. Echo intensity, however, increases only a little from 103 to 104 dB. This also suggests less contribution of large zooplankton to echo intensity.

The latter property, namely maximums and minimums of the biomass in a vertical profile, is well correlated with echo intensity, although the correlation is

different by station and by size of zooplankton. At station A, the biomass is maximum at 0–100 and 300–400 dbar and minimum at 200–300 dbar for both small and large zooplanktons. This is highly correlated with the maximums and the minimum of echo intensity. Small zooplankton has another maximum at 800–1000 dbar, and large zooplankton has a slight maximum at 600–800 dbar. These are not correlated with echo intensity. These maximums disappear for the total biomass of small and large zooplanktons, and the total biomass may be effective for echo intensity.

At station B, echo intensity has small maximums at 0–100, 200–300, and 400–600 dbar and slight maximum at 2000–3000 dbar. The maximum at 0–100 dbar corresponds to the maximums of both small and large zooplanktons. The maximum at 200–300 dbar may correspond to the maximum band at 200–400 dbar of small zooplankton, although the correspondence of depth is not so good. The maximum at 400–600 dbar corresponds to the huge maximum of large zooplankton, and that at 2000–3000 dbar also to large zooplankton. The maximums at 800–1000 dbar of both small and large zooplanktons are not correlated with echo intensity.

The results at A and B show that the maximums of echo intensity at depths less than 600 dbar are correlated with both or either of small and large zooplanktons, although the maximums of zooplankton at 600–1000 dbar are not correlated with echo intensity, and suggest a possibility of contribution of large zooplankton to the maximum of echo intensity at 2000–3000 dbar.

At station C, biomass of small zooplankton is highly correlated with echo intensity. The maximums at 200–300 dbar during the daytime and at 0–100 and 200–300 dbar during the nighttime correspond well to those of echo intensity. On the other hand, biomass of large zooplankton is maximum markedly at 400–600 dbar

during both the daytime and nighttime and slightly at 0–100 dbar during the nighttime. The remarkable maximums at 400–600 dbar are not correlated with echo intensity at all. The results at C strongly suggest large contribution of small zooplankton to echo intensity in the layer of 0–600 dbar. It should be noticed that echo intensity at near-surface is markedly different between the daytime and the nighttime. The temporal variations at near-surface of echo intensity may not be explained by suspended particles, because their amount must not significantly change between the daytime and the nighttime. Moreover, it should be noted that the crowded depth of zooplankton in the layer of 0-800 dbar shifts upward from the daytime to the nighttime, due to the migration of both small and large zooplanktons.

Integrating the results at A, B, and C, it is concluded that the biomass of small zooplankton primarily contributes to maximums and minimums of echo intensity at depths of 0–600 dbar, whereas the biomass of large zooplankton partly contributes, like the maximum at 400–600 dbar at B, and partly strengthens the contribution of small zooplankton, like the maximums at A.

This conclusion may be strange. Theoretically, echo intensity of 300-kHz sound waves with wavelength of approximately 5 mm is large commonly for scatterers with sizes larger than 1 mm, and decreases gradually as the size of scatterer decreases (Holliday and Piper, 1980). Therefore, echo intensity reflected by large zooplankton with size of 1–4 mm must be stronger than that by small zooplankton. Moreover, large zooplankton is much more abundant in weight at the stations. Why is the contribution of small zooplankton to echo intensity more primary than that of large zooplankton? This may be related to a difference in a style of living in water, forming patches of zooplankton or not. The current conclusion may imply that small zooplankton forms

patches which are effective for scattering sound pulses. Another possibility is that the volume of small zooplankton is larger than that of large zooplankton due to a difference in density of the body, although the biomass weight of small zooplankton is much less than that of large plankton.

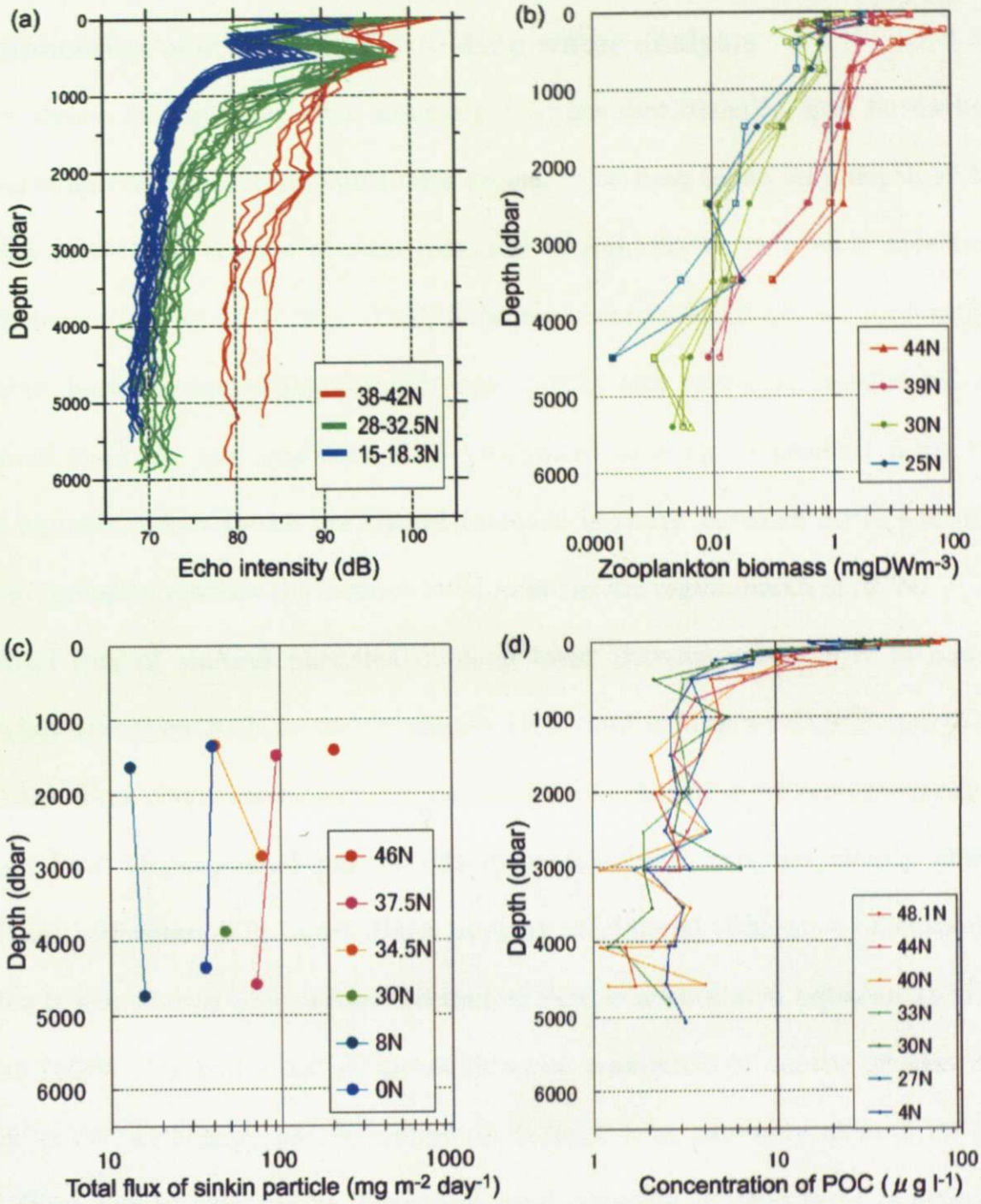

Fig. 3.3: Latitudinal differences of vertical profile in the western North Pacific, (a) echo intensity at 15°-18.3°N (blue, 166°-170°E), 28°-32.5°N (green, 152°-157°E) and 38°-42°N (red, 170°E), (b) zooplankton biomass at 137°-155°E (solid squares in Fig. 1), (c) flux of sinking particles mostly at depths of approximately 1500 m and 4500 m along 175°E (pluses in Fig. 1), and (d) suspended particles along 175°E (large open circles in Fig. 1). The data of zooplankton biomass, sinking particle flux and concentration of POC are sited from Yamaguchi et al. (2004), Kawahata (2002) and NEDO (1993, 1995), respectively.

3.4. Application of echo intensity to deep water analysis

As shown in Fig. 3.3a, echo intensity changes meridionally, and is markedly larger in subarctic region than subtropics especially in deep layer. At a depth of 3000 dbar, the meridional change of echo intensity is remarkable in a wide meridional range between 2° and 45°N (Fig. 3.4a). Echo intensity is small almost uniformly in subtropics between approximately 12° and 30°N, and increases southward and northward from the low intensity. The southward increase is gradual from 12°N toward equator, whereas the northward increase is sharp between 30°N and 35°N, and echo intensity reaches the highest level in subarctic region north of 35°N.

Total flux of sinking particles in deep layer increases from 8°N to equator moderately and from 30°N to 34.5°N significantly, and is large at 34.5°N and 37.5°N (Fig. 3.4b). This corresponds well to the meridional variation of echo intensity. In contrast, POC of suspended particles is dispersive, and does not clearly show a meridional difference (Fig. 3.4c). Such unclear meridional difference of suspended particles is also shown in a vertical section of POC concentration between 15°S and 55°N at 155°W (Ichikawa, 1975), although weak maximum at depths greater than 1000 m at 35°-45°N may partly contribute to high echo intensity around 39°N at 165°W (Fig. 2.4a in Chapter 2). Therefore, echo intensity in deep layer is primarily due to sinking particles.

We should noticed that echo intensity deviates in a range of approximately 5 dB from the average at each latitude (Fig. 3.4a). The deviation of echo intensity may be due to concentration of the scatterers which are included in the water masses carried by the deep currents. At the 18.3°N and Melanesian lines, the Lower Circumpolar Water (LCPW) is carried northward by the deep western boundary current in the

lower deep layer at depths greater than 3500 m. In the deep layer at the 18.3°N line, echo intensity ranges within 5 dB and has two minimums reaching nearly 68 dB at 147°-152°E and 154°-159°E in the East Mariana Basin (Figs. 3.5a and 3.6a). These minimums correspond to the maximums of dissolved oxygen which show the pathways of LCPW due to the western branch current of the deep circulation concluded by Kawabe et al. (2003). The minimum of echo intensity having relatively high value at 160°-162°E, corresponding to relatively low oxygen maximum, may show that water mixed with LCPW exists at 18.3°N, 160°-162°E.

In the southwestern part of the Melanesian line (2°-9°E, 159°-163°E), echo intensity in deep layer increases slightly southwestward due to the meridional variation (southward gradual increase) of echo intensity indicated in Fig. 3.4a, but markedly reaches minimums at 161°E, 161.6°-162°E, and 162.7°E, corresponding clearly to the maximums of dissolved oxygen which show the pathways of the western branch current carrying LCPW (Kawabe et al., 2003) (Figs. 3.5b and 3.6b).

Therefore, low echo intensity characterizes LCPW together with high oxygen, low temperature, high salinity, and low nutrients. Echo intensity can be used as a parameter for analysis of water masses such as LCPW.

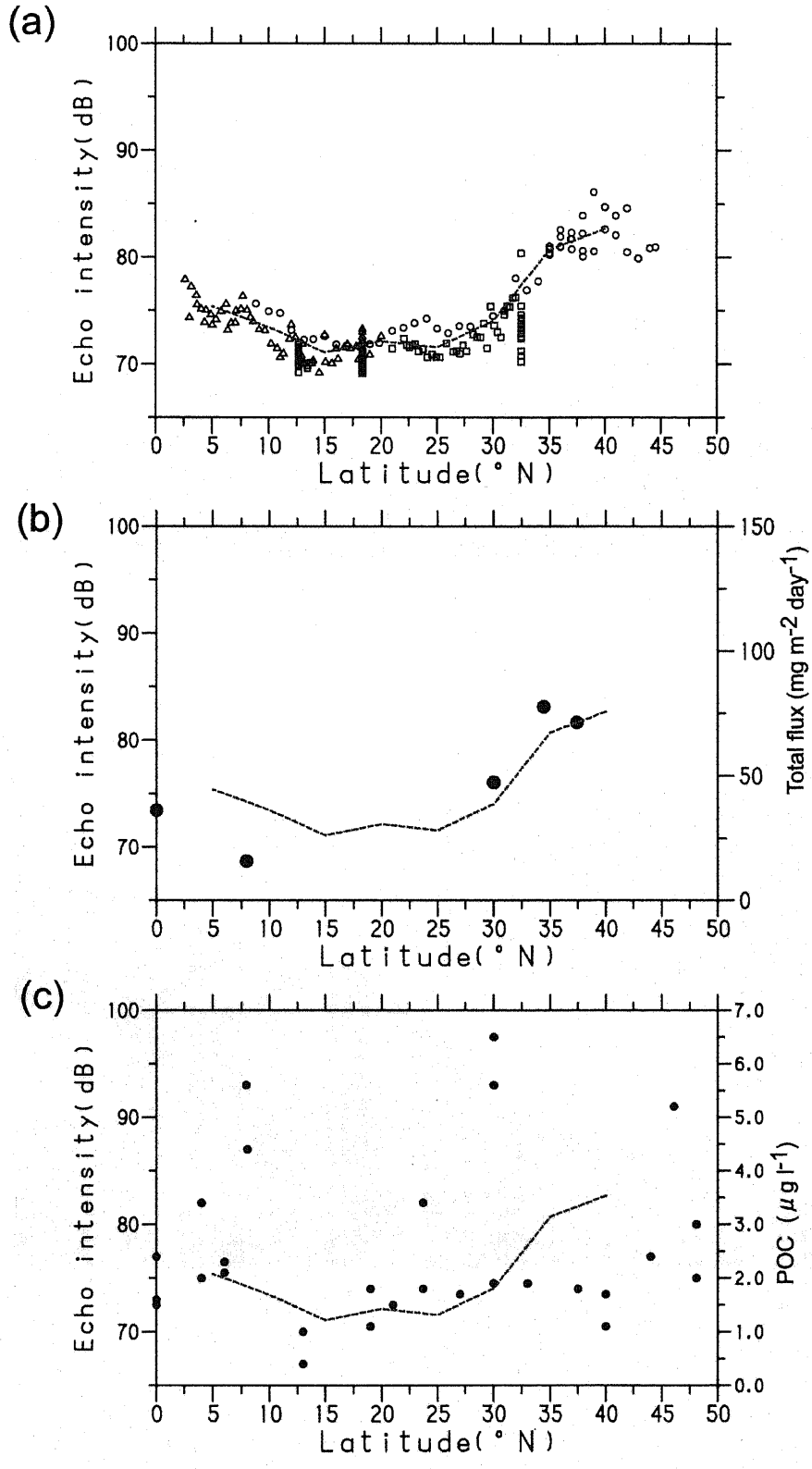

Fig. 3.4: Latitudinal distributions of (a) echo intensity averaged at depths of 2750-3250 dbar at all stations in *Hakuho-maru* KH-99-1, KH-03-1 and KH-04-4 cruises, (b) total flux of sinking particle at depths of 2848-4743 m on 175°E, and (c) POC concentration at depths of 3050 m on 175°E. Broken line indicates echo intensity which is averaged at 5°N intervals. The total fluxes in (b) are cited from Kawahata (2002).

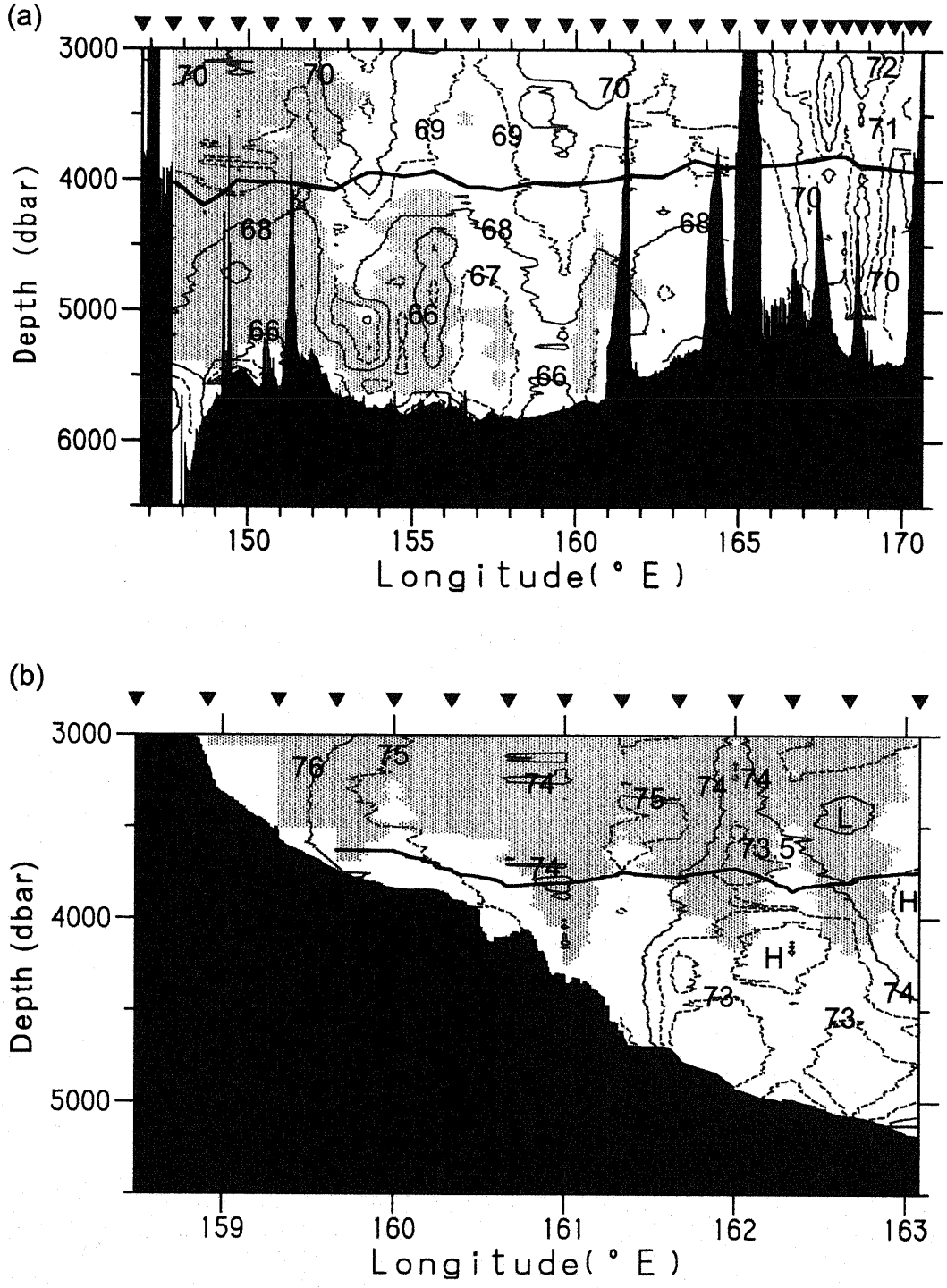

Fig. 3.5: Vertical distribution on the (a) 18.3°N line and (b) Melanesian line of echo intensity (dB) and dissolved oxygen anomaly (ml l^{-1}) on the potential density surfaces from averages at 4 stations (163°-164.3°E) on the MEL line. Shade shows oxygen anomaly of higher than (a) -0.025, and (b) 0.025. Thick line indicates the potential density surface of $\sigma 4 = 45.865$.

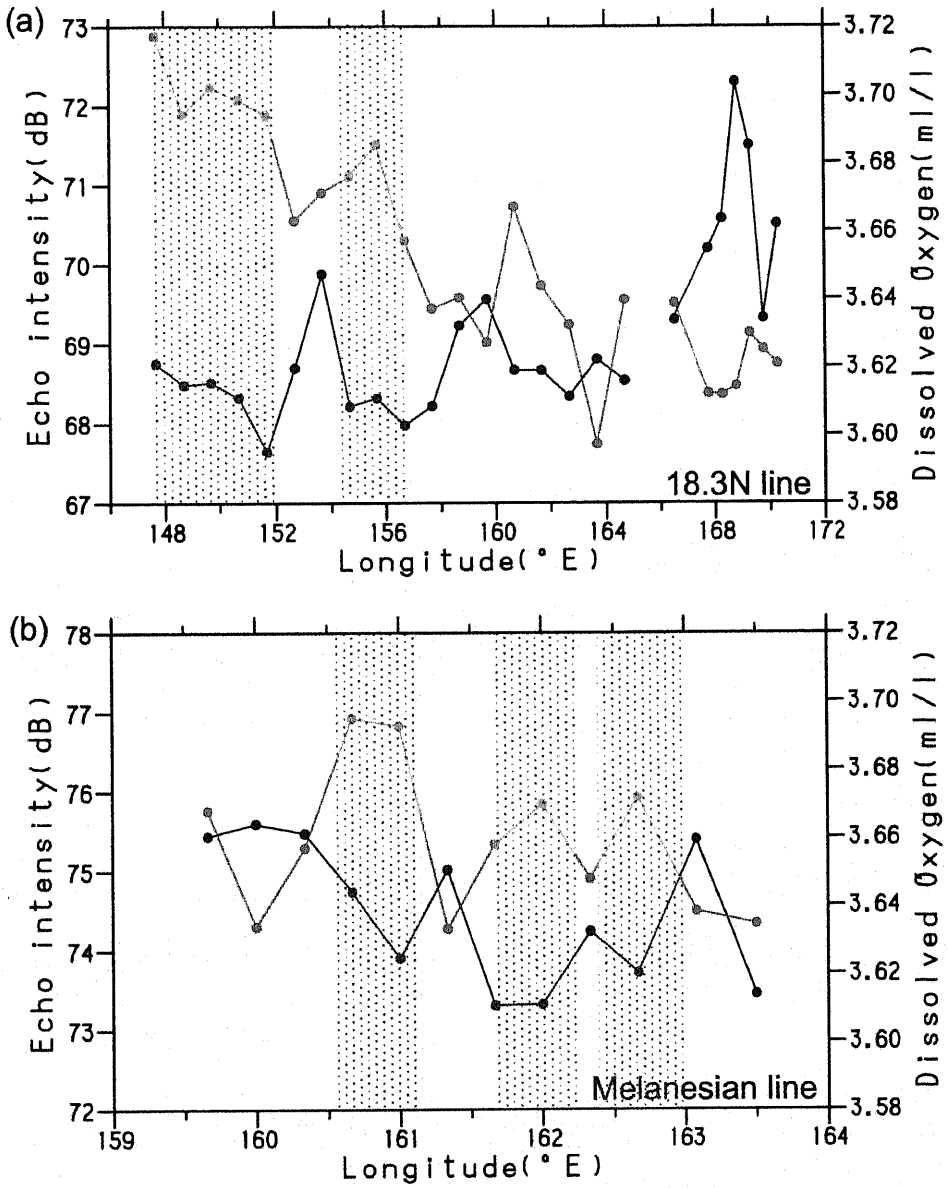

Fig. 3.6: Longitudinal distributions of echo intensity (black) and dissolved oxygen (grey) averaged in a layer of densities between $45.865\sigma_4$ and $45.880\sigma_4$ (4000-4500 m), at the 18.3°N line (a) and between $45.865\sigma_4$ and $45.868\sigma_4$ (3700-3800 m) at the Melanesian line (b). Shading indicates the pathways of the western branch current of the deep circulation carrying LCPW concluded by Kawabe et al. (2003).

3.5. Conclusions

Echo intensity measured with an LADCP in the North Pacific shows remarkable meridional variations particularly in deep layer at depth greater than 3000 m, that echo intensity is uniformly small in subtropics between 12° and 30°N, and increases southward gradually and northward sharply from 30°N to 35°N, reaching the highest level of echo intensity in subarctic region north of 35°N. The present study concluded that the meridional variations of echo intensity in the deep layer are primarily due to the meridional difference in amount of sinking particles, and that the deviation from the average at each latitude, which ranges in approximately 5 dB, is due to the characteristics in echo intensity of inflowing water masses such as LCPW.

LCPW is markedly characterized by low echo intensity, like low temperature, high salinity, high oxygen, and low nutrients. Therefore, a marked minimum of echo intensity corresponding to maximum of dissolved oxygen shows a pathway of the deep circulation current carrying LCPW. Echo intensity is a useful parameter for analysis of water masses such as LCPW.

Moreover, the present study concluded that a contribution of zooplankton to echo intensity increases as a depth decreases from 3000 dbar, and that echo intensity at depth less than 800 dbar is mainly due to zooplankton, in particular small zooplankton with size of less than 1 mm.

Chapter 4

Pathways and structure of deep currents in the North Pacific

4.1. Introduction

In the deep layer at depths of greater than 3500 m in the North Pacific, hereafter termed the lower deep layer, the Lower Circumpolar Water (LCPW) is carried by the deep western boundary current (DWBC) separating from the Antarctic Circumpolar Current (ACC). DWBC in the lower deep layer separates into several branch currents and finally enters the Northeast Pacific Basin. In the Northeast Pacific Basin, LCPW characterized by high oxygen and low silicate loses dissolved oxygen and obtains silicate from sediment and POC, and changes into the North Pacific Deep Water (NPDW) in the upper deep layer at depths of 2000–3500 m.

DWBC in the lower deep layer is separated into the eastern and western branches immediately after entering the Central Pacific Basin (Johnson and Toole, 1993; Kawabe and Taira, 1995; Kawabe et al., 2003). The eastern branch current proceeds northward along the western boundary of the Central Pacific Basin, passes the Wake Island Passage at 18°N 170°E, and enters the Northwest Pacific Basin. The western branch current proceeds at the western boundary of the Melanesian and East Mariana Basins, and enters the Northwest Pacific Basin. These branch currents probably join east of Japan. The confluence flows along the Kuril-Kamchatka and the Aleutian Trenches i.e., the northern boundary of the North Pacific, and enters the Northeast Pacific Basin (Mantyla and Reid, 1983). This is the main pathway of the deep circulation current in the North Pacific.

Other pathways of DWBC carrying LCPW have been expected to be located at south of the Hawaiian Ridge (Mantyla and Reid, 1983) and the Main Gap (30°N, 170°E) in the Emperor Seamounts Chain (Hamann and Taft, 1987). At the former pathway, the separation from DWBC passes the Horizon and Clarion Passages (Edmond et al., 1971; Wong, 1972). At the latter pathway, Hamann and Taft (1987) measured the extremely steady northeastward

current at a depth of 4000 m with a moored current meter for 9 months over a slope eastern side of the Main Gap, and the direction is almost parallel to the axis of an extension of the Main Gap. Thus, the current probably flows through the Main Gap, but it should be exactly clarified within the Gap.

In the present chapter, the deep inflow into the Northeast Pacific Basin through the Main Gap in terms of structure and pathway, by analyzing current velocity and echo intensity data obtained using an LADCP.

The second subject in this chapter is the deep circulation current from the South Pacific existing in the upper deep layer at depths of 2000-3500 m. The current continues from the anticyclonic gyre in the South Pacific separating from the ACC, as shown by Reid (1997) and flows into the equatorial North Pacific (Kawabe et al., 2003). The deep circulation current in the upper deep layer flows along the 2500-m isobaths in the equatorial Pacific, passing through the northeastern slope of the Solomon Rise in the Melanesian Basin on the onshore side of the deep circulation current in the lower deep layer (Kawabe et al., 2003).

Kawabe et al. (2006) found that the structure of the upper deep current has two states and that it changes sharply between them using moored current meters. In the state observed during the first half of the observation period, a strong countercurrent flows at ML1 and the upper deep current flows at ML2 and ML3.

They inferred that the upper deep current during the first half of the observation period extended to the west of ML1 and was divided into western and eastern cores by the countercurrent. I confirm the double-core structure of the upper deep current in the Melanesian Basin and the lateral extension of the current cores and the countercurrent, and discuss the origin of the countercurrent, using LADCP data.

4.2. Data

Current velocity data from LADCP were obtained at full depths, and the data at the stations shown in Fig. 4.1 were processed by the method in Chapter 2. Most of the stations are between the Emperor Seamounts Chain and 165°W in the subarctic region north of 35°N, and at northeastern slope of the Solomon Rise in the Melanesian Basin. Therefore, we used the current velocity profiles at 170°E (ES1–ES8, ES line), 180° (A1–A4, A line), 175°W (B1–B4, B line), and 165°W (C026–C36, C line) collected during the period 19 May–15 June 2003 on the R.V. *Hakuho Maru* KH-03-1 cruise (Fig. 4.2a) to examine the lower and upper deep currents, and at nine stations (M1–M9, M line) located between 2°05′N, 158°30′E and 5°46′N, 161°20′E within the Melanesian Basin (Fig. 4.12a) collected during the period 30 January–2 February 1999 on the R.V. *Hakuho Maru* KH-99-1 cruise to examine the upper deep current. The barotropic tidal velocity estimated using the tide model of Egbert (1994) was removed from the processed LADCP velocity.

Echo intensity data from LADCP were also used for water-mass analysis, using the character of low echo intensity of LCPW clarified in Chapter 3. Moreover, velocity data from moored current meters at M line were used (Fig. 4.12a). The velocity data obtained from three current meters at a depth of approximately 2000 m at ML1 (located between M3 and M4), ML2 (between M5 and M6) and ML3 (between M7 and M8) (Kawabe et al., 2006), where the upper deep current flowed, were averaged for five-day period around the day of LADCP observations. These averages were used for a comparison with LADCP velocity data.

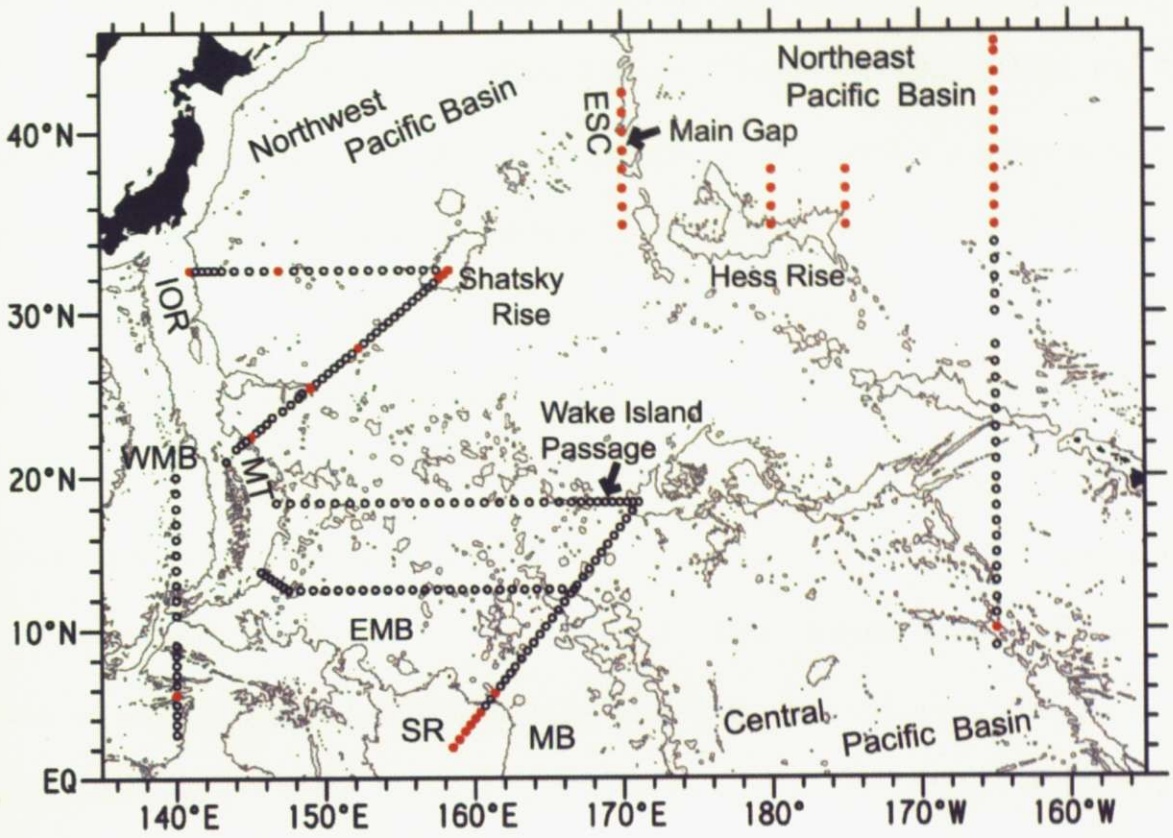

Fig. 4.1: LADCP stations in *Hakuho-Maru* cruises KH-99-1, KH-03-1 and KH-04-4 in the North Pacific (open circles). Red dots show stations at which the corrected velocity by means of the correction method in Chapter 2 is available. Solid lines indicate 4000 m isobaths. MB, Melanesian Basin; SR, Solomon Rise; MT, Mariana Trench; EMB, East Mariana Basin; WMB, West Mariana Basin; IOR, Izu-Ogasawara Ridge; ESC, Emperor Seamounts Chain.

4.3. Inflow through the Main Gap into the Northeast Pacific Basin

At the center of the Main Gap in the Emperor Seamounts Chain (ES5, Fig. 4.2a), eastward current exists at depth greater than 5000 dbar with a strong velocity core of more than 5 cm s^{-1} centered at 5400 dbar (Fig. 4.3a). The LADCP current vector averaged in a bottom layer of potential temperatures lower than 1.12°C (~ 4200 m) orients southeastward (Fig. 4.2b). This is consistent with the eastward current observed by Hamann and Taft (1987). In the bottom layer north of the Main Gap, strong westward current exists at ES6-ES8, carrying water with high echo-intensity which is different from LCPW (Figs. 4.3a, d). This current may continue to the westward current between 39° and 41°N at 165°E observed with mooring current meters by Schmitz (1987), which is different from the global deep circulation, and may form a meso-scale circulation.

Water properties at the ES line show that coldest (< 1.05°C) and highest oxygen (> 3.7 ml l^{-1}) water exists at the southernmost stations at ES1 and ES2, and cold, oxygen-rich water extends northward to south of ES6 with high oxygen water more than 3.64 ml l^{-1} at near-bottom at ES5 in the Main Gap (Figs. 4.3b and 4.3c). The minimums of echo intensity less than 79 dB correspond well to the cold, oxygen-rich water at ES1, ES2, and ES5 (Fig. 4.3d). These characteristics suggest that the water in the bottom layer at ES1-ES5 is LCPW, and LCPW flows northward along the Emperor Seamounts Chain to the Main Gap. This is supported by northward velocity from LADCP in the bottom layer at ES2 and ES4 (Fig. 4.2b). The northward current is probably bifurcated from the eastern branch current of deep circulation, and carried part of the LCPW which is transported by the eastern branch current as shown by (Kenyon, 1983; Kawabe and Taira, 1995). Therefore, part of LCPW flows

into the Northeast Pacific Basin through the Main Gap, being carried by the northward current along the Emperor Seamounts Chain and the eastward currnet in the Main Gap.

In a bottom layer at the A (180°) and B (175°W) lines, eastward current exists at A2-A4 and around B2 at the foot of the northern slope of the Hess Rise (Figs. 4.2b, 4.4a, and 4.5a). Eastward current was also observed over this slope at 179°E by Roden (2000) using LADCP. The eastward current carries colder (< 1.12°C) water with high oxygen (> 3.5 ml l^{-1}) and low echo-intensity (< 80 dB) which is less characteristic of LCPW than the bottom water in the Main Gap (Figs. 4.4b-d and 4.5b-d).

At the C line (165°W), characteristics of bottom water are markedly different between couth and north of the seamount at 37°N (Figs. 4.6b-d). The southern water is quite cold (< 1.09°C) with high oxygen (> 3.62 ml l^{-1}) and low echo intensity (< 80 dB), that is similar to bottom water in the Main Gap. Near-bottom current south of 37°N (C26-C28) is eastward with velocity more than 5 cm s-1 (Figs. 4.6a).

The characteristics of zonal velocity and water in a bottom layer are clearly shown by averages in a layer of potential temperature lower than 1.12°C (Fig. 4.7). This is suggests that the inflow of LCPW from the Main Gap flows eastward along the northern slope of the Hess Rise and reaches south of 37°N (at least, 35°-37°N) at 165°W (Fig. 4.8).

It should be noticed that dissolved oxygen south of 37°N at the C line is much less than that at the A and B lines and goes back to the level in the Main Gap. Between 37° and 41°N in the C line, zonal velocity is very weal, and bottom water may be stagnant. This may cause low oxygen and high echo intensity. North of 42°N,

eastward current is significant, and echo intensity is low like LCPW, but dissolved oxygen is very low, much lower than LCPW. The water may be originated from LCPW but loses oxygen by significant consumption. These suggest a complicated distribution of current in the lower deep layer in the Northeast Pacific Basin.

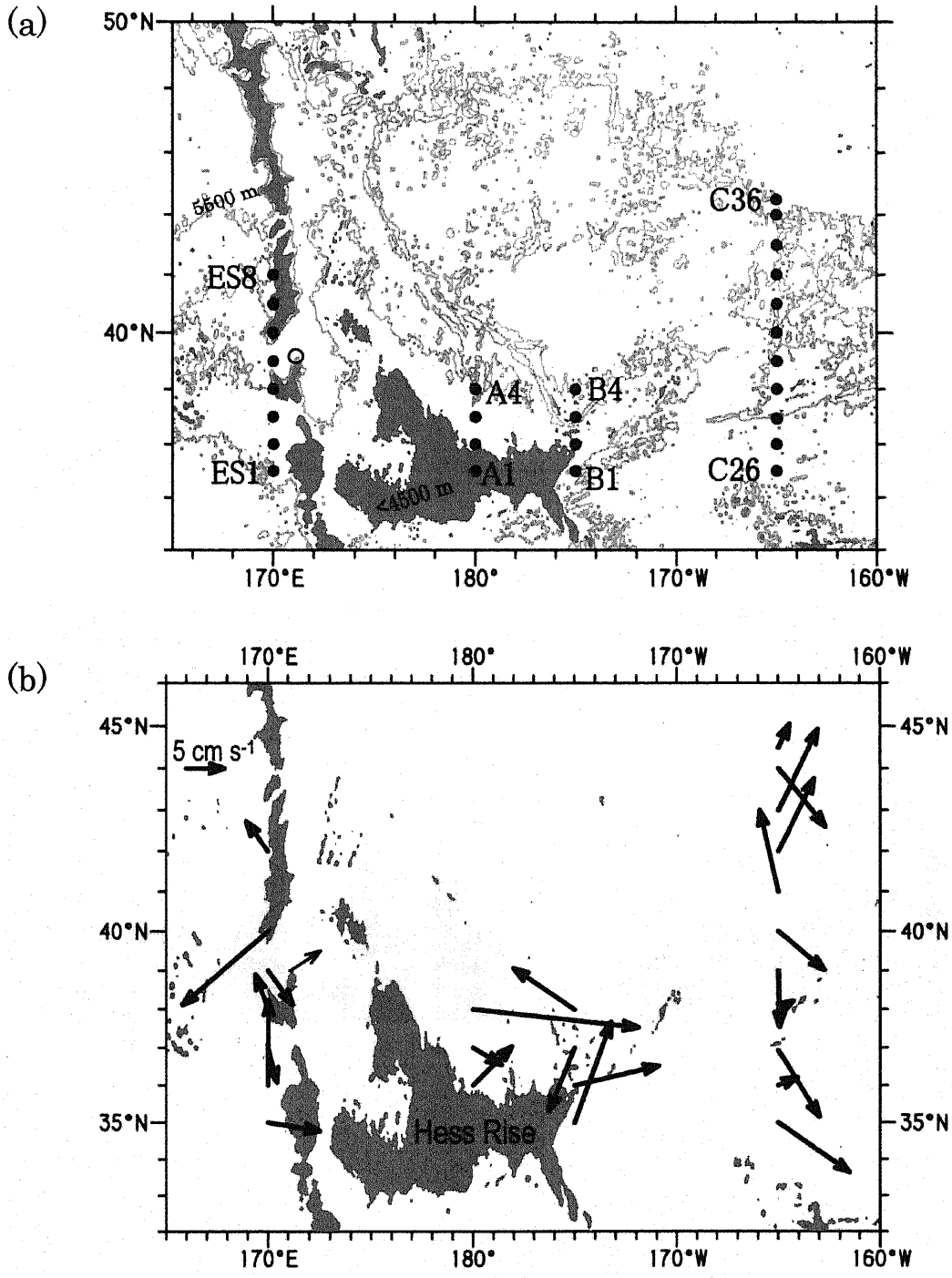

Fig. 4.2: (a) LADCP stations (dots) by the present study and a mooring station of current meter by Hamann and Taft (1987) (open circle) in northwestern region of the Northeast Pacific Basin, (b) velocity vectors from LADCP averaged in a bottom layer greater than $45.873\sigma_4$ ($\theta < 1.12$°C, 4200 m ~ sea bottom) and a velocity vector from the current meter at 3947 m depth. Areas of shallower than 4500 m are shaded, and grey lines in (a) indicate 5500 m isobaths.

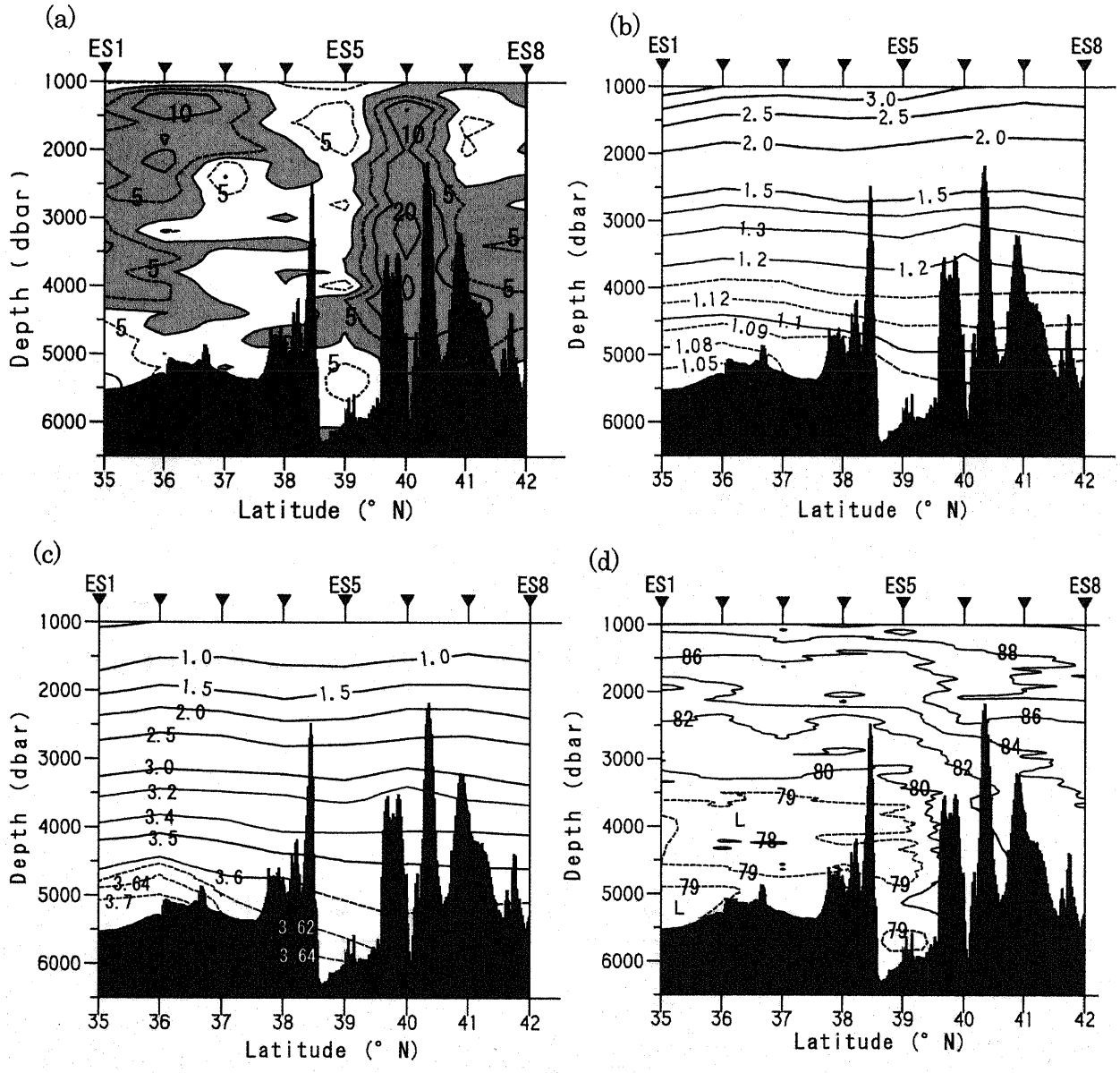

Fig. 4.3 Vertical sections at the ES line (170°E) of (a) zonal velocity (cm s^{-1}), (b) potential temperature (°C), (c) dissolved oxygen (ml l^{-1}) and (d) echo intensity (dB). Shading in (a) indicates westward velocity.

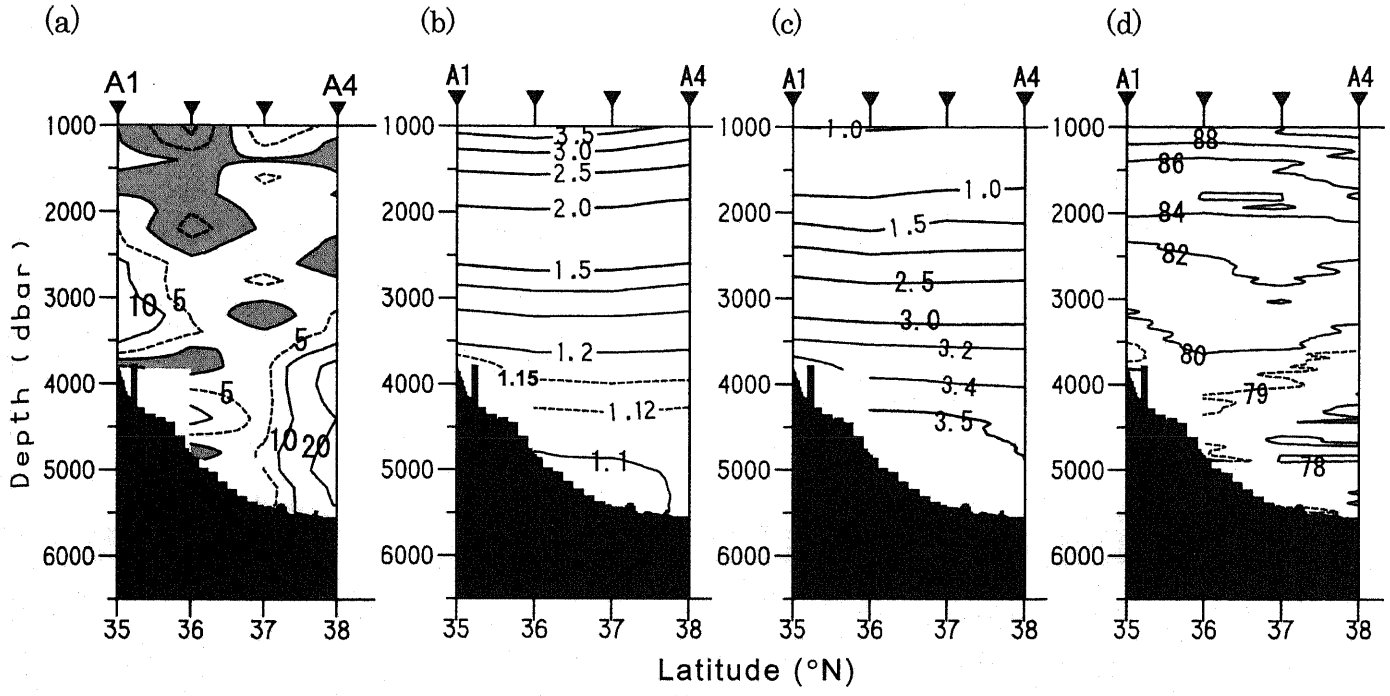

Fig. 4.4: Same as Fig. 4.3 but for the section at the A line (180°).

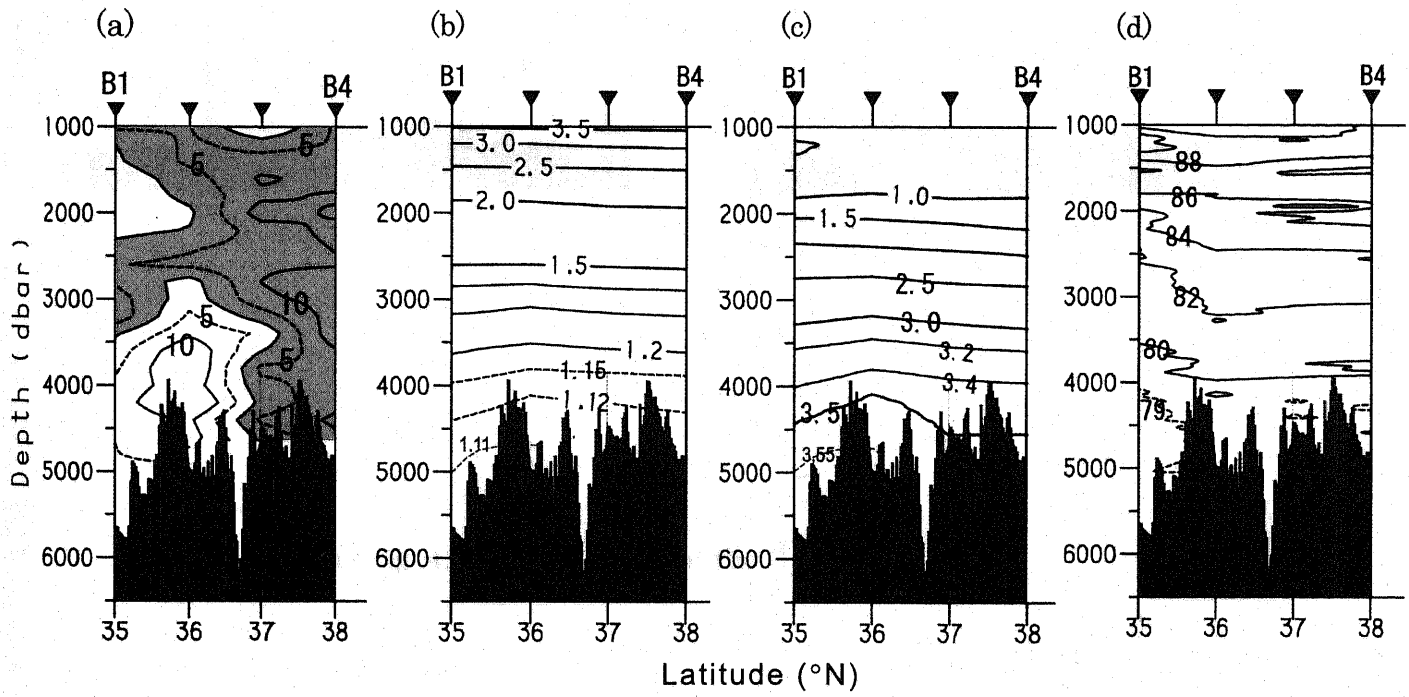

Fig. 4.5: Same as Fig. 4.3 but for the section at the B line (175°W).

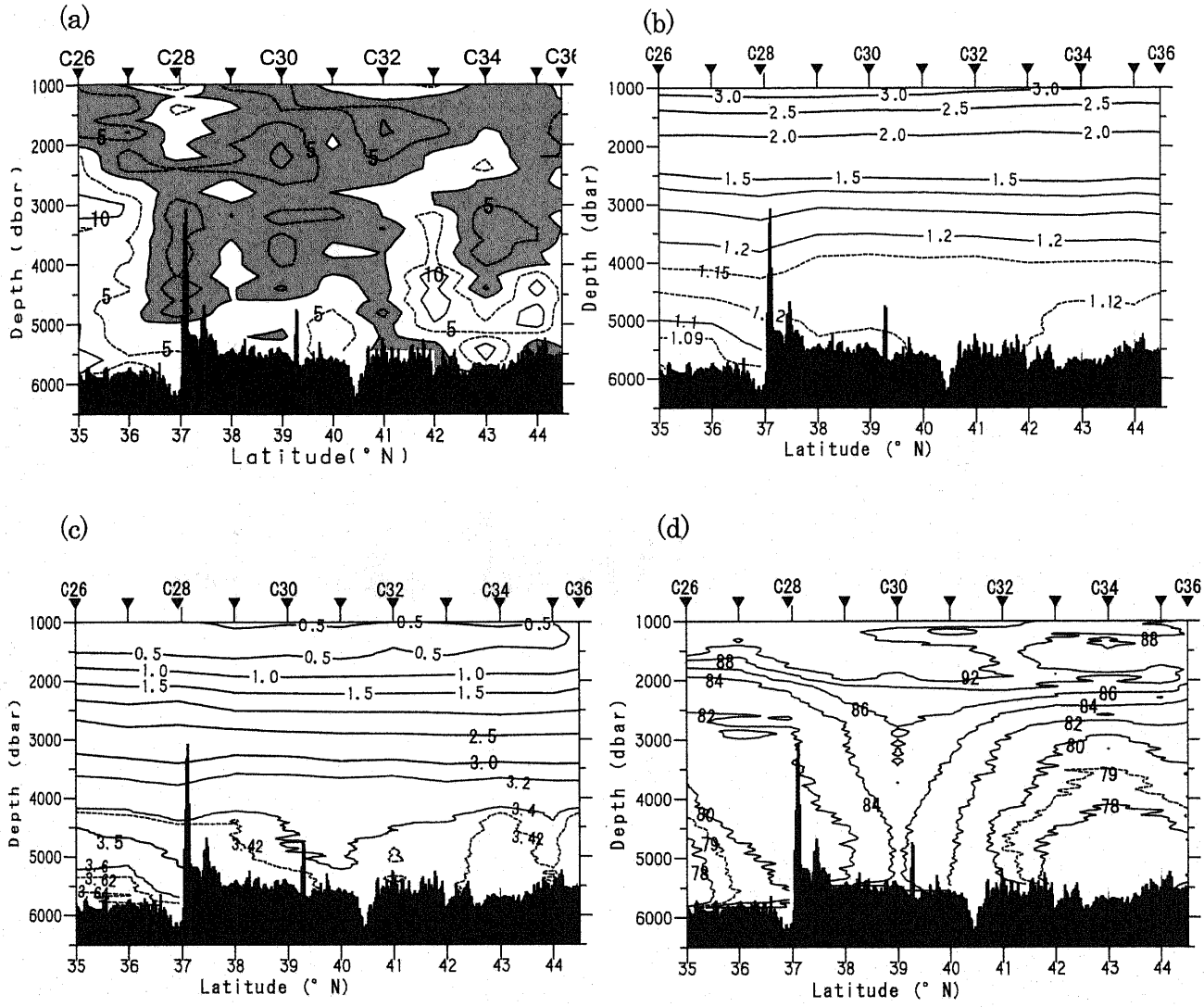

Fig. 4.6: Same as Fig. 4.3 but for section at the C line (165°W).

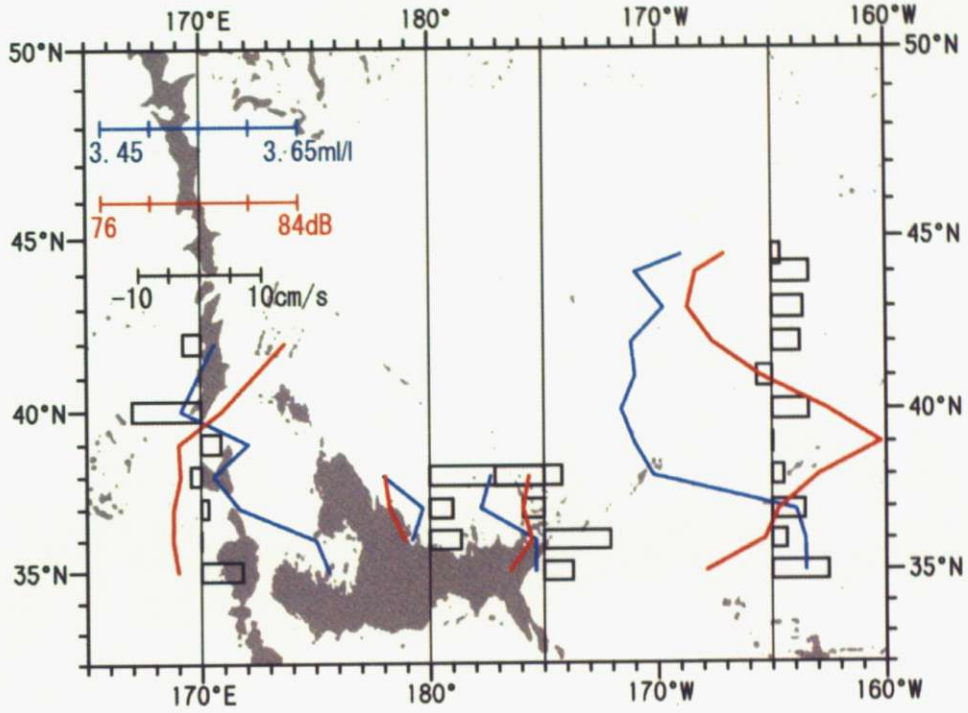

Fig. 4.7: Distribution of zonal velocity (bow), echo intensity (red line), and dissolved oxygen (blue line) averaged in a layer of potential temperature less than 1.12°C ($\sigma_4 > 45.873$) approximately.

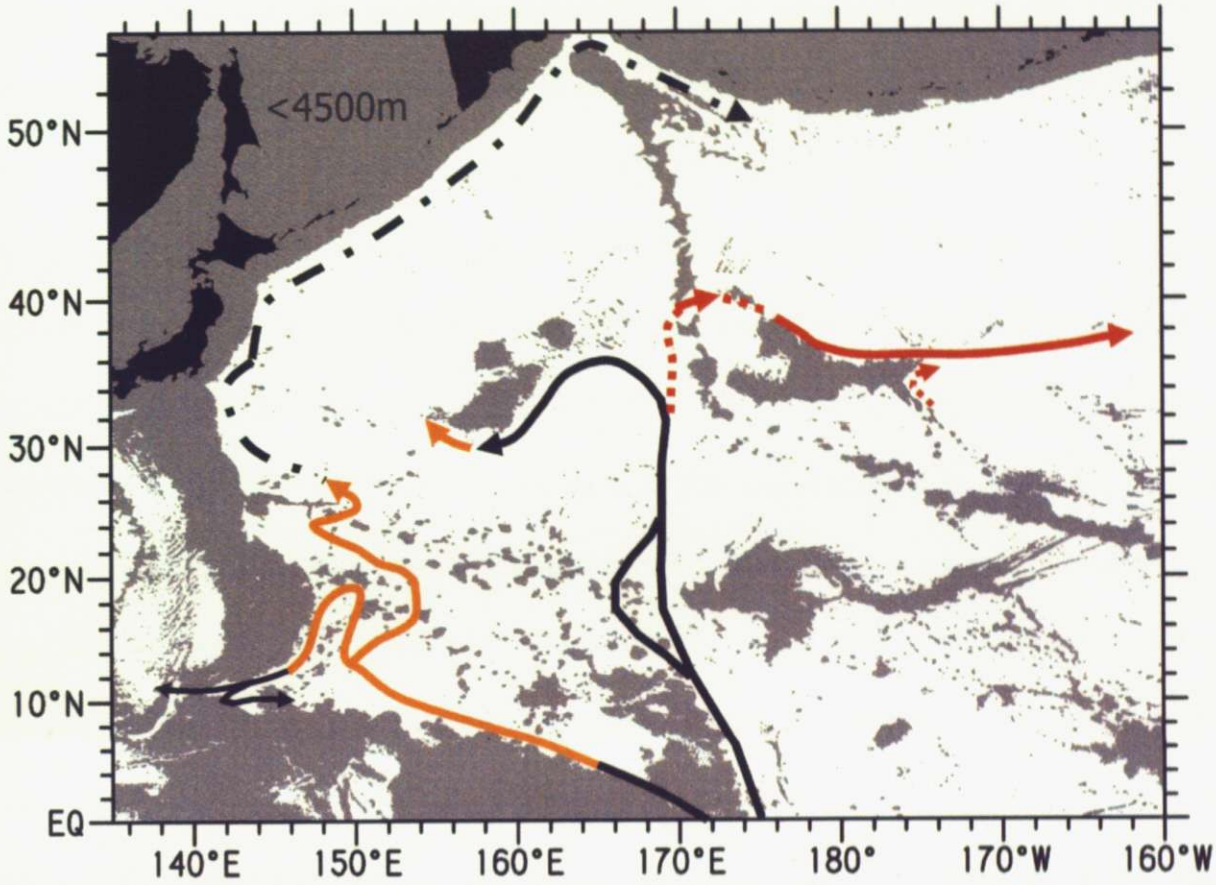

Fig. 4.8: Schematic of the pathways of LCPW due to the deep circulation current in the lower deep layer in the North Pacific. Red solid lines represent the pathway concluded using current velocity and echo intensity from LADCP. Red broken lines represent the pathway suggested from water-mass properties, including LADCP echo intensity, and bottom topography. Black and orange lines are the pathway of the eastern and western branch currents concluded by Kawabe et al. (2003). The orange lines were confirmed by echo intensity data from LADCP in the present study. Black broken lines represent the pathway deduced by earlier studies.

4.4. Pathway of the western branch current of deep circulation

Low echo intensity is characteristic of LCPW (Chapter 3), and is expected to be useful to examine the pathway of the western branch current of the lower deep current. Then, the vertical distribution of echo intensity at the 12.7°N, Shatsky and 32.5°N lines are examined. At the 12.7°N line, water with significantly low echo intensity (< 69 dB) exists at depths of 3700-5300 dbar between 146°-152°E, and is divided by a ridge at 148°E into two minima over the Mariana Trench and the western region of the East Mariana Basin (Fig. 4.9c). The minima of echo intensity at 146°-147°E and 149°-152°E are clearly seen in the zonal variation of the average in a layer of $45.865\sigma_4$-$45.880\sigma_4$, and correspond to two maxima of oxygen averaged in the same layer (Fig. 4.10c). It should be noted that the minima of echo intensity are much remarkable than the maxima of oxygen. The location of the low echo-intensity water confirms that of the western branch current of deep circulation flowing northward around 150°-151°E which was concluded by Johnson and Toole (1993), Kawabe (1993) and Kawabe et al. (2003), and the return flow of the western branch current flowing southward along the Mariana Trench and partly entering the Philippine Sea suggested by Kawabe et al. (2003) and Siedler et al. (2004).

At the 18.3°N line, the most remarkable minimum of echo intensity exists around 155°-156°E and corresponds well to the location of the western branch current concluded by Kawabe et al. (2003) as indicated in Figs. 3.5b and 3.6b in Chapter 3. At the Shatsky line, minimum of echo intensity less than 69 dB exists at 146°-152°E in the southern and northern regions of the Ogasawara Plateau located at 148°-149°E, although LADCP data are missing immediately north of the plateau. Moreover, minimum of echo intensity less than 71 dB exists at 154°-156°E. These are

consistent with the pathway of the deep circulation current deduced by Kawabe and Taira (1995) and Kawabe et al. (2003), and specify the location of the western branch current probably at 149°-152°E north of the Ogasawara Plateau and the location of the eastern branch current at 154°-156°E immediately south of the Shatsky Rise.

At the 32.5°N line, marked minimum of echo intensity less than 71 dB exists at 145°-151°E (Figs. 4.9a and 4.10a). This suggests that the deep circulation current, probably the eastern branch current, flows in the area of this echo-intensity minimum, although this suggestion must be investigated by further study.

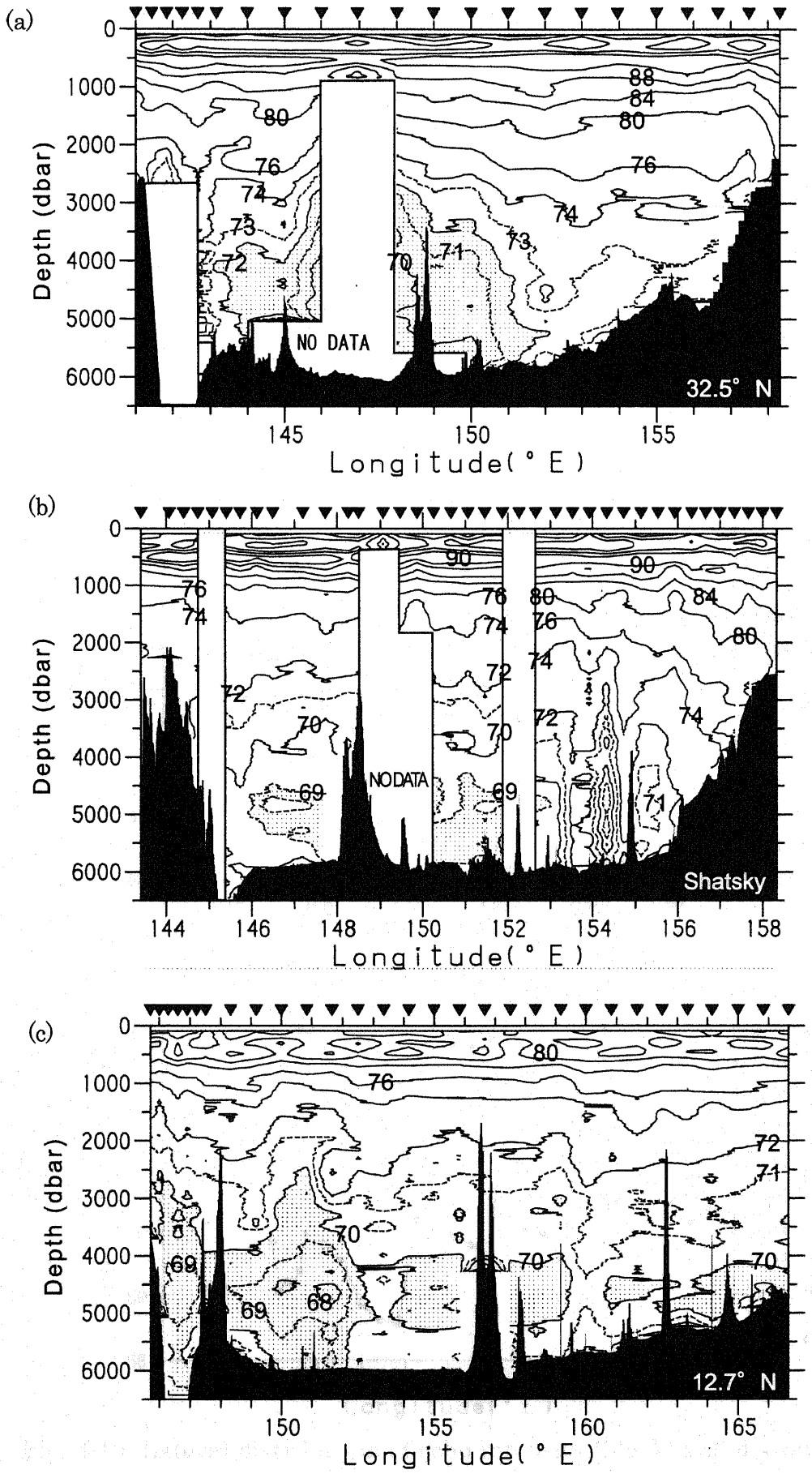

Fig. 4.9: Vertical distributions of echo intensity (dB) at (a) 12.7°N, (b) Shatsky and (c) 32.5°N lines.

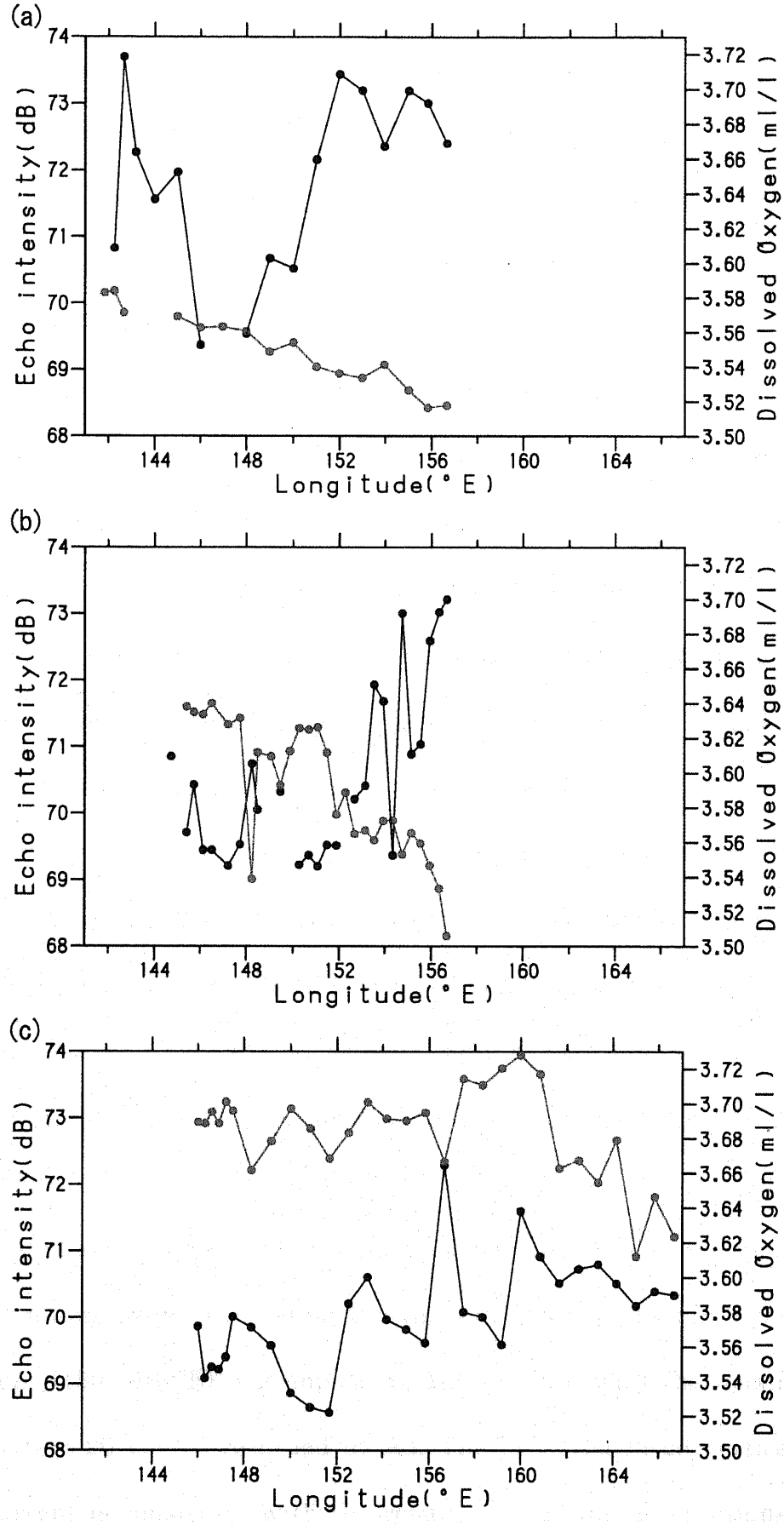

Fig. 4.10: Lateral distribution of echo intensity (black) and dissolved oxygen (grey) averaged in a layer of densities of $45.865\sigma_4$-$45.880\sigma_4$ which corresponds to 4000-4500 dbar approximately at (a) the 32.5°N line, (b) Shatsky line and (c) 12.7°N line.

4.5. Currents in the upper deep layer in the Melanesian Basin

4.5.1. Vertical structure of the upper deep currents

Figure 4.12 shows velocity vectors from LADCP on an isothermal surface of potential temperature, $\theta = 2.1°C$, which is close to the top of the upper deep layer at a depth of approximately 2000 m (Kawabe et al., 2003). The current is eastward at M3, southward at M4, northward at M5, southwestward at M6, northwestward at M7, and southwestward at M8. The vector mean of LADCP velocity between pairs of stations is southeastward for M3 and M4, southwestward for M5 and M6, and westward for M7 and M8. These current directions are similar to those measured using current meters at ML1, ML2 and ML3, respectively, although the amplitude of velocity is much larger. The southeastward current at ML1 and the westward current at ML3 are the countercurrent and the eastern core of the upper deep current, which continued for seven months during the first half of the mooring observation (Kawabe et al., 2006). The northwestward current at M2 may represent the western core of the upper deep current inferred by Kawabe et al. (2006). These results demonstrate that the LADCP velocity data provide the correct direction of the velocity component perpendicular to the observation line.

The distribution of the perpendicular component of velocity (Fig. 4.13) indicates that the countercurrent has a great thickness at depths less than 3500 dbar and has a wide extent (159°–160°E), encompassing M3 and M4, with the maximum velocity of approximately 20 cm s^{-1} recorded at A3. The observed large vertical extent of the countercurrent is consistent with the results of mooring observations undertaken at ML1, as described by Kawabe et al. (2006). The width of the countercurrent spans more than two intervals between the LADCP stations, which is larger than that speculated

by Kawabe et al. (2006). The amplitude of velocity exceeds 10 cm s^{-1} at every measurement depth and exceeds 20 cm s^{-1} at 2000 dbar and 2700–3200 dbar. These values may represent an overestimate, although such a strong current may be possible over short time periods.

West of the countercurrent, a northwestward current core exists at depths between 1600 and 2500 dbar at 158.5°–159°E (M1–M2), with a maximum velocity of 10 cm s^{-1} recorded at 2000 dbar at M2 (Fig. 4.13). This current likely represents the western core of the upper deep current. In contrast, the northwestward velocity at M7 represents the eastern core of the upper deep current. This may include a cyclonic eddy formed in combination with the countercurrent at M6. High velocities in excess of 30 cm s^{-1} within the eastern core may partly reflect this eddy. The cyclonic eddy (or the countercurrent at M6) was not present in the current-meter results for the eastern core averaged during the first half of the mooring period; however, the current-meter data at 2650 m at ML2 show the countercurrent component around the time of the LADCP observation (Kawabe et al., 2006). The structure of the eastern core of the upper deep current may be affected by the existence of an eddy (or small-scale countercurrent), but the location of the core is largely unaltered.

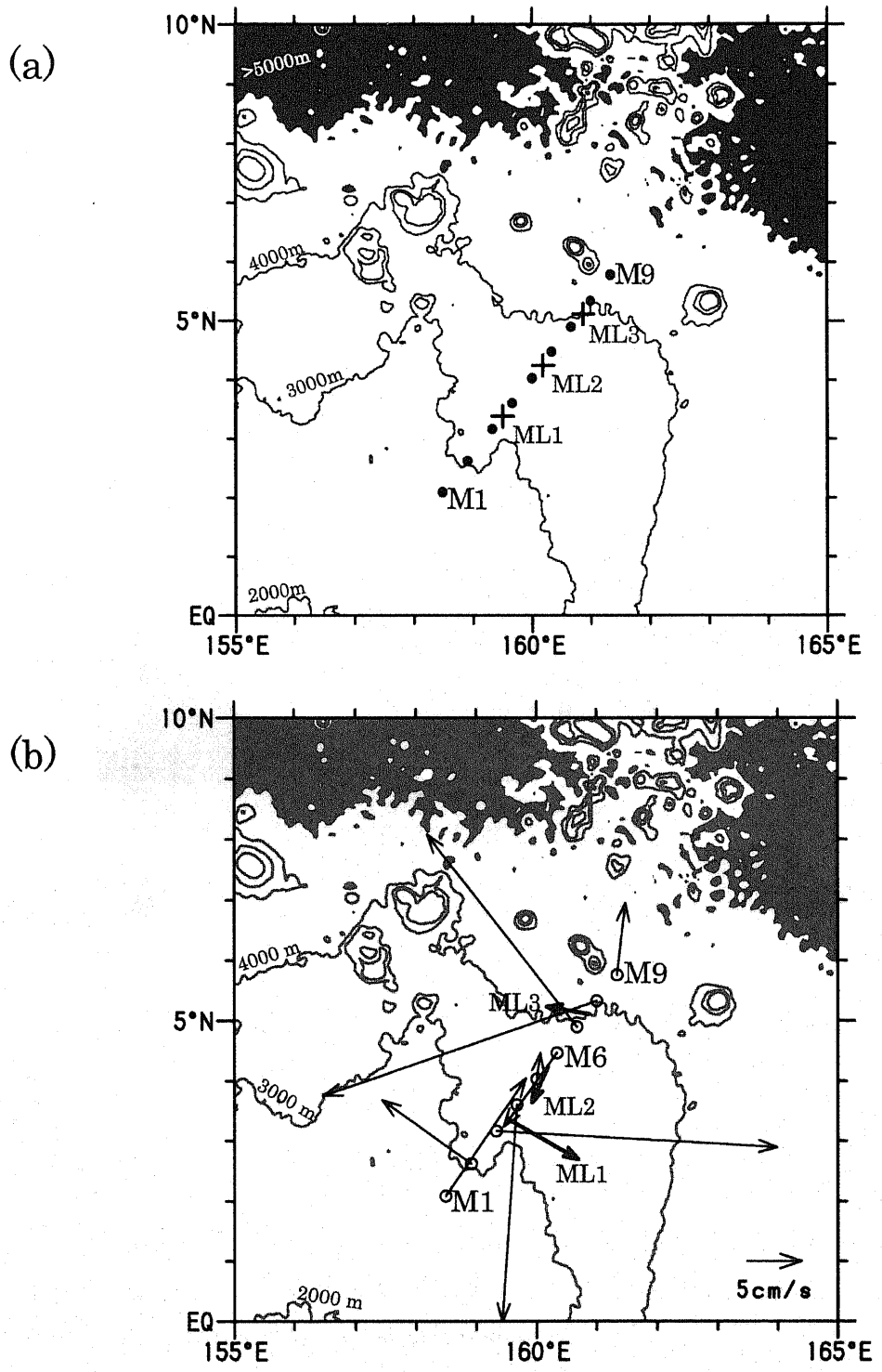

Fig. 4.11 (a) Enlarged maps of LADCP stations (dots) in the Melanesian Basin. Pluses indicate mooring stations of current meters, areas of greater than 5000 m are shaded, and grey lines indicate 2000, 3000, 4000 m. (b) Velocity vectors measured using LADCP at M1–M9 at depths of $\theta = 2.1°C$ (thin arrows) and current meters at depths of approximately 2000 m at ML1–ML3 averaged for the five-day period around the time of the LADCP observations (thick arrows). Contours are isobaths at 2000, 3000, and 4000 m. Shading represents areas at depths greater than 5000 m.

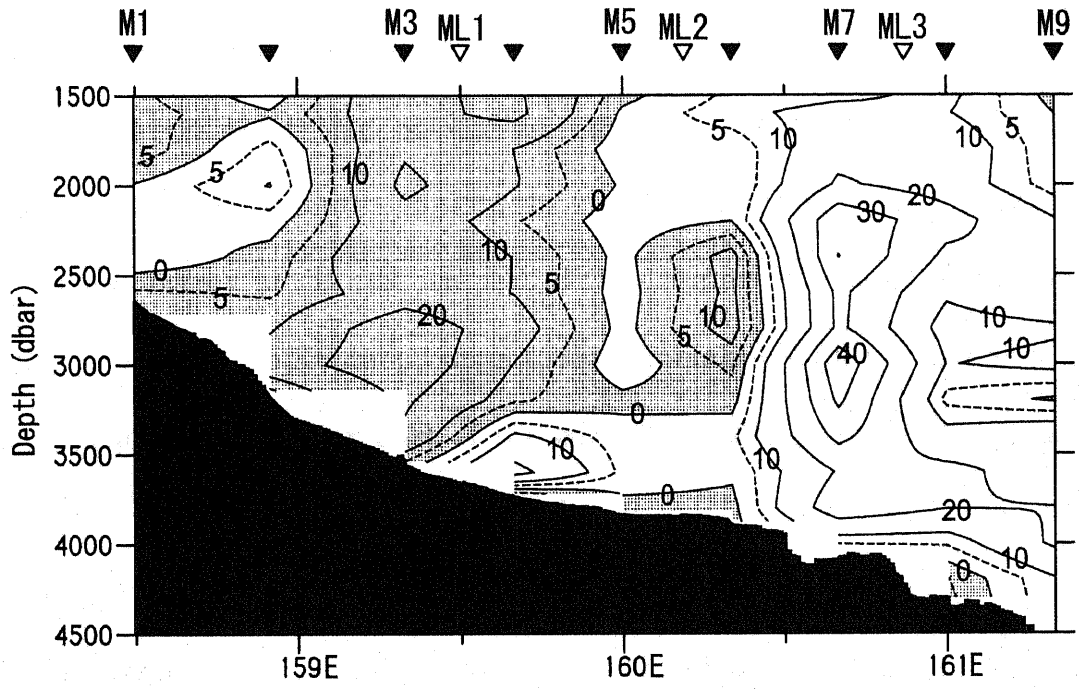

Fig. 4.12: Vertical sections of the velocity component (cm s^{-1}) perpendicular to the section measured at M1–M9 in the Melanesian Basin using LADCP. Shading represents a southeastward velocity. The barotropic tidal velocity estimated using the tide model of Egbert (1994) was removed from the data. The LADCP stations are shown by solid triangles at the top of the panel. For reference, the mooring positions ML1–ML3 are shown by open triangles.

4.5.2. Characteristics of the countercurrent

The western core of the upper deep current carries oxygen-rich water. This is especially pronounced in the upper part of the core above the 1.9°C isotherm, which has a large dissolved-oxygen anomaly of more than 0.20 ml l^{-1}, as determined from the averages at M14–M17 located at 8.0°–9.7°N, 163.1°–164.3°E in a small deep valley farther northeast of M9 (Fig. 4.14). The oxygen anomaly extends to M3, the center of the countercurrent, at depths shallower than the 1.9°C isotherm. The oxygen anomaly decreases markedly in the eastern part of the countercurrent to the east of M3. In the eastern core of the upper deep current, the anomaly is still positive but is relatively weak, occupying the upper part of the core. The oxygen anomaly in the lower part (below the 1.8°C isotherm) is almost uniformly weak in the western and eastern cores of the upper deep current and the intervening countercurrent.

Echo intensity is relatively strong in the upper part (above the 1.8°C isotherm) of the countercurrent, with the maximum intensity recorded at the center of the countercurrent. The intensity in the upper part of the countercurrent is much higher than that in the western and eastern cores of the upper deep current, being much higher than that in the eastern core. The highest echo intensity in the countercurrent and lowest in the eastern core are also seen in the lower part of the upper deep layer, although they are less pronounced than those in the upper part.

Thus, the differences in water-mass characteristics between the different currents are especially marked in the upper part of the currents (Fig. 4.15). The countercurrent contains an intermediate oxygen anomaly between the eastern and western cores of the upper deep current. This suggests that the countercurrent carries a mixture of the UCPW carried by the two cores of the upper deep current; however, echo intensity in

the countercurrent is much higher than that in the cores. This indicates that the countercurrent carries the upstream water, which is characterized by high echo intensity. If the countercurrent flows into the Melanesian Basin by proceeding along the 3000 or 3500 m isobaths, then the countercurrent in the upstream region must flow eastward along the southern boundary of the East and West Caroline Basins near the equator, carrying water with high echo intensity peculiar to the near-equator region. During eastward transportation, the water mixes with high-oxygen UCPW carried by the upper deep current.

Firing et al. (1998) observed an eastward deep current at depths of 2000–3500 m at 0–1°S, 150°E on the southern boundary of the East Caroline Basin in August 1985 and January 1986. This eastward current may be steered into the Melanesian Basin by the bottom slope at a depth of approximately 3500 m, thereby becoming the countercurrent observed in the present study. The equatorial eastward current, however, was not found at 146°E in October 1993 (Firing et al., 1998). This may imply that the equatorial eastward current on the bottom slope is not always present. Even if the equatorial eastward current is always present, it does not detour around the Solomon Rise when it is detached from the bottom slope at the change in vertical structure. In such a case, the current probably continues eastward along the equator. The absence of the countercurrent on the Solomon Rise during the second half of the mooring observation described by Kawabe et al. (2006) may reflect the disappearance of the equatorial eastward current or the release of the current from topographic controls.

(a)

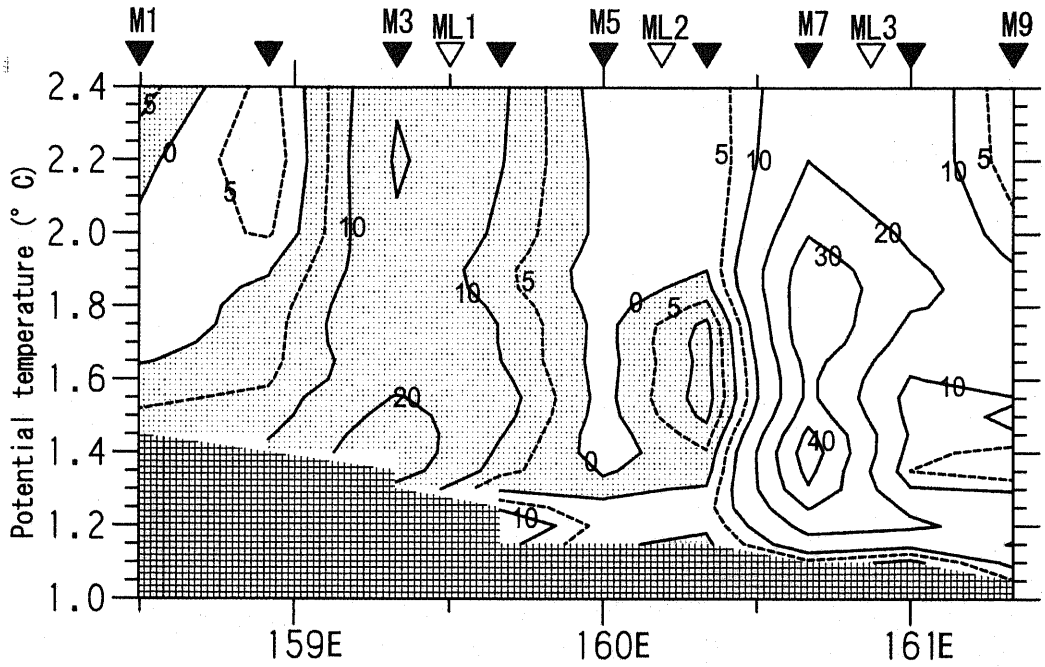

Fig. 4.13: Vertical sections at M1-M9 in the Melanesian Basin of the velocity component (cm s-1) perpendicular to the section measured using LADCP (a). The hatched areas in the lower part represent areas of no data due to the sea bottom. Shading in (a) indicates southeastward velocity.

(b)

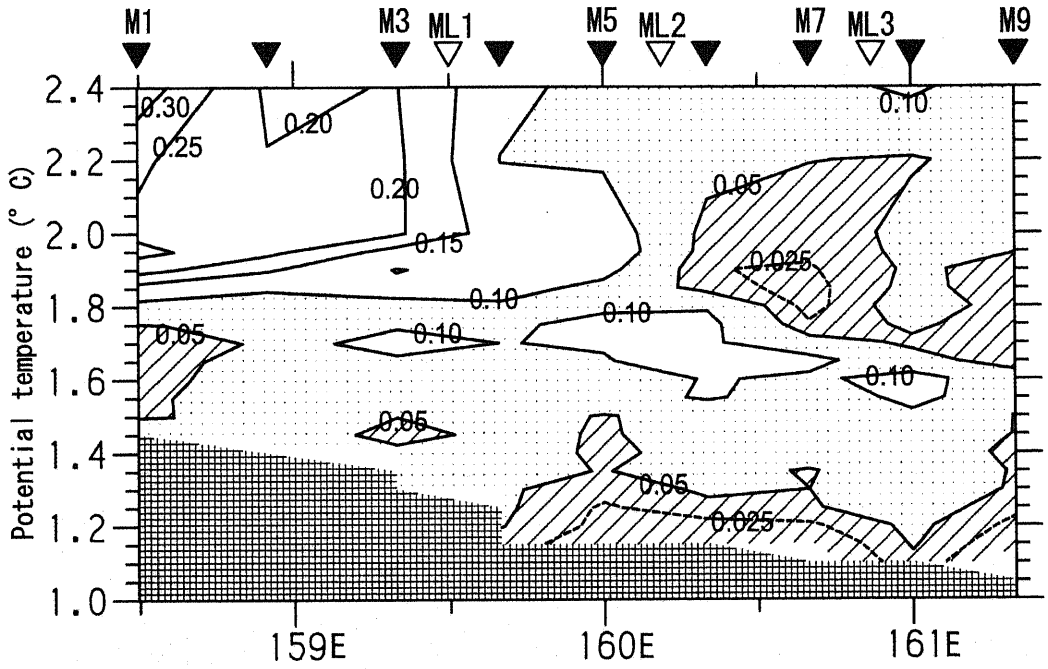

(c)

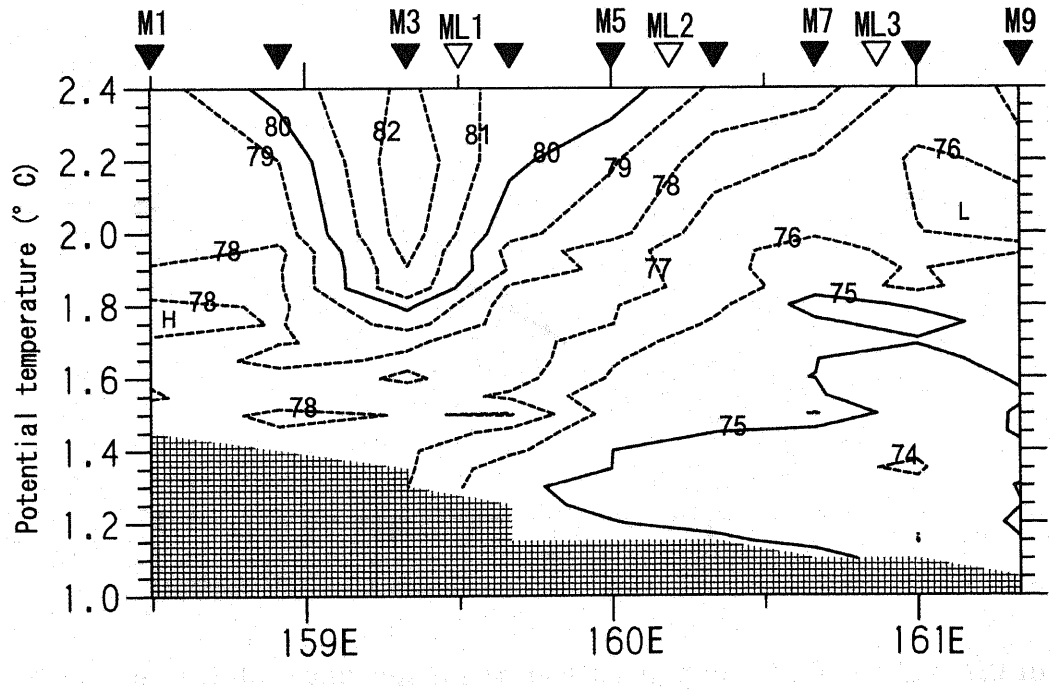

Same as (a) but for the anomaly on isotherms of dissolved oxygen (ml l-1) derived from the average of values at M14-M17 (163.1 -164.3 E) as in Kawabe et al. (2003) (b), and echo intensity (dB) measured using LADCP (c). Potential temperature is taken as the ordinate. Areas of oblique lines and dotted areas in (b) indicate values of less than 0.05 and 0.10 ml l-1, respectively.

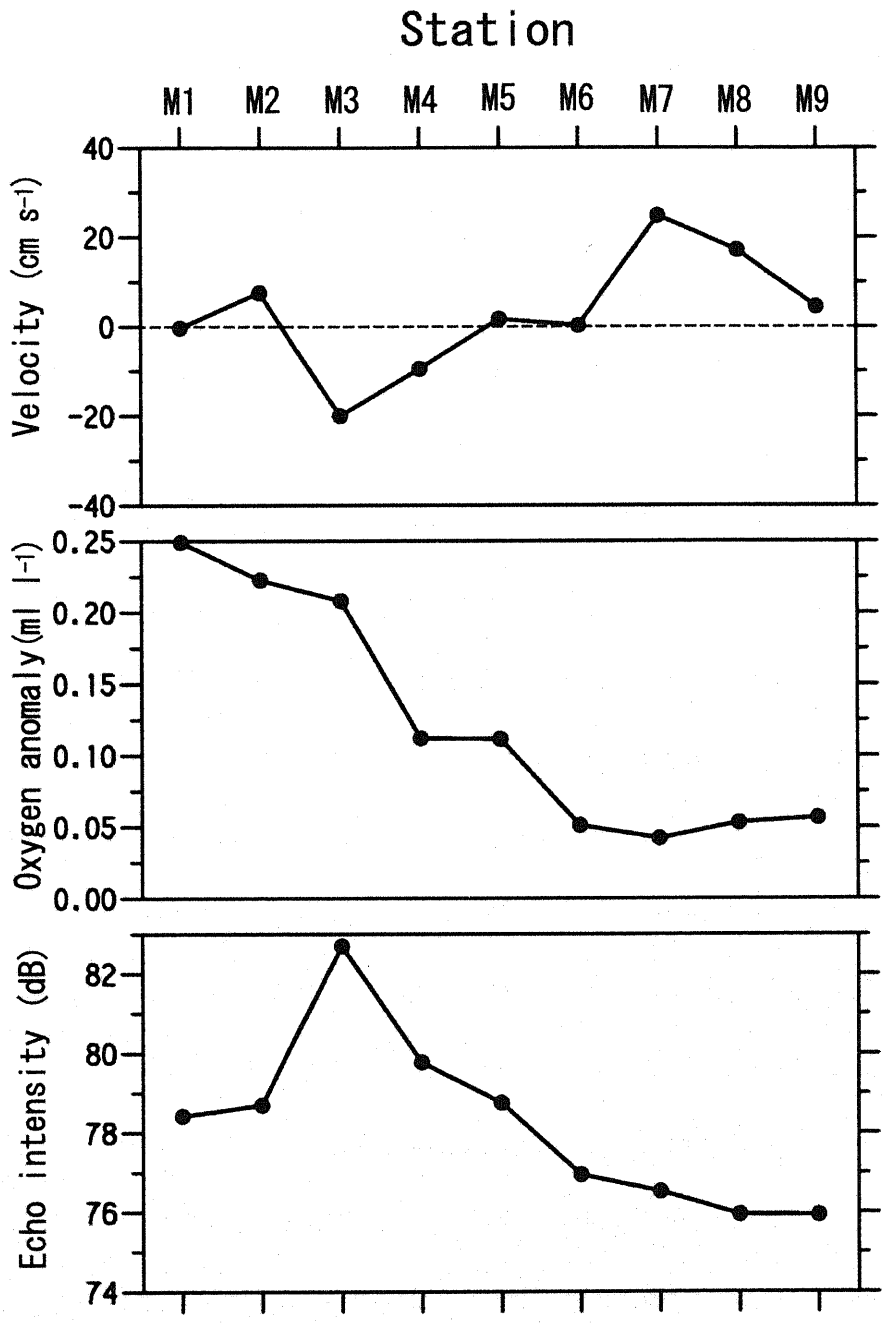

Fig. 4.14: Lateral distributions on an isotherm of θ = 2.1°C at M1–M9 in the Melanesian Basin of current velocity perpendicular to the observation section measured using LADCP (upper panel), the anomaly of dissolved oxygen from M14–M17 (middle panel), and echo intensity measured using LADCP (lower panel).

4.6. Conclusions

First, we examined current velocity and echo intensity data from LADCP to clarify an inflow of the eastern branch through the Main Gap and the pathway in the Northeast Pacific Basin, and to confirm pathways of the western branch.

In the Main Gap, the southeastward velocity core with approximately 10 cm s^{-1} at maximum was observed at depths greater than 4750 dbar, at water depth of approximately 6500 m, carrying LCPW with high oxygen and low echo-intensity similar to in the southern region of the Main Gap. This current continues to eastward current observed on the northern slope of the Hess Rise, at water depth of approximately 4000-5500 m, and passes 165°W at water depth of approximately 6000 m. Thus, a pathway of a inflow of LCPW from the Main Gap to the Northeast Pacific Basin was clarified from this study as described with a schematic in Fig. 4.8 The deep water carried into the Northeast Pacific Basin is gradually transformed into NPDW in the upper deep layer, and carried by the westward current. The westward current was observed in a wide latitudes at the central of the basin.

As for the western branch, the pathways in the earlier studies after passing the Melanesian Basin was confirmed from echo intensity (Fig. 4.8). Suggesting by Johnson and Toole (1993) and Kawabe et al. (2003), the western branch flows northwestward in the East Mariana Basin, at water depths greater than 4000 m approximately, turns northward at small seamounts at the eastern side of the Mariana Trench, and enters the western North Pacific. A portion of LCPW entering the Mariana Trench turns southward, and proceeds along the Mariana Trench toward the West Mariana Trench observed by Kawabe et al. (2003) and Siedler et al. (2004). Echo intensity on the these pathways is much less than the other longitudes, suggesting LCPW more clearly than

dissolved oxygen.

Next, we used current velocity and echo intensity data from LADCP to clarify the structure of the western and eastern cores of the upper deep current and the countercurrent at depths of 2000–3500 m over the northeastern slope of the Solomon Rise in the Melanesian Basin. We used the echo intensity and dissolved oxygen characteristics of the water to infer the upstream pathway of the countercurrent.

The western core of the upper deep current was observed at depths of 1600–2500 dbar over the bottom slope, at water depths of approximately 3000 m, carrying UCPW with very high dissolved oxygen. The eastern core was observed in the eastern region over the bottom slope at water depths of approximately 4000 m. Between these two cores of the upper deep current, a thick countercurrent flowed with a large width of more than 100 km.

The countercurrent is located over the bottom slope at water depths of approximately 3500 m, carrying water that is characterized by extremely high echo intensity. Based on these facts, we inferred that the equatorial eastward deep current along the southern boundary of the East Caroline Basin, as observed by Firing et al. (1998), is steered by the bottom slope at water depths of approximately 3500 m. This current is connected to the countercurrent within the Melanesian Basin observed in the present study.

The equatorial water carried by the equatorial eastward current mixes with high-oxygen UCPW carried by the upper deep current. This explains the fact that the water in the countercurrent has an oxygen content that is intermediate between that of the western and eastern cores of the upper deep current. Moreover, the long-time disappearance of the countercurrent in the Melanesian Basin (Kawabe et al., 2006)

may occur when the equatorial eastward current disappears or detaches from the bottom slope.

Chapter 5

General conclusions

Current velocity and echo intensity from a lowered acoustic Doppler current profiler (LADCP) are important parameters for analysis of deep ocean circulation which influences the global environment. This thesis presented new methods to correct LADCP velocity that is processed by the ordinal processing method, and to apply LADCP echo intensity to a parameter of deep water-mass. Then, using these methods, deep circulation was examined from LADCP data observed in the North Pacific.

In Chapter 2, we obtained the fact that echo intensity of a reflected sound pulse is highly correlated with the magnitude of the difference in vertical shear of velocity between downcast and upcast, indicating an error in velocity shear. Thus, the correction method is tried to feature that the velocity shear is corrected using echo intensity, and that the correction values are determined as to fit LADCP velocity to shipboard ADCP (SADCP) and LADCP bottom-tracked velocities. This method is valid for a full-depth LADCP cast throughout which the echo intensity is relatively high, and produced qualitatively good current structures that were consistent with the deep current structures inferred from silicate distribution.

In Chapter 3, we clarified a meridional difference of echo intensity which is higher in the subpolar and equatorial regions and lowest in the subtopics. The main contributor to echo intensity at depths greater than 3000 m is probably sinking particle. At the vicinity of each latitudes, a significant deviation of echo intensity from the mean at the latitudes exists. In the lower deep layer, the deviation has a significant negative relationship with high-oxygen water which indicates water originating from the Lower Circumpolar Water (LCPW). Thus, we presented a new application of echo intensity to water-mass analysis in the deep layer. This property of echo intensity is extremely useful in the North Pacific where water-mass properties are weakened to be analyzed.

In Chapter 4, using current velocity and echo intensity data from LADCP, we obtained a new pathway of deep current carrying LCPW from the Main Gap into the Northeast Pacific Basin, and clarified the current structure which carries North Pacific Deep Water (NPDW) from direct current observation. LCPW carried by the eastern branch of the lower deep current through the Main Gap continues along the northern slope of the Hess Rise and along approximately 38°N toward 165°W in the Northeast Pacific Basin, overturns to be carried by the westward current as NPDW.

In the Melanesian Basin, we clarified the structure of the upper deep current at depths of 2000–3500 m over the northeastern slope of the Solomon Rise. The current comprised western and eastern cores located over the bottom slope at water depths of approximately 3000 and 4000 m, respectively. Between the double cores of the current, a thick countercurrent was observed with a width of more than 100 km. The countercurrent flowed over the bottom slope at a water depth of approximately 3500 m and carried water that is characterized by extremely high echo intensity, indicating the water carried from the equatorial region.

This thesis indicates that the use of current velocity from LADCP is limited to depths shallower than 1000 m approximately in low echo intensity region, but simultaneously, suggests that the current velocity in the high echo intensity region such as subpolar region is enough useful for a qualitative analysis of deep circulation. These results and a new application of echo intensity to water-mass analysis enable to help the LADCP users, an improvement of LADCP instrument, and studies of deep ocean circulation.

References

Ashjian, C. J., S. L. Smith, C. N. Flagg, A. J. Mariano, W. J. Behrens and P. V. Z. Lane (1994): The influence of a Gulf Stream meander on the distribution of zooplankton biomass in the Slope Water, the Gulf Stream, and the Sargasso Sea, described using a shipboard acoustic Doppler current profiler. Deep-Sea Research I, 41, 23-50.

Ashjian, C. J., S. L. Smith, C. N. Flagg and C. Wilson (1998): Patterns and occurrence of diel vertical migration of zooplankton biomass in the Mid-Atlantic Bight described by an acoustic Doppler current profiler. Continental Shelf Research, 18, 831-858.

Braithwaite, H. (1974): Some Measurements of Acoustic Conditions in Rivers. Journal of Sound and Vibration, 37, 557-567.

Cunningham, S. A., M. J. Griffiths and B. A. King (1997): Comparison of Bottom-Tracking and Profiling LADCP Data in a Section Across the ACC at Drake Passage. International WOCE Newsletter, 26, 39-40.

Edmond, J. M., Y. Chung and J. G. Sclater (1971): Pacific Bottom Water Penetration east around Hawaii, Journal of Geophysical Research, 84, 7809-7826.

Egbert, G. D., A. F. Bennett and M. G. G. Foreman (1994): TOPEX/Poseidon tides estimated using a global inverse model. Journal of Geophysical Research, 99, 24,821-24,852.

Firing, E. and R. L. Gordon (1990): Deep Ocean Acoustic Doppler Current Profiling. Proc. IEEE Fourth Working Conf. on Current Measurements, Clinton, MD,

Current Measurement Technology Committee of the Oceanic Engineering Society, 192-201.

Firing, E. (1998): Lowered ADCP Development and Use in WOCE. International WOCE Newsletter, 30, 10-14.

Firing, E., S. Wijffels and P. Hacker (1998): Equatorial subthermocline currents across the Pacific. Journal of Geophysical Research, 103, 21,413-21,423.

Fischer, J. and M. Visbeck (1993): Deep velocity profiling with self-contained ADCPs. Journal of Atmospheric Oceanic Technology, 10, 764-774.

Hall, M. M., T. M. Joyce, R. S. Pickart, W. M. Smethie Jr. and D. J. Torres (2004): Zonal circulation across 52°W in the North Atlantic, Journal of Geophysical Research, 109, C110088, doi:10.1029/2004JC002384.

Hamann, I. and B. A. Taft (1987): The Kuroshio extension near the Emperor Seamounts. *Journal of Geophysical Research*, 92,3827-3839.

Hay, A. E. (1983): On the Remote Acoustic Detection of Suspended Sediment at Long Wavelengths. Journal of Geophysical Research, 88, 7525-7542.

Heywood, K. J., S. Scrope-Howe and Barton E. D. (1991): Estimation of zooplankton abundance from shipborne ADCP backscatter. Deep-Sea Research, 38, 677-691.

Holliday, D. V. and R. E. Piepper (1980): Volume scattering and zooplanktondistributions at acoustic frequencies between 0.5 and 3 MHz. Journal of Acoustic Society America, 67, 135-146

Honjo, S., J. Dymond, R. Collier and S. J. Manganini (1995): Export production of particles to the interior of the equatorial Pacific Ocean during the 1992 EqPac experiment., Deep-Sea Research II, 42, 831-870.

Ichikawa, T. (1975): Particulate Organic Carbon and Nitrogen in the Adjacent Seas of

the Pacific Ocean. Marine Biology, 68, 49-60.

Johnson, G. C. and J. M. Toole (1993): Flow of deep and bottom waters in the Pacific at 10° N. *Deep-Sea Research I*, 40, 371-394.

Johnson, G. C. and J. M. Toole (1993): Flow of deep and bottom waters in the Pacific at 10°N, Deep Sea Research I, 40, 371-394.

Johnson, H. P., S. L. Hautala, T. A. Bjorklund and M. R. Zarnetske (2006): Quantifying the North Pacific silica plume. Geochemistry Geophysics Geosystems, 7, Q05011, electronic journal (http://www.agu.org/journals/gc/).

Kaneko, A., Zhu X. H. and Radenac M. H. (1996): Diurnal Variability and Its Quantification of Subsurface Sound Scatterers in the Western Equatrial Pacific. Journal of Oceanography, 52, 655-674.

Kawabe, M. (1993): Deep water properties and circulation in the western North Pacific. In: Teramoto, T. (Ed.), Deep Ocean Circulation, Physical and Chemical Aspects. Elsevier Science Publishers, Amsterdam, pp. 17-37.

Kawabe, M., S. Fujio and D. Yanagimoto (2003): Deep-water circulation at low latitudes in the western North Pacific, Deep Sea Research I, 50, 631-656.

Kawabe, M, D. Yanagimoto, S. Kitagawa and Y. Kuroda (2005): Variations of the deep western boundary current in Wake Island Passage, *Deep-Sea Research I*, 52, 1121-1137.

Kawabe M., D. Yanagimoto and S. Kitagawa (2006): S. Variations of deep western boundary currents in the Melanesian Basin in the western North Pacific, *Deep-Sea Research I*, 53, 942-959.

Kawabe, M. and K. Taira (1995): Flow distribution at 165° E in the Pacific Ocean. in *Biogeochemical Processes and Ocean Flux in the Western Pacific*, edited by H.

Sakai and Y. Nozaki, pp. 629-649,Terra Sci., Tokyo.

Kawahata, H., Yamamuro, M. and Ohta, H. (1998c): Seasonal and vertical variations of sinking particle fluxes in the West Caroline Basin. Oceanologica Acta, 21, 521-532.

Kawahata, H. (2002): Suspended and settling particles in the Pacific. Deep-Sea Research Ⅱ, 49, 5647-5664.

Kenyon, K. E. (1983): Sections along 35° N in the Pacific. *Deep-Sea Research A*, 30, 349-369.

Lilijebladh, B. and Thomasson, M. A. (2001): Krill behaviour as recorded by acoustic doppler current profilers in the Gullmarsfjord. Journal of Marine Systems, 27, 301-313.

Mantyla, A. W. and J. L. Reid (1983): Abyssal characteristics of the World Ocean waters, Deep Sea Research 20, 871-885.

NEDO (1993): Reports on North Pacific Carbon Cycle Study during NH92, New Energy and Industrial Technology Development Organization, Ministry if International Trade and Industry, pp. 1-284 (in Japanese).

NEDO (1995): Reports on North Pacific Carbon Cycle Study during NH94, New Energy and Industrial Technology Development Organization, Ministry if International Trade and Industry, pp. 1-259 (in Japanese).

O'Brien, T. D., M. E. Conkright, T. P. Boyer, C. Stephens, J. I. Antonov, R. A. Locarnini, H. E. Garcia (2002): World Ocean Atlas 2001, Volume 5: Plankton. NOAA Atlas NESDIS 53, U.S. Government Printing Office, Wash., D.C., 95 pp.

Owens, W. B. and B. A. Warren (2001): Deep circulation in the northwest corner of the Pacific Ocean. *Deep-Sea Research I*, 48, 959-993.

Reid, J. L. (1997): On the total geostrophic circulation of the pacific ocean: flow patterns, tracers, and transports. *Progressive Oceanography*, **39**, 263-352.

RD Instruments (1996): Principles of Operation, A Practical Primer.

Roden, G. I. (2000): Flow and water property structures between the Bering Sea and Fiji in the summer of 1993. Journal of Geophysical Research, 105, 28,595-28,612.

Schmitz, W. J. (1987): Observations of new, large, and stable abyssal currents at midlatitudes along 165° E. *Journal of Physical Oceanography*, 17, 1309-1315.

Siedler, G., J. Holfort, W. Zenk, T. J. Muller and T. Csernok (2004): Deep-Water Flow in the Mariana and Caroline Basins. *Journal of Physical Oceanography*, 34, 566-581.

Stramma, L., J. Fischer and F. Schott (1996): The flow field off southwest India at 8°N during the southwest monsoon of August 1993. Journal of Marine Research, 54, 55-72.

Talley, L. D. and T. M. Joyce (1992): The Double Silica Maximum in the North Pacific. *Journal of Geophysical Research*, **97**, 5465-5480.

Vincent, C. A., R. A. Young and D. J. P. Swift (1982): The relationship between bedload and suspended sand transport on the inner shelf, Long Island, New York. Journal of Geophysical Research, 87, 4163-4170.

Visbeck, M. (2002): Deep Velocity Profiling Using Lowered Acoustic Doppler Current Profilers: Bottom Track and Inverse Solutions. Journal of Atmospheric Oceanic Technology, 19, 794–807.

Warren, B. A. and W. B. Owens (1988): Deep currents in the central subarctic Pcific Ocean. *Journal of Physical Oceanography.*, **18**, 529-551.

White J. R, Zhang Xinsheng, Welling L. A. (1995): Latitdinal gradients in zooplankyon biomass in the tropical Pacific at 149W during the JGOFS EqPc: Effect of El Nino. Deep-Sea Research Ⅱ, 42, 715-1313.

Wijffels, S., M. Hall, T. Joyce, D. J. Torres, P. Hacker and E. Firing (1998): Multiple deep gyres of the western North Pacific: A WOCE section along 149°E. Journal of Geophysical Research, 103, 12,985-13,009.

Wong, C. S. (1972): Deep Zonal Waters in the Equatorial Pacific Ocean Inferred from Anomalous Oceanographic Properties, Journal of Geophysical Research, 77, 7196-7202.

Yamaguchi, A., Watanabe, Y., Ishida, H., Harimoto, T., Furusawa, K., Suzuki, S., Ishizaka, J., Ikeda, T., and Takahashi, M. M. (2004): Latitudinal Differences in the Planktonic Biomass and Community Structure Down to the Greater Depths in the Western North Pacific. Journal of Oceanography, 60, 773-787.

Young, R. A., J. T. Merrill, T. L. Clarke and J. R. Proni (1982): Acoustic profiling of suspended sediments in the marine bottom boundary layer. Geophysical Research Letter, 9, 175-178.

Acknowledgements

I express the deepest gratitude to my supervisor Dr. Masaki Kawabe for improving the dissertation and elevating my mind as a scientist. I am grateful to Dr. Shinzou Fujio for his appropriate and profitable suggestions for LADCP data analysis. Valuable discussions with Drs. Yutaka Michida, Eitarou Oka, Daigo Yanagimoto, Kiyoshi Tanaka and the other members of Ocean Circulation Group in Ocean Research Institute, the University of Tokyo, broadened my acquaintances and interests in physical oceanography. Trans-field advises on zooplankton and particulate matters kindly received from Drs. Jun Nishikawa, Hiroyuki Matsuura and Hodaka Kawahata, respectively, were most precious in my study experience. This dissertation owes its completion largely to graphic libraries and UNIX machines produced and maintained by Drs. Shinzou Fujio and Daigo Yanagimoto, and to perfect maintenances of LADCP and CTD by Mr. Shoji Kitagawa. Lunch time discussions with the supervisor's secretary Ms. Fukuko Sogo were pleasant in my study life, so I send her special thanks.